January 2015

SOUND SCATTERING OF AN OBSTACLE PLACED NEAR A NON-LOCALLY REACTING GROUND

Yiming Wang
Purdue University

Recommended Citation

Wang, Yiming, "SOUND SCATTERING OF AN OBSTACLE PLACED NEAR A NON-LOCALLY REACTING GROUND" (2015). *Open Access Theses*. 1181.
https://docs.lib.purdue.edu/open_access_theses/1181

Graduate School Form 30
(Revised 08/14)

PURDUE UNIVERSITY
GRADUATE SCHOOL
Thesis/Dissertation Acceptance

This is to certify that the thesis/dissertation prepared

By Yiming Wang

Entitled

SOUND SCATTERING OF AN OBSTACLE PLACED NEAR A NON-LOCALLY REACTING GROUND

For the degree of Master of Science in Engineering

Is approved by the final examining committee:

Kai Ming Li

Marcial Gonzalez

Ganesh Subbarayan

To the best of my knowledge and as understood by the student in the Thesis/Dissertation Agreement, Publication Delay, and Certification/Disclaimer (Graduate School Form 32), this thesis/dissertation adheres to the provisions of Purdue University's "Policy on Integrity in Research" and the use of copyrighted material.

Approved by Major Professor(s): Kai Ming Li

Approved by: Ganesh Subbarayan 04/29/2015

Head of the Department Graduate Program Date

SOUND SCATTERING OF AN OBSTACLE PLACED NEAR A NON-LOCALLY REACTING GROUND

A Thesis

Submitted to the Faculty

of

Purdue University

by

Yiming Wang

In Partial Fulfillment of the

Requirements for the Degree

of

Master of Science in Engineering

May 2015

Purdue University

West Lafayette, Indiana

TABLE OF CONTENTS

Page

LIST OF FIGURES

ABSTRACT

Wang, Yiming, M.S.E, Purdue University, May 2015. Sound Scattering of an Obstacle Placed Near a Non-Locally Reacting Ground. Major Professor: Kai Ming Li, School of Mechanical Engineering.

The Boundary Element Method (BEM) is widely used in outdoor sound scattering problems due to its computational efficiency when compared to the FEM (FEM) for certain propagation geometries. The advantage of the BEM is apparent for problem geometries where the scattering surface is much smaller than the computational domain of the problem. The Green's function can be used in the BEM formulation to represent a non-locally reacting porous ground surface. The Weyl Van der Pol formula is often used to accurately calculate the Green's functions above a locally reacting surface. However, the Green’s function representation for the sound field above and below a non-locally reacting ground has not yet been established. Nevertheless, the steepest descent method can be used to derive these functions.

An efficient solution for several different types of Green’s functions are derived in the present study. The simulation results are computed via the BEM and validated against analytical solutions and/or physical experimental measurements. The scattering effect due to an obstacle in the vicinity of a porous ground is also investigated.

CHAPTER 1. INTRODUCTION

1.1 Introduction

Sound scattering due to an impedance boundary is a fundamental problem in acoustics with practical noise control engineering applications. Typical examples of obstacles placed above the ground are: noise barriers, vegetation, and tires. Constructing a noise barrier is a common method to reduce noise pollution in outdoor environments. A large body of research has been conducted on the effects of diffraction due to the presence of noise barriers. The interface between a rolling tire and the road surface forms a horn-like region, which acts as an amplifier for the noise generated around the contact region. The amplified noise from the horn-like structure contributes significantly to the total noise generated by a moving vehicle. Another example is the scattering of sound due to objects embedded below the ground. Objects below the ground can be identified via acoustical detection methods.

There are many different methods for solving a variety of scattering problem configurations. For the sound field scattered by infinitely long cylinders and spheres, analytical solutions can be derived based on previous studies by Rayleigh and Morse, (Rayleigh, 1896); (Morse, 1948). For a finite sized objects, analytical solutions may not be readily available. Various different approximation methods can be used to solve these kinds of problems: the transfer matrix method, optical method, and Kirchhoff method (Stephens, 1984); (Junger and Feit, 1972) have been suggested in the literature. Numerical solutions are needed for more complicated problem configurations.

To solve the problem of scattering by an irregularly shaped object, we should consider numerical methods such as the FEM (FEM) and/or the Boundary Element Method (BEM). Over the last few decades, the development of computer technology has made numerical approaches more readily available. Regardless of how complicated the shape of an obstacle may be, we can always find a satisfactory solution via the BEM or FEM approximations. Figure 1-1 shows some typical scattering problem configurations in the context of outdoor sound propagation.

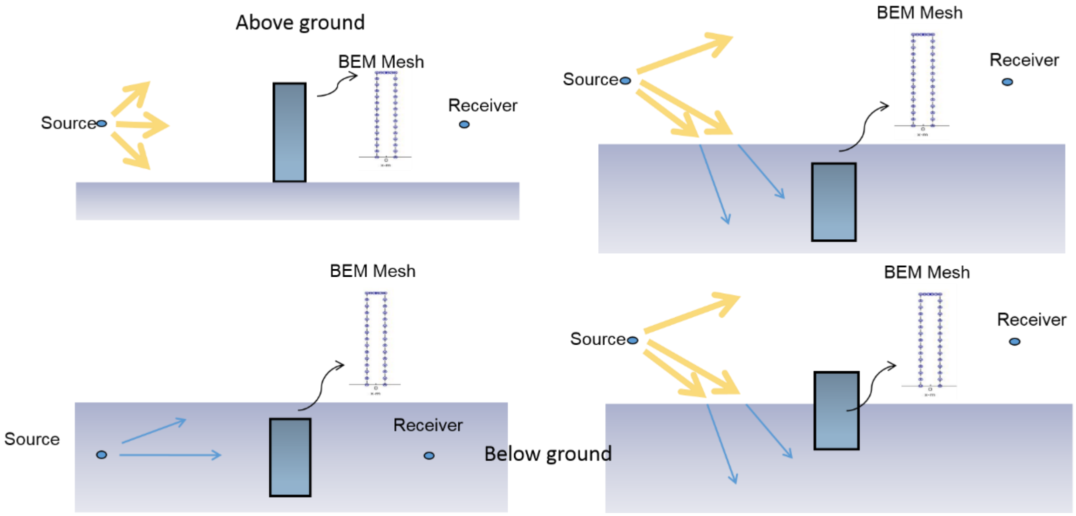

Figure 1-1. Typical scattering geometries considered in the present study.

In order to solve a problem via the FEM approach, one needs to discretize the entire domain of interest into a collection of ‘finite’ elements. Alternatively, the BEM approach only requires discretization along the surface of the scattering objects (e.g., the perimeter of the noise barrier’s surface). Typically, outdoor sound propagation involves large domain sizes which can be modelled as an infinite boundary. Due to modeling constraints in the FEM, a finite domain must be discretized to approximate an infinitely large domain. The infinite boundary conditions must be approximated by artificial boundary conditions such as the perfectly matched layer, (Abarbanel et al., 1999) which may introduce considerable errors in the final result. The mesh size must be sufficiently small to ensure the accuracy of the numerical solutions. Hence, the computational time for the FEM can become substantial.

In the BEM formulation, the dimension of the problem is reduced by one dimension and the discretization only needs to be carried out along the surface of the obstacle. Hence, the BEM approaches are more suitable for sound scattering problems involving an infinite domain. There are several different methods for solving the scattering problem within two domains simultaneously.

The first method is to approximate the boundary condition along the air/ground interface as a locally reacting impedance plane. The sound field above a locally reacting ground can be approximated by using the steepest descent method (Chandler-Wilde and Hothersall, 1985). However, the boundary condition on the surface of the non-locally reacting ground require more thought. A non-locally reacting ground surface has acoustical properties which depends on the angle of incidence (e.g., porous mediums such as foam, soil, and sand). A two-domain method is used to satisfy the boundary conditions along the medium interface: (1) continuity of the normal particle velocity, and (2) continuity of the acoustic pressure (Seybert, Cheng and Wu, 1990). However, the regions need to be discretized in this method include the interface between the air and the porous medium and also the obstacle’s surface. Hence, this method requires a large numbers of elements to represent the sound pressure field along the surface of the obstacle. This requirement can diminish the advantages of the BEM over the FEM for tackling these types of problems.

In order to solve the problem more efficiently with the BEM, a two-medium boundary element approach has been suggested (Berry et al, 1994). This method only requires discretization along the surface of the obstacles. However, the method requires an accurate representation for four different types of Green’s function. The first Green’s function corresponds to the source and receiver located above the porous ground interface. The second Green’s function represents a source located above the air/ground interface while a receiver is situated within the porous medium. The third Green’s function describes the source and receiver located within the porous medium. And the fourth Green’s function provides the remaining permutation which is a crucial component in the subsequent analysis. By the principle of reciprocity (Fokkema and van den Berg, 2013), the last Green’s function can be obtained via the second Green’s function described above. The various Green’s functions are assembled to compute the pressure along the surface of the objects using the BEM approach. Thus, the sound field in the air and in the underground medium can be solved by means of a set of Boundary Integral Equations (BIE). Perhaps the most challenging part in this two-domain BEM approach is in the derivation of the three different types of Green’s function. Although the functions can be expressed in integral form, numerical calculation can be computationally intensive due to the large number of boundary elements required.

The Fast Field Program (FFP) techniques may be implemented to compute the necessary Green’s functions more efficiently. However, the locations of the receivers are not always aligned along a straight line of equal spacing required by the FFP formulation. In fact, the location of the receivers in the two-domain BIE are on the surface of the obstacle itself. Nonetheless, the FFP provides an alternative method for calculating the Green's function for simple propagation geometries (e.g., a semi-infinite plane).

Most of the earlier asymptotic solutions for the Green's function are either not sufficiently accurate for application in the BEM, or are only valid for certain limiting cases. One of the objectives in the current research is to derive a fast and accurate solution for each of the three types of Green's function proposed. These Green's function can be implemented in the boundary integral formulation to predict the scattered sound field due to various arrangements of obstacles. Figure 1-2 depicts the processes involved in implementing the two-domain BIE formulation.

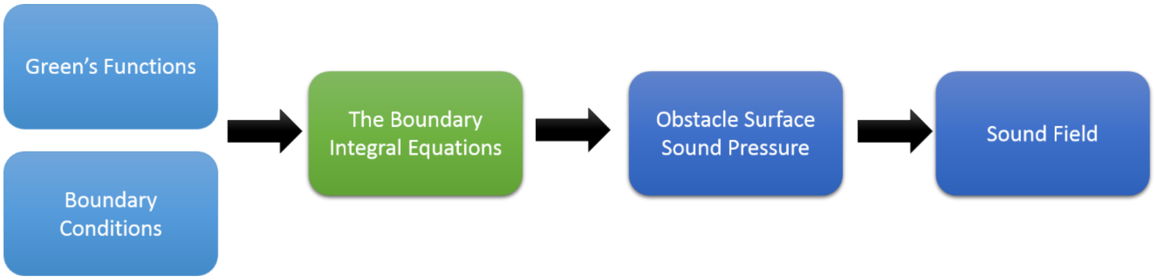

Figure 1-2. Process diagram for the two-domain BEM approach.

1.2 Literature Review

1.2.1 The Boundary Element Method

The BEM is commonly used to predict the sound field in the presence of scattering from various obstacles. In order to solve the BIE along the boundary of the obstacle, one needs to discretize the surface of the scattering object. This method has been widely applied in many areas, such as noise barrier design, underground object detection, and outdoor sound propagation.

Compared to the standard FEM approach, the BEM can oftentimes be more efficient when the problem of interest involves unbounded domains. In order to solve the problem via the FEM, the domain needs to truncated into bounded region using a large number of finite elements distributed throughout the domain. Alternatively, a BEM approach can be combined with a Sommerfeld boundary condition to model the unbounded domain. Discretization is only required along the surface of the scattering obstacle. For many acoustics problems, meshing is among the most difficult and time consuming steps. Modifying of the surface mesh is more convenient following the BEM approach. Hence, the FEM may be useful for smaller domain sizes while the BEM is of greater interest for outdoor sound propagation conditions over large distances.

The origin of the BEM dates back to as early as the 1750s. Euler, Lagrange, Fourier, among other mathematicians and scientists have shaped the method into what it is today. One of the most important contribution to the development of the BEM came from George Green. According to Green’s second theorem, we can reduce the dimension of the problem from 3D to 2D and from 2D to 1D via:

$$\iiint_{\Omega} (\Phi\Delta\Psi - \Psi\Delta\Phi) dV = \iint_{\Gamma} (\Phi \frac{\partial \Psi}{\partial n} - \Psi \frac{\partial \Phi}{\partial n}) dS \qquad (1.1)$$

which demonstrates the dimensional difference between the FEM and BEM approach. Fredholm formulated the BIE and proved the existence and uniqueness of the solution of the BIE.

Although some BIE were already developed at the beginning of the twentieth century, solving the numerical equations without the aid of digital computers was nearly impossible. It wasn't until the 1960s (after digital computers became accessible to many scientists) that research concerning numerical methods such as the FEM, the finite difference method, and the BEM began to develop as a field. Many methods for solving the BIE were developed during this period. The work completed by Jaswon, Ponter, and Symm (Jaswon, 1963) on the direct and indirect methods for potential problems has greatly influenced the development of the BEM during the 1960s. Jaswon et al. applied the free-field Green's function, which is the solution to the Helmholtz equation with Sommerfeld boundary conditions, along with Green's second theorem, to develop the BIE which we still use today. The work by Kupradze from Tbilisi State University on potential function solutions is another substantial contributions to the BEM community. Work by Chen (Chen, 1963), and Rizzo on the Somigliana integral equation are also noteworthy.

In the early years of BEM developments, the functions and the acoustical variables were assumed to be constant in each element. In order to have a decent approximation with the BEM, one needs to have a large number of boundary elements. Seybert introduced the first order and second order interpolation methods into the BIE from the FEM (Seybert, 1985). A detailed history of the BEM could be found in the work by Cheng (Cheng, 2005).

When a scattering obstacle is positioned above a porous non-locally reacting surface, the ground is sometimes assumed to be locally reacting ground to simplify the calculations. With an impedance boundary condition and the Green's second theorem, one can calculate the acoustic pressure at any location above the ground (Chandler-Wilder, 1984). However, this assumption is not always valid for certain mediums, especially when the sound speed within the ground is very close to the speed of sound in air. The air/ground interface can no longer be treated as an impedance boundary. A set of different Green's functions must be calculated first to solve these types of problems via the BEM.

When the scattering of the obstacle is below the ground and in the vicinity of the air/ground interface, the contribution due to the scattering of the obstacle is non-negligible. In order to solve problems of this type, a two-medium BEM approach must be applied. Ahmad (Ahmad, 1988) and Seybert (Seybert, Cheng and Wu, 1990) developed multi-domain BEM methods for problems of elastodynamics and acoustics. The idea is to couple the BIE on the interface between the different mediums. They proposed that the surface of the interface needs to be discretized into boundary elements. As a result, the number of equations is substantially increased. Later, Berry introduced a BEM for two mediums by utilizing three types of Green's functions without increasing the number of equations. Discretization of the boundary is only performed on the surface of the below ground obstacle. Asymptotic solutions for the Green's functions were used in the study, which were valid only for limited scattering geometries. Among the most challenging aspect of the method is in the derivation of the Green's functions.

1.2.2 Green's Function

The study of sound propagation above an infinitely large ground can be dated back to the first half of the twentieth century. Acoustic wave propagation was adapted from the study of electromagnetic wave propagation (Norton, 1936 and Morse, 1944). In the work of Morse and Bolt, the sound field above an impedance ground was expressed as the sum of two different terms: a direct wave term and a mirror wave term (due to an image source). The calculation of the reflection term can be computationally expensive following the BEM approach.

Ingard built on previous developments (Ingard, 1951). Several different source types were considered including monopole, dipole and quadrupole. The steepest descent method was used to approximate the reflection wave contribution. Then the method of pole subtraction was applied to evaluate the integration when the path is close to the singular points (Chien and Soroka, 1975). These types of approximated Green's function can be simplified to a form of the Weyl Van der Pol formula.

For a non-locally reacting ground such as an infinite porous ground or a hard-backed porous ground, the above approximating methods are invalid. The exact solution for the sound field above a non-locally reacting ground can be found in Sommerfeld's work (Sommerfeld, 1909). Asymptotic solutions of the sound field above a porous half-space has been investigated by multiple researchers (Paul, 1957) (Attenborough, 1980). An experimental study on the Green's function above a non-locally reacting ground was conducted by Lawhead and Rudnick (Lawhead and Rudnick, 1951). The asymptotic solution of the sound field above a hard-backed porous layer was developed by Allard (Allard, 2002). Most recently, Li and Liu researched the sound field above an impedance-backed porous layer (Li and Liu, 2012). Later, Li and Tao used a modified double saddle point method to obtain the prediction of the sound field above several different types of non-locally reacting porous grounds based on the work by Ott (Ott, 2013) and Kawai (Kawai, Hidaka and Nakajima, 1984). The asymptotic solution for sound propagation above a semi-infinite porous ground, impedance-backed ground, and hard-backed ground are developed in their work.

The sound field due to a coherent line source is similar to that of a point source. The formula is simpler due to the absence of the Bessel function term in the solution. An accurate and efficient solution for a coherent line source propagating over an impedance plane is presented by Chandler-Wilde and Hothersall (Chandler-Wilde, 1995). The method of the steepest descent and pole subtraction are used to obtain the solution, similar to the approach used in the point source case. The integrals can be evaluated by Gaussian quadrature integration for increased numerical efficiency. The solutions for the pressure and the directional derivatives are obtained, which are necessary in the BEM implementation.

For the sound field below the ground, the study on the subject was investigated by Berry, Chandler-Wilde and Attenborough (Berry, 1994), and later by Li (Li, 2008). In the current investigation, the solution for a point source is extended to consider a coherent line source. The integration is calculated along the steepest descent path instead of at the stationary points.

For the sound field below the ground due to an underground noise source, the solution is complicated by the introduction of a lateral wave term. When the incidence angle of the plane wave is larger than the critical angle, most of the energy will be reflected back into the lower medium (i.e., total internal reflection). Lateral waves travel along the air/ground interface for some distance, then go back into the porous medium when this occurs. The effect was first discovered in optics. An explanation for the phenomena can be found in (Brekhovskikh, 2012). The contribution due to the lateral wave term is calculated via the method of steepest descent. Here, the path of the integration is different from that of the direct wave. An asymptotic solution for this type of Green's function (based on the ray theory) is provided by Berry (Berry, 1994). However, the solution is only valid for limited situations where analytical solutions are readily available. This topic is of great interest in underwater water acoustics and seismo-acoustic research communities.

Fast and accurate solutions need to be developed to evaluate the below ground Green's function required in the BIE formulation. The Fast Field Program (FFP) is often used to compute the Green's function above and below the ground. The method was developed for electromagnetic wave propagation and introduced to the acoustics community by (Dinapoli, 1970). Originally, it was applied to underwater acoustics problems to investigate the relationship between the speed of sound and the water depth. Later, the method was used in the study of the atmospheric sound propagation. The FFP is applicable in range independent propagation conditions (Richards and Attenborough, 1972).

The sound field along a horizontal line or on the surface of a horizontal plane can be computed efficiently via the FFP. However, this requires the receivers to be on the same elevation. In the BEM formulation described in the later chapters, the receivers need to be on the surface of the arbitrarily shaped scattering obstacles. Even though the FFP is an efficient numerical method for computing the Green's function, the method is not as robust as the BEM for arbitrary scattering objects. However, it can serve as a validation tool to verify the BEM formulation under limiting cases.

1.3 Outline

This thesis is divided into six chapters. A literature review is presented in the first chapter along with a discussion of the advantage/disadvantage of various computational tools (e.g., method of steepest descent, FEM, BEM, and FFP). Figure 1-3 provides an outline of the various topics examined in this thesis. Two different propagation configurations are investigated in the current research: (1) scattering above the ground (i.e., Chapter 2 and 3), and (2) below ground scattering problems (i.e., Chapter 4 and 5).

An application of the BEM for calculating the sound field above the ground is described in Chapter 2. Starting from Helmholtz's equation along with the associated boundary conditions, the BIE is derived with the help of Green's second theorem. A fast asymptotic solutions for the above ground Green's function and the directional derivatives are introduced in the second chapter. The steepest descent method and pole subtraction method are also described. The sound field due to a coherent line source are compared against those calculated via direct numerical integration methods.

Chapter 3 describes the method of colocation. Sound field predictions are validated against experimental measurements and other data available in the literature. The last section in Chapter 3 illustrates the above ground sound field predictions obtained using the BEM. It highlights the necessity for an efficient method to compute the below ground Green's function.

The BEM for an underground scattering problems is introduced in Chapter 4. The boundary condition along the air/ground interface is coupled with the BIE in the two mediums. The underground Green's function and the sound field below the ground due to an above ground coherent line source are approximated by asymptotic solutions. The method of steepest descent is used in the derivation, and a branch cut integral is introduced. The sound field above the ground due to a below ground monopole source is obtained from the saddle path method by identifying two saddle points. The efficiently approximated Green's function are compared to exact solutions to help determine their applicability. Acoustic reciprocity in the two mediums is also discussed.

Chapter 5 presents the predictions for the sound field above and below the ground due to a scattering object positioned below the ground. A detailed formulation of the colocation method is provided. The acoustic pressure along the rigid surface of the hard-backed layer is compared against the analytical solution. Scattering due to a cylindrical object embedded in the ground is investigated using the BEM in a case study.

Conclusions are drawn in Chapter 6. A discussion of future work is provided to extend the topics presented in the current investigation to areas of potential growth.

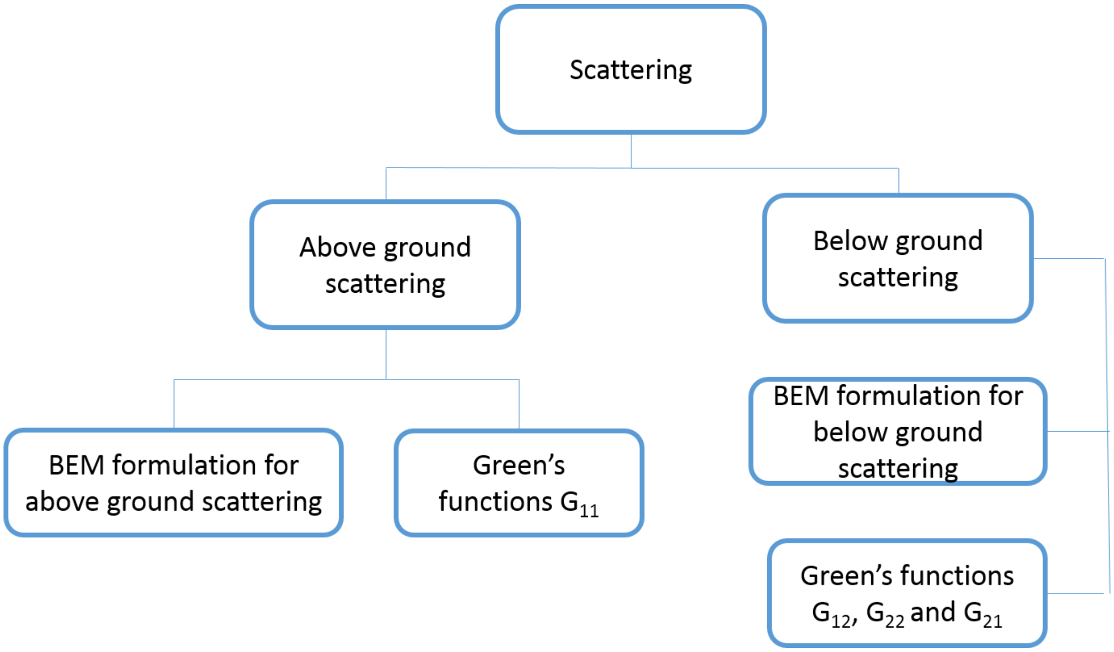

Figure 1-3. Schematic diagram for classifying sound scattering problems.

CHAPTER 2. THE BEM FOR THE SCATTERING ABOVE THE GROUND

2.1 Introduction

The development of the BIE can be traced back to one hundred years ago, however, without the help of the numerical methods brought by the advancement in the computer technology, the application of the BEM is nearly impossible. In the 1960s, the BEM was first put into application together with the FEM, which is a very powerful numerical tool in the area of structural mechanics. Nonetheless, the BEM has several advantages in the analysis of outdoor sound propagation. The most important reason is that the domains in many outdoor acoustic problems are unbounded, and it is time consuming to truncate and discretize the whole problem domain with the FEM. However, with the BEM, one only needs to discretize the surface of the scattering obstacle, which saves a lot of computer memories and calculation time.

The purpose of the current study is to develop an approach to calculate the sound field in the air and in the porous medium with the influence of an obstacle which can be both above or below the ground. When the shapes of the obstacles are not complicated, the results based on analytical methods have been presented by Bowman. (Bowman, 1970). However, if the shape of the scattering obstacle is arbitrary, the BEM is more suitable, in which the surface boundary of an obstacle with arbitrary shape, as long as it is continuous, can be approximated with finite number of polygons. There have been many studies on the formulations of the BIE for acoustic scattering problems. (Morgan, 1998) Particularly, for predicting the acoustic influence of near-surface obstacles in the porous medium, a method involved BIE was developed by Berry, Chandler-Wilde and Attenborough. (Berry, 1994) However, the asymptotic solutions for the Green's functions are only valid for certain geometries.

The purpose of the current study is to extend the previous work on the BEM scattering problems to more general geometries. To solve the BIE with BEM introduced by Berry, the fast and accurate solutions of several types of Green's functions are indispensable.

2.2 Basic Theory

2.2.1 The Sound Wave Equation

In an isotropic and homogeneous medium, the propagation of sound is governed by the wave equation.

$$\nabla^2 p + \frac{1}{c^2}\frac{\partial^2 p}{\partial t^2} = 0, \tag{2.1}$$

where p denotes the sound pressure, t is the time and c is the speed of sound in the medium. The solutions are assumed as time-harmonic, which can be expressed as

$$p(\mathrm{x},\mathrm{t}) = \mathrm{Re}(u(\mathrm{x})\,\mathrm{e}^{-i\omega t}), \tag{2.2}$$

where the spatial variable x is the sound source location and $\omega = 2\pi f$ denotes the angular frequency with f representing the source frequency. The time dependent factor, $e^{i\omega t}$ is used as an alternative expression in some textbooks.

Substituting (2.2) into (2.1), we get the Helmholtz equation

$$\Delta p + k^2 p = 0, \quad in\ D \tag{2.3}$$

D is the domain of propagation and $\Delta \equiv \nabla^2$. In the current study, we only consider a 2-dimensional condition. The variable k denotes the wave number, which can be calculated as

$$k = \frac{\omega}{c} = \frac{2\pi f}{c} \ . \tag{2.4}$$

As an alternative to the pressure, Sound Pressure Level is often used, which is more directly related to the human perception of sound. Sound pressure can be converted to SPL by

$$SPL = 10\log_{10} \left| \frac{p^2}{p^2_{ref}} \right| = 20\log_{10} \left| \frac{p}{p_{ref}} \right| , \tag{2.5}$$

where the reference pressure $p_{ref} = 20\mu pa$ is the threshold of human hearing for sound propagation in the air.

In order to derive the BEM formulation, we need to obtain the Green's function for the sound field. If the monopole sound source is placed at position r_s and the receiver location is r, the Green's function can be expressed as $p(\mathrm{r}, \mathrm{r}_s) = G(r, r_s)$. The Green's function is the solution for the inhomogeneous Helmholtz equation

$$\Delta p + k^2 p = -\delta(r - r_s), r, r_s \in D_s \text{ ,} \tag{2.6}$$

where δ is the Dirac delta distribution function. In 2D, it means a coherent line source of sound is located at r_s point.

$$\delta(\mathrm{r} - \mathrm{r}_s) = \begin{cases} +\infty, r = r_s \\ 0, \quad r \neq r_s \end{cases} \tag{2.7}$$

An additional boundary conditions is often assumed for sound propagation in a unbounded field, which is known as the Sommerfeld radiation condition. It can be expressed as

$$\frac{\partial p(\mathrm{r}, \mathrm{r}_s)}{\partial r} - ikp(\mathrm{r}, \mathrm{r}_s) = \mathrm{o}(|\mathrm{r} - \mathrm{r}_s|^{-\frac{1}{2}}), \ as\, r \to \infty \tag{2.8}$$

The free field Green's function can be expressed as

$$G_f(\mathrm{r}, \mathrm{r}_s) = \frac{i}{4} H_0^{(1)}(\mathrm{k}\,|\mathrm{r} - \mathrm{r}_s|), \quad \mathrm{r}, \mathrm{rs} \in D \tag{2.9}$$

where $H_0^{(1)}$ denotes the zeroth order Hankel function of the first kind. The Hankel function is given by

$$H_0^{(1)}(\mathrm{z}) = J_0(\mathrm{z}) + \mathrm{i}\mathrm{Y}_0(\mathrm{z}), \tag{2.10}$$

which can be found in many mathematic handbooks. (Abramowitz, 1972) And $|r - r_s|$ is the Euclidean distance between r and r_s. If the value of $z = k\,|r - r_s|$ is small enough, we can use the near field approximation

$$H_0^{(1)}(\mathrm{z}) = 1 + i\frac{2}{\pi}[\ln(\frac{1}{2}\mathrm{z}) + \gamma]. \tag{2.11}$$

The term γ is Euler's constant which is approximately 0.577215. (Abramowitz, 1972) The approximation is necessary when we need to calculate the improper integral in the sound source element. In the 3D case

$$G_f(\mathrm{r},\mathrm{r}_s)=\frac{e^{ik|r-r_s|}}{4\pi|\mathrm{r}-\mathrm{r}_s|},\quad \mathrm{r},\mathrm{rs}\in D \tag{2.12}$$

The normal derivative of the Green's function, which is necessary in the boundary element formulation, is given by

$$\frac{\partial G_f(\mathrm{r},\mathrm{r}_s)}{\partial n(\mathrm{r})}=-\frac{ik}{4}H_1^{(1)}(\mathrm{k}|\mathrm{r}-\mathrm{r}_s|)\frac{\partial|\mathrm{r}-\mathrm{r}_s|}{\partial n},\quad \mathrm{r},\mathrm{rs}\in D \tag{2.13}$$

where $H_1^{(1)}$ is the first kind Hankel function.

The most common problem is the monopole scattering problem, which usually has boundary surfaces with sound rigid property or impedance boundary condition. The impedance boundary condition is given by

$$\frac{\partial p(\mathrm{r},\mathrm{r}_s)}{\partial n(\mathrm{r})}+ik\beta p(\mathrm{r},\mathrm{r}_s)=0 \tag{2.14}$$

where β denotes the normal admittance of the surface. If the sound speed ratio $n=c_1/c_2$ is large enough, the surface is named as locally reacting ground. The Green's function for locally reacting ground is relatively easier to model compared to porous ground, where solving the problem involves solving the wave equations in both media and then applying continuity conditions.

2.2.2 Free Field Scattering BEM Formulation

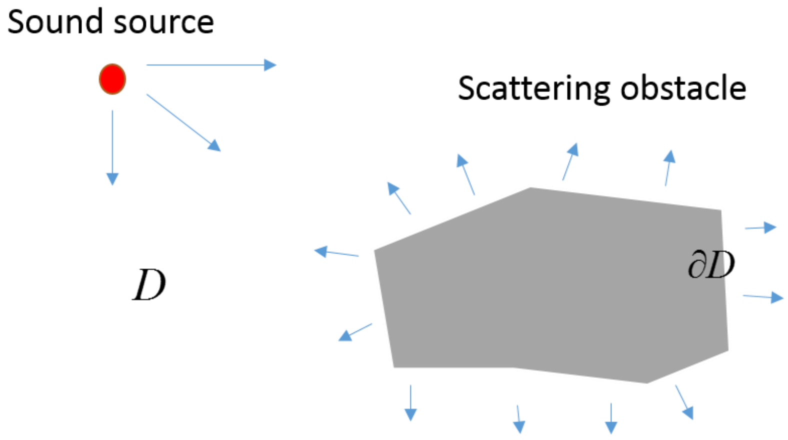

Figure 2-1. Free field scattering.

The governing equation for the acoustic pressure in the sound scattering problem in free field is $\Delta p + k^2 p = -\delta(\mathrm{r} - \mathrm{r}_s)$. The first boundary condition is $\frac{\partial p(\mathrm{r},\mathrm{r}_s)}{\partial n(\mathrm{r})} + ik\beta p(\mathrm{r},\mathrm{r}_s) = 0$ on the surface ∂D, which is an impedance boundary condition. ∂D denotes the surface of the scattering obstacle. Another boundary condition is the Sommerfeld boundary condition.

The free field Green's function G and p are both solutions to the homogeneous Helmholtz equation in the propagation domain D. We can apply the Green's theorem to the equation

$$p\Delta G - G\Delta p = Gk^2 p - pk^2 G = 0\,. \tag{2.15}$$

We will have

$$\int_{\Omega}(G\frac{\partial p}{\partial n}-p\frac{\partial G}{\partial n})dr_0=0, \tag{2.16}$$

where the Ω is the same as D except that Ω does not include a point at the source location of the function $G(r_0,r)$ and a point at the source location of the function $p(r,r_s)$, which are r point and r_s point. After some integrations around r_s and r, we can get the expression of the BIE

$$\epsilon p(\mathrm{r},\mathrm{r}_s)=G(\mathrm{r}_s,\mathrm{r})+\int_{\partial D}[G(\mathrm{r}_0,\mathrm{r})\frac{\partial p(\mathrm{r}_0,\mathrm{r}_s)}{\partial n(\mathrm{r})}-\mathrm{p}(\mathrm{r}_0,\mathrm{r}_s)\frac{\partial G(\mathrm{r}_0,\mathrm{r})}{\partial n(\mathrm{r}_0)}]\mathrm{dr}_0 \tag{2.17}$$

with

$$\epsilon=\begin{cases}0 & r_0\notin D\\ 1 & r_0\in D\\ \alpha/2\pi & r_0\in\partial D\end{cases}, \tag{2.18}$$

where D is the propagation domain and ∂D is the boundary of the propagation domain. $n(r)$ is the unit normal at point r pointing from the scattering surface to the outside of the propagation domain. α is the solid angle in the region of the domain, which is equal to π at most points on the scattering surface except at the corner points. $G(r_s,r)$ is the free field Green's function in the 2D case.

After substituting the impedance boundary condition into the BIE, we can obtain

$$\epsilon(r)p(\mathrm{r},\mathrm{r}_s)=G(\mathrm{r}_s,\mathrm{r})+\int_{\partial D}[G(\mathrm{r}_0,\mathrm{r})(-ik\beta(r_0)p(\mathrm{r}_0,\mathrm{r}_s))-\mathrm{p}(\mathrm{r}_0,\mathrm{r}_s)\frac{\partial G(\mathrm{r}_0,\mathrm{r})}{\partial n(\mathrm{r}_0)}]\mathrm{dr}_0, \tag{2.19}$$

The Green's function and the directional derivative are always known. With the numerical method of colocation, we can solve the pressure distribution.

2.2.3 Above the Ground BEM Formulation

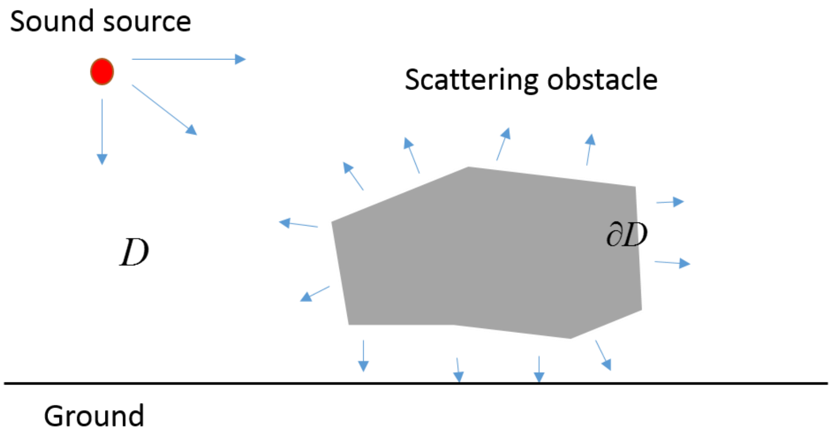

Figure 2-2. The scattering above an infinitely long ground.

The BIE for the sound field above the ground is similar to the previous one.

$$\epsilon(r)p(\mathrm{r},\mathrm{r}_s)=G_1(\mathrm{r}_s,\mathrm{r})+\int_{\partial D}[G_1(\mathrm{r}_0,\mathrm{r})(-ik\beta(r_0)p(\mathrm{r}_0,\mathrm{r}_s))-\mathrm{p}(\mathrm{r}_0,\mathrm{r}_s)\frac{\partial G_1(\mathrm{r}_0,\mathrm{r})}{\partial n(\mathrm{r}_0)}]\mathrm{dr}_0, \quad (2.20)$$

The only difference between (2.20) and (2.19) is the Green's function. The Green's function in (2.19) is the free field Green's function, however, the Green's function G_1 in the (2.20) is the Green's function for the sound field in the air. The ground can be locally reacting, hard-backed, impedance backed or rigid porous. The derivation of the Green's function can be found in the section 2.3.

2.2.4 Mixed Ground Types BEM Formulation

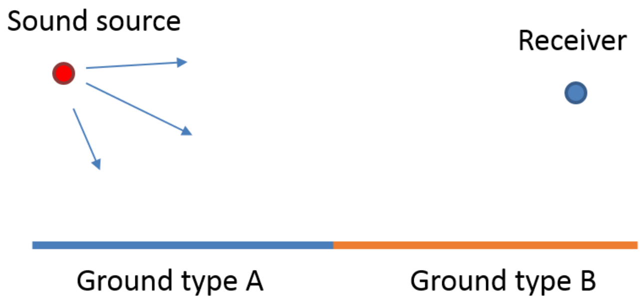

Figure 2-3. Scattering above a discontinuous ground.

The geometry is in the Figure 2-3. If the surfaces on the left and on the right are both locally reacting, the ground can be described with impedance boundary conditions. With a similar approach, we can obtain

$$\begin{aligned} &p(\mathrm{r},\mathrm{r}_s)=G_1(\mathrm{r}_s,\mathrm{r}) \\ &+\int_{\partial D}[G_1(\mathrm{r}_0,\mathrm{r})(-ik\beta(r_0)\,p(\mathrm{r}_0,\mathrm{r}_s))-\mathrm{p}(\mathrm{r}_0,\mathrm{r}_s)(-ik\beta_0(r_0)G_1(\mathrm{r}_0,\mathrm{r}))]\,\mathrm{dr}_0, \end{aligned} \tag{2.21}$$

which can be simplified as

$$p(\mathrm{r},\mathrm{r}_s)=G_1(\mathrm{r}_s,\mathrm{r})+\int_{\partial D}[-p(\mathrm{r},\mathrm{r}_s)ikG_1(\mathrm{r}_0,\mathrm{r})(\beta_0(r_0)-\beta(r))]\,\mathrm{dr}_0\,. \tag{2.22}$$

The integration is performed on the surface part where the ground type has changed, and the Green's function G_1 is the Green's function for the sound field above the original type of ground. (Chandler-Wilde & Hothersall, 1984)

If the ground is porous on the right but locally reacting on the left, we can derive a different BIE equation by assuming the contribution from the below ground is small. This assumption is proper when the sound source is located above the locally reacting part. The BIE equation can be expressed

$$p(\mathrm{r},\mathrm{r}_s)=G_p(\mathrm{r}_s,\mathrm{r})+\int_{\partial D}[G_p(\mathrm{r}_0,\mathrm{r})(-ik\beta(r_0)\,p(\mathrm{r}_0,\mathrm{r}_s))-\mathrm{p}(\mathrm{r}_0,\mathrm{r}_s)\frac{\partial G_p(\mathrm{r}_0,\mathrm{r})}{\partial n(\mathrm{r}_0)}]\,\mathrm{dr}_0 \quad (2.23).$$

The integration is performed on the part of ground with the impedance boundary condition, and the Green's function G_p is the above ground Green's function for the porous ground.

If the location of the sound source is above the porous ground part, the assumption is not accurate because of the reflection from the underground interface between the porous ground and the locally reacting ground, which makes an innegligible contribution to the total sound pressure.

2.3 Green's Functions for Sound Field Above the Ground

2.3.1 Introduction of the Green's Functions Above the Ground

The prediction of the sound fields above and below a two-medium interface is a subject of great interest and the study has been conducted for decades. The method was first introduced from the study of electromagnetic waves by Sommerfeld (Sommerfeld, 1909) and he dipole prediction by Banos. (Banos, 1966) Later studied by Chien and Soroka (Chien, 1975), and Attenborough. (Attenborough, 2006) Most recently, the propagation above and below a porous ground was studied by Li and Liu. (Li, 2011)

For the prediction of the sound field in the air, the interface was often treated as a locally reacting ground, where boundary condition were modeled as an impedance boundary condition. The prediction of the sound field in the air could be calculated with an asymptotic solution known as the Weyl-van der Pol equation. (Attenborough, 2006)

However, assuming the surface as locally reacting is not always proper. In order to make the BEM possible for more general cases, the fast solution for the Green's functions must be solved.

2.3.2 Fast Solutions for Sound Fields Above Ground with an Above Sound Source.

In the case of two dimensions, R_1 is the distance between the sound and the receiver. R_2 is the distance between the location of the sound source image below the ground and the location of the receiver. r is the distance between the sound source and the receiver in the *x* direction. z_s and z_r are the indicated in the figure 2-4.

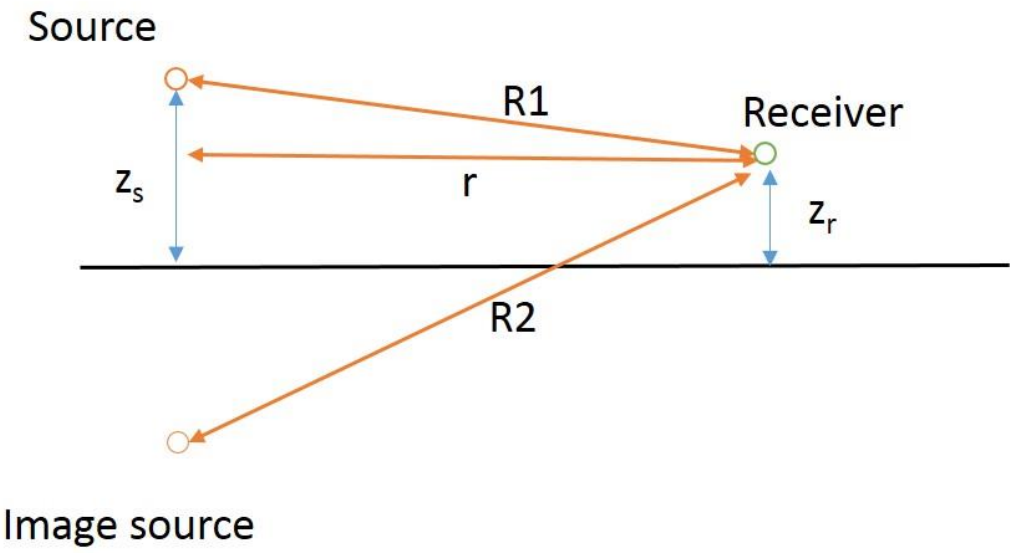

Figure 2-4. Geometry of the problem.

Li and Liu (Li & Liu, 2011) suggested that the sound fields above a porous ground due to a point source can be expressed as

$$p^{(m)}\left(r,z_s,z\right)=\frac{e^{ikR_1}}{4\pi R_1}+\frac{e^{ikR_2}}{4\pi R_2}+p_a^{(m)} \quad . \tag{2.24}$$

In the 2D case, the function is similar

$$p^{(m)}\left(r,rs\right)=\frac{iH_0^{(1)}(kR_1)}{4}+\frac{iH_0^{(1)}(kR_2)}{4}+p_a^{(m)} \quad . \tag{2.25}$$

The diffraction term in the 3D case can be expressed as

$$p_a^{(m)}\left(r,r_s\right)=\frac{-ik}{4\pi}\int_C \frac{\zeta\sqrt{n^2-\sin^2\mu}\,\sin\mu G_0\left(\mu\right)\exp\left[ikf_a(\mu)\right]}{\cos\mu+\zeta\sqrt{n^2-\sin^2\mu}}\,d\mu \quad . \tag{2.26}$$

Based on Li and Liu’s work for a point source, the p_a for a corrent line source can be expressed as

$$p_a\left(\mathrm{r},\mathrm{r}_s\right)=\frac{-i}{2\pi}\int_C \frac{\chi^{(m)}\exp\left[ikf_a(\mu)\right]}{\cos\mu+\chi}\,d\mu\,, \tag{2.27}$$

where

$$f_a\left(\mu\right)=r\sin\mu+\left(z_s+\mathrm{z}\right)\cos\mu=R_2\cos\left(\mu-\theta\right) \quad . \tag{2.28}$$

In the Equation (2.28), ζ is the density ratio, n is the sound speed ratio between the above ground medium and the below ground medium. χ is the admittance of the ground surface, which is a function of μ . The variable m represents the type of the ground. The incident angle of the mirror wave is θ and the horizontal separation between the source and receiver is denoted by *r*. The integration path for the integration can be found in many textbooks. μ travels from $-\pi/2+i\infty$ to $-\pi/2$, then it goes to $\pi/2$ and to $\pi/2-i\infty$. The path does not cross any branch cuts here.

The integral could be evaluated with the directly numerical integration, however, the method is extremely time comsuming. To improve the speed of calculation, the steepest descent method is used. The method of steepest descent is known to be one of the fastest method to evaluate an integration along an infinitely long path in the complex plane. In order to perform the steepest descent method, we need to change the path of integration to the steepest descent path first. Also, the residue due to the singularity must be included into the result. The detailed analysis can be found in work of Li and Liu (Li & Liu, 2011).

The pole location can be solved by setting the denominator of the integrand to zero, and the solution can be solved with

$$\cos\mu_p = -\zeta\sqrt{\left(n^2-1\right)/\left(1-\zeta^2\right)} = -\chi_p \qquad (2.29)$$

and

$$\sin\mu_p = \sqrt{\left(1-\zeta^2 n^2\right)/\left(1-\zeta^2\right)} = +\sqrt{1-\chi_p^2}\ . \qquad (2.30)$$

A conformal mapping needs to be introduced, which can be expressed as

$$\frac{1}{2}W^2 = ikR_2[1-\cos(\mu-\theta)] \ . \tag{2.31}$$

The steepest descent path is found by setting the imaginary part of the Equation (2.31) to zero, which is the real axis in the W plane. Then, the diffraction term could be expressed as

$$p_a = P_{SDP} + H\{-\mathrm{Im}[i[1-\cos(\mu_p-\theta)]]\}\, p_p \ , \tag{2.32}$$

where p_p is the pole contribution which can be evaluated with the residue theorem. The expression of p_p is not given here because it will be cancel later. The term P_{SDP} can be expressed as

$$P_{SDP} = \frac{-i}{2\pi}\int_{C_\mu} \frac{\chi \exp\left[ikf_a(\mu)\right]}{\cos\mu+\chi}\, d\mu \ . \tag{2.33}$$

With Equation (2.31) and Equation (2.33) we can obtain

$$P_{SDP} = -\frac{i}{2\pi}e^{ikR_2}\int_{C_X} \frac{A(W)e^{-W^2/2}}{\cos\mu+\chi} dW \ , \tag{2.34}$$

where

$$A(W) = \chi / \sqrt{ikR_2 - W^2/4} \ . \tag{2.35}$$

The integral along the steepest descent path can be evaluated with an asymptotic expansion, but it does not work well if the pole is in the vicinity of the integration path, where the influence of pole brings a large oscillation near the pole location.

In order to evaluate the integration appropriately, we need to take advantage of the method of pole subtraction. The method introduces an additional term to the integral, which has the same limit as the singular term when the integration variable μ goes to the singular point. As a result, the singularity at the pole location will be canceled by the additional term, and at the same time, the additional term could be evaluated with the error function.

The integration term in the Equation (2.34) can be rearranged through pole subtraction method, which can be written as

$$\frac{P_{SDP}}{(-\frac{i}{2\pi})e^{ikR_2}} = A_p \int_{Cx} \frac{e^{-W^2/2} dW}{W - W_p} + \int_{Cx} [\frac{A}{\cos\mu + \chi} - \frac{A_p}{W - W_p}] e^{-W^2/2} dW \ , \tag{2.36}$$

where W_p is the location of the singularity in the W plane and A_p is chosen to eliminate the singularity at the pole location. To match the limit at the pole location, we need

$$A_p = \lim_{W \to W_p} A(W) = \frac{\chi_p}{E(\mu_p)\sin\mu_p} \tag{2.37}$$

For different types of ground, $E\mu_p$ has different expressions. Detailed solution for $E\mu_p$ can be found in Li's work. (Li & Liu, 2011)

Now P_{SDP} can be cast as a summation of the following two terms

$$P_{SDP} = p_s + \phi_s \ , \tag{2.37}$$

where

$$p_s = (-\frac{i}{2\pi})e^{ikR_2} A_p \int_{Cx} \frac{e^{-W^2/2} dW}{W - W_p} \ , \tag{2.38}$$

and

$$\phi_s = (P_{SDP} - p_s) \ . \tag{2.39}$$

At the same time, p_s can be computed with the complementary error function

$$P_s = P_{erfc} - H[-\mathrm{Im}(W_p)]p_p \ , \tag{2.40}$$

where

$$P_{erfc} = -\frac{\chi_p e^{-W_p^2/2} erfc(-iW_p / \sqrt{2})}{2E(\mu_p)\sin \mu_p} e^{ikR_2} \ . \tag{2.41}$$

This correction term can be evaluated with numerical methods. The expressions for the integrals in the W plane are

$$P_{SDP} = -\frac{i}{2\pi} e^{ikR_2} \int_{Cx} \frac{\chi e^{-W^2/2}}{(\cos \mu + \chi)\sqrt{ikR_2 - W^2 / 4}} dW \tag{2.42}$$

and

$$\overline{P_{erfc}} = \frac{i}{2\pi} e^{ikR_2} \int_{Cx} \frac{\cos\mu_p}{(W-W_p)E(\mu_p)\sin\mu_p} e^{-W^2/2} dW \ . \tag{2.43}$$

In order to give the asymptotic solution with a physical meaning, we could express the solution for the sound pressure with an easy expression, which contains a direct wave term and a mirror wave term with an acoustic reflection coefficient Q. The solution can be expressed as

$$p \approx \frac{iH_0^{(1)}(kR_1)}{4} + Q\frac{iH_0^{(1)}(kR_2)}{4} \ , \tag{2.44}$$

where

$$Q = V_\theta + g_w \ . \tag{2.45}$$

The plane wave reflection coefficient is named as V_θ and the ground wave tern g_w is defined by

$$g_w \frac{iH_0^{(1)}(kR_2)}{4} = P_{erfc} - \overline{P}_{erfc} \tag{2.46}$$

and

$$g_w = \frac{2\beta_p}{E_p \sin\mu}\{(2[1-\cos(\mu_p-\theta)])^{-1/2} + i\sqrt{\pi}(ikR_2/2)^{1/2} e^{-w_a^2} erfc(-iw_a)\} \ . \tag{2.47}$$

In the next step, the ground wave term can be expressed as

$$g_w = \frac{\beta_p}{E_p \sin\mu} \frac{F(w_a)}{\sqrt{1-\cos(\mu_p-\theta)}} = \frac{\sqrt{2ikR_2}\,\beta_p F(w_a)}{E_p w_a \sin\mu} \ . \tag{2.48}$$

The g_w can also be written as

$$g_w = A(1-V_\theta)F(w_a) \ , \tag{2.49}$$

where

$$A = \frac{r_\beta / r_w}{E_p \sin\mu_p} \ , \tag{2.50}$$

which is a diffraction factor.

Now, the total sound field can be written as

$$p \approx \frac{iH_0^{(1)}(kR_1)}{4} + [V_\theta + A(1-V_\theta)F(w_a)]\frac{iH_0^{(1)}(kR_2)}{4} \ . \tag{2.51}$$

It might be interesting to mention that, the asymptotic solution of ground wave g_w in the 2D case is more accurate than that in the 3D case when the range is small. The results are compared with the three dimensional solutions for the Green's function by Li. We can see in the Figure 2-5 that, there is a singularity when the horizontal distance is very close to 0 for the three dimensional Green's function.

The singularity in the 3D case is originated from the hankel function term, however, the integral for the two dimentional Green's function has no hankel function term in the integrand. This comparison could be seen from the Figure 2-5 and Figure 2-6. The values of the diffraction term are compared for different types of ground surface at different frequencies.

There is no singularity in the two dimensional case, however, we can observe in the figure 2-6 that a disagreement between the asymptotic solution and the exact solution appears when the range is smaller than 0.1 m. However, the error gradually becomes a constant as the range decreases. Poor agreement in this region is inevitable, but the error can usually be satisfactory in practical applications because the value of the direct wave term is far larger than the value of the diffraction term when the horizontal range is close to zero. We can also conclude that the value of the diffraction term is important only when the distance between the sound source and the receiver is large.

It may be important to point out that the aysmptotic results in Figure 2-5 and Figure 2-6 are calculated with the Gaussian quadrature with one term. The fast solutions calculated with 20 Gaussian quadrature terms are shown in Figure 2-7 and Figure 2-8, where the agreement is excellent for any geometries.

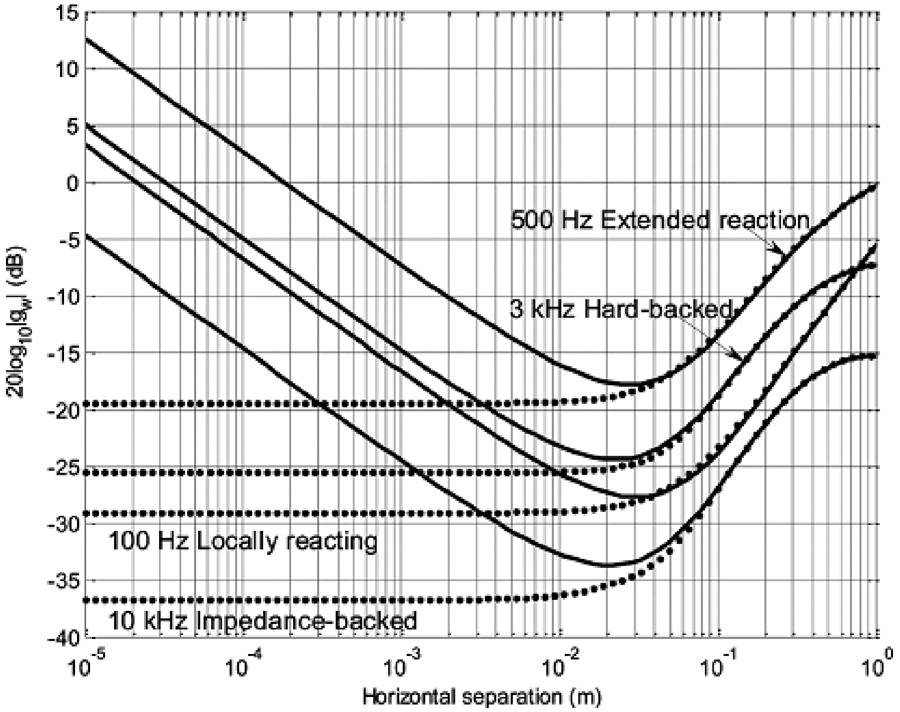

Figure 2-5. The ground wave term above the ground due to an above ground point source (Li and Tao, 2014). Dotted: asymptotic solution; Solid: exact solution.

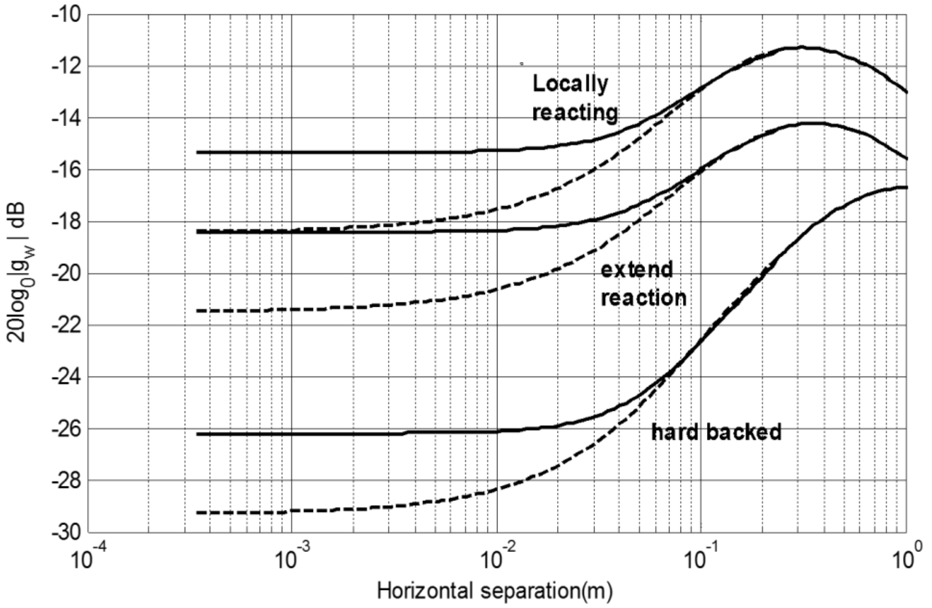

Figure 2-6. The ground wave term above the ground due to a coherent line source. Dotted: asymptotic solution; Solid: exact solution.

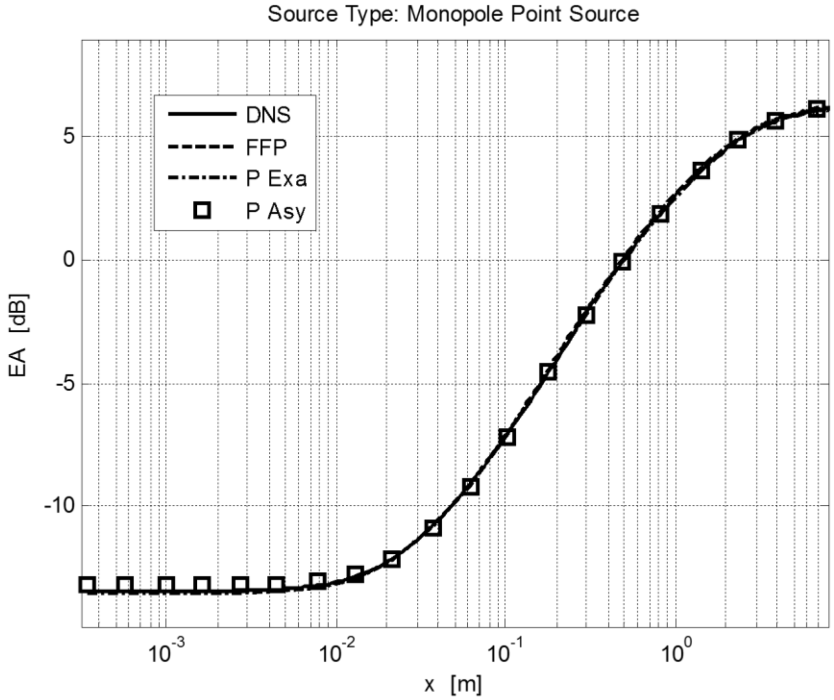

Figure 2-7. The predicted excess attenuation of the diffraction term along a horizontal line above a locally reacting ground surface. Source frequency is 1 kHz. The source is placed at 0.02m and the receiver at 0.04m above the ground. Solid line: DNS method. Dashed line: FFP method. Dashed dotted line: Exact solution (EXA). Square mark: asymptotic solution.

The exact solutions of the diffraction term calculated with Gaussian quadrature with 20 terms and the asymptotic solutions agree well with DNS method and the FFP method solutions. A comparison of the excess attenuation for the Green's function with different frequencies is shown in the Figure 2-8. The agreement between the fast asymptotic solutions and the accurate solutions is excellent.

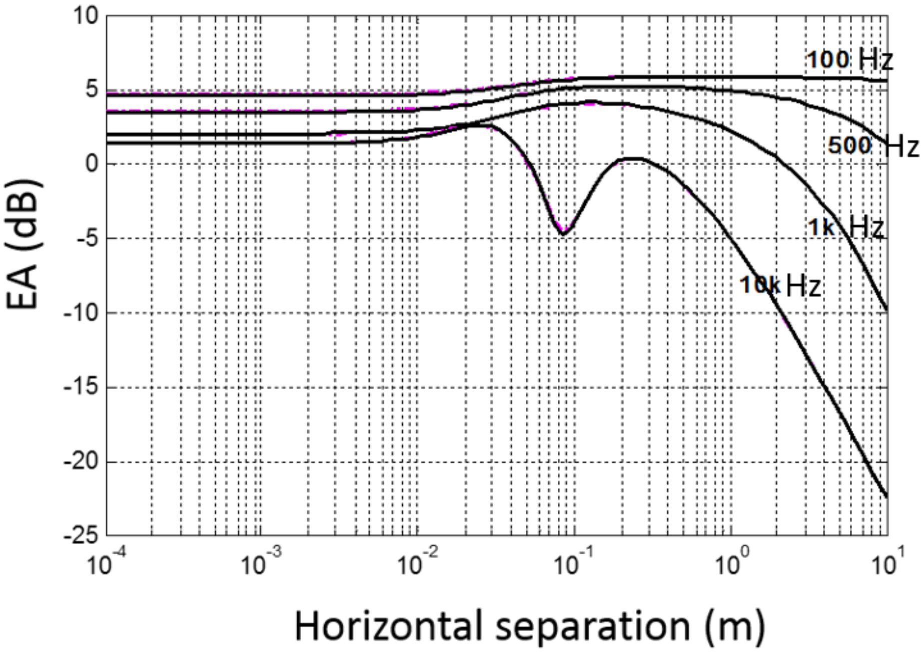

Figure 2-8. The predicted excess attenuation of the green function (G/Gf, where Gf is the free field green function) versus horizontal separation above a hard backed extend reaction ground for 100 Hz, 500 Hz, 1k Hz and 10k Hz. The same geometrical configuration as Fig 2-7 is used.

Horizontal directional derivative is also required in the BEM formulation. A similar method is used to find the solution for the horizontal directional derivative. Also, the solution for a vertical dipole will be discussed.

The path of the integration is changed to the steepest descent path, which is the same as the path in the last section. The equation for the horizontal directional derivative is

$$\begin{aligned}\partial_r p_a^{(m)} &= \frac{k}{2\pi}\int_{C_\mu} \frac{\zeta N(\mu)\sin\mu e^{ikR_2\cos(\mu-\theta)}}{\cos\mu+\zeta N(\mu)}\,d\mu \\ &+H\left[-\mathrm{Im}\left\{i\left[1-\cos(\mu_p-\theta)\right]\right\}\right]P_p\end{aligned} \quad . \tag{2.52}$$

After mapping to the *W* space as in the last section

$$P_{SDP} = \frac{k}{2\pi}\int_{C_\mu} \frac{\zeta N(\mu)\sin\mu e^{ikR_2\cos(\mu-\theta)}}{\cos\mu+\zeta N(\mu)}\,d\mu = \frac{k}{2\pi}e^{ikR_2}\int_C \frac{A(W)e^{-W^2/2}}{\cos\mu+\chi}dW \ , \tag{2.53}$$

where

$$A(W) = \chi\sin\mu \,/\, \sqrt{ikR_2 - W^2/4} \ . \tag{2.54}$$

Using the same pole subtraction method, we can get

$$\frac{P_{SDP}}{(\frac{k}{2\pi})e^{ikR_2}} = A_p\int_C \frac{e^{-W^2/2}dW}{W-W_p} + \int_C [\frac{A}{\cos\mu+\chi} - \frac{A_p}{W-W_p}]e^{-W^2/2}dW \ , \tag{2.55}$$

where

$$A_p = \lim_{W\to W_p} A(W) = \frac{\chi_p}{E(\mu_p)} \ . \tag{2.56}$$

Now P_{SDP} can be written as

$$P_{SDP} = p_s + \phi_s \ , \tag{2.57}$$

where

$$p_s = (-\frac{i}{2\pi})e^{ikR_2} A_p \int_{Cx} \frac{e^{-W^2/2} dW}{W - W_p} \tag{2.58}$$

and

$$\phi_s = (P_{SDP} - p_s) \ . \tag{2.59}$$

Evaluating p_s with the similar complementary error function

$$P_s = P_{erfc} - H[-\mathrm{Im}(W_p)]p_p \ , \tag{2.60}$$

where

$$P_{erfc} = -\frac{ik\chi_p e^{-W_p^2/2} erfc(-iW_p/\sqrt{2})}{2E(\mu_p)} e^{ikR_2} \ . \tag{2.61}$$

The correction terms are

$$P_{SDP} = \frac{k}{2\pi} e^{ikR_2} \int_C \frac{\chi \sin \mu e^{-W^2/2}}{(\cos\mu + \chi)\sqrt{ikR_2 - W^2/4}} dW \tag{2.62}$$

and

$$P_{SDP} = \frac{k}{2\pi} e^{ikR_2} \int_C \frac{\chi \sin \mu e^{-W^2/2}}{(\cos\mu + \chi)\sqrt{ikR_2 - W^2/4}} dW \ . \tag{2.63}$$

The horizontal directional derivative is derived similarly. The path of the integration is changed to the steepest descent path, the derivative can be written as

$$\begin{aligned}\partial_r p_a^{(m)} &= \frac{k}{2\pi}\int_{C_\mu} \frac{\zeta N(\mu)\cos\mu e^{ikR_2\cos(\mu-\theta)}}{\cos\mu+\zeta N(\mu)}d\mu \\ &+H\left[-\operatorname{Im}\left\{i\left[1-\cos(\mu_p-\theta)\right]\right\}\right]P_p\end{aligned} \quad . \tag{2.64}$$

After mapping to the W plane

$$P_{SDP} = \frac{k}{2\pi}\int_{C_\mu}\frac{\zeta N(\mu)\cos\mu e^{ikR_2\cos(\mu-\theta)}}{\cos\mu+\zeta N(\mu)}d\mu = \frac{k}{2\pi}e^{ikR_2}\int_C \frac{A(W)e^{-W^2/2}}{\cos\mu+\chi}dW \quad , \tag{2.65}$$

where

$$A(W) = \chi\cos\mu / \sqrt{ikR_2 - W^2/4} \quad . \tag{2.66}$$

Using the pole subtraction method, we can get

$$\frac{P_{SDP}}{(\frac{k}{2\pi})e^{ikR_2}} = A_p\int_C \frac{e^{-W^2/2}dW}{W-W_p} + \int_C [\frac{A}{\cos\mu+\chi} - \frac{A_p}{W-W_p}]e^{-W^2/2}dW \quad , \tag{2.67}$$

where

$$A_p = \lim_{W\to W_p} A(W) = \frac{\chi_p}{E(\mu_p)}\cot(\mu_p) \quad . \tag{2.68}$$

P_{SDP} can be expressed as

$$P_{SDP} = p_s + \phi_s \ , \tag{2.69}$$

where

$$p_s = (-\frac{i}{2\pi})e^{ikR_2} A_p \int_{Cx} \frac{e^{-W^2/2}dW}{W - W_p} \tag{2.70}$$

and

$$\phi_s = (P_{SDP} - p_s) \ . \tag{2.71}$$

Also,

$$P_s = P_{erfc} - H[-\mathrm{Im}(W_p)]p_p \ , \tag{2.72}$$

where

$$P_{erfc} = -\frac{ik\chi_p e^{-W_p^2/2} erfc(-iW_p/\sqrt{2})}{2E(\mu_p)} \cot(\mu_p) e^{ikR_2} \ . \tag{2.73}$$

The correction term is the sum of

$$P_{SDP} = \frac{k}{2\pi} e^{ikR_2} \int_C \frac{\chi \cos \mu e^{-W^2/2}}{(\cos\mu + \chi)\sqrt{ikR_2 - W^2/4}} dW \tag{2.74}$$

and

$$\overline{P}_{erfc} = -\frac{k}{2\pi} e^{ikR_2} \int_C \frac{\cos\mu_p \cot(\mu_p)}{(W - W_p)E(\mu_p)} e^{-W^2/2} dW \tag{2.75}$$

The fast solutions for the Green’s functions of the first type are derived in the section 2.3. In the next chapter, the solutions are implemented into the BEM formulation to solve the sound scattering problems.

CHAPTER 3. BEM RESULTS FOR ABOVE GROUND SCATTERING

There are several different empirical and analytical methods for predicting the sound field due to a scattering object positioned above a ground surface. The first method is based on ray theory, which expresses the sound field in terms of the Fresnel integrals. Later, methods which introduced the effects of reflection due to an impedance ground were considered. The predictions based on these methods were shown to be accurate based on experimental evidence. However, the shapes of the barriers were required to be thin to obtain good agreement.

With the development of digital computers, the scattering of sound from noise barriers above the ground can be computed effectively. The shape of the barrier can be arbitrary in the BEM approach, and the reflection from the ground can be incorporated using the relevant Green's function. A major disadvantage of the BEM is that computational times can be substantial when the frequency is high and/or the scattering surface is complicated.

Even with a vast number of studies on the problems mentioned above, the sound field predictions above a non-locally reacting porous ground have not yet been satisfactorily completed. The Green's function above a porous ground are usually difficult to obtain due to the non-locally reacting boundary condition.

A fast solution for the Green's function for the above ground cases were derived in Chapter 2 via the steepest descent method. The proposed method is more efficient than the direct numerical integration approaches or the FFP. Results obtained from the proposed BEM implementation are first compared against the standard BEM approach from the previous studies. Next, experimental validation is conducted and shown in this chapter.

3.1 Numerical Implementation

The geometry for the above ground propagation condition is shown in the Figure 3-1.

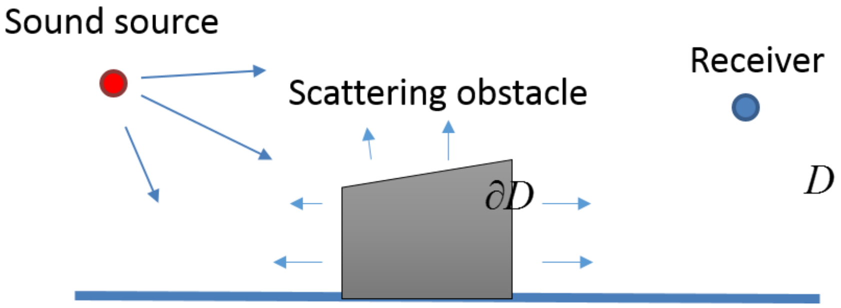

Figure 3-1. Problem geometry for an above ground noise barrier. The receiver location of interest are those positioned behind the barrier.

In the figure 3-1, r_s denotes the location of the monopole point source, r denotes the location of the receiver. An obstacle is placed above the ground and the ground is assumed to be either: semi-infinite and locally/non-locally reacting, or finite thickness with a hard/impedance backed termination boundary condition.

The BIE on the surface of the obstacle can be expressed as:

$$\varepsilon\, p(r,r_s) = G(r_s,r) + \int_{\partial D} [G(r_0,r)\frac{\partial p}{\partial n}(r_0,r_s) - p(r_0,r_s)\frac{\partial G}{\partial n}(r_0,r)]ds(r_0)\ , \tag{3.1}$$

which can be simplified into:

$$\varepsilon Ax = B + \sum_{n=1}^{N} Cx\ . \tag{3.2}$$

The mesh has *N* elements and *N*+1 nodes. Colocation points in the BEM are chosen as the midpoints between two adjacent nodes. We can see that there are *N*+1 unknowns but only *N* constraints. In the current problem, the sound pressure for the N^{th} and *N*+1 nodes are assumed to be the same. This serves as the last constraint.

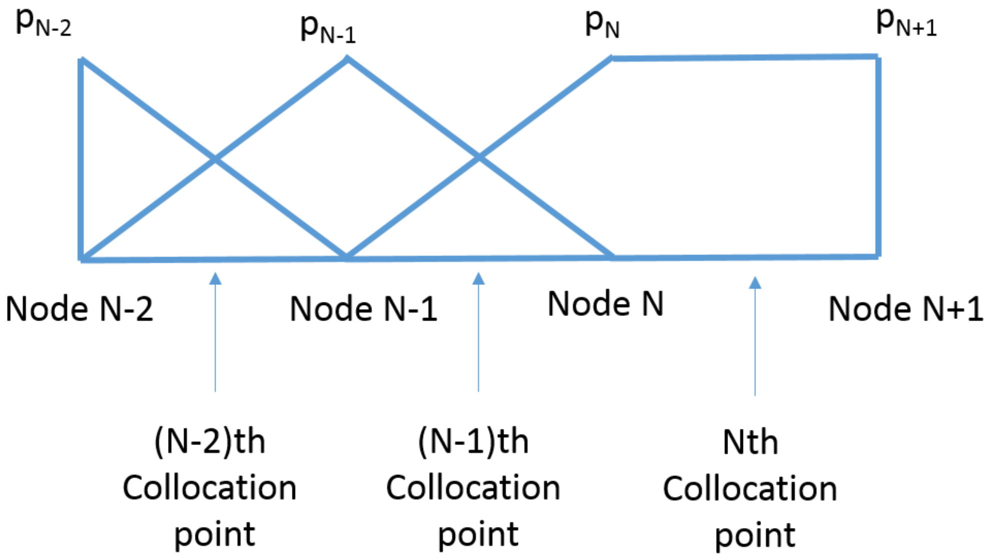

Figure 3-2. The structure of the mesh.

$x = x_1, x_2, x_3 \ldots x_m \ldots x_N$, $r_s = (x_s, z_s)$ denotes the source position and $r = (x,z)$ denotes the receiver position. Let $p(r,r_s)$ denote the acoustic pressure at r due to the monopole source at r_s, and let ∂D denote the barrier's surface. When $\varepsilon = 1$, the receiver lies in the propagating medium. If $\varepsilon = \frac{1}{2}$, the receiver lies on the barrier's surface. If the receiver is at a corner point, $\varepsilon = \frac{\Omega}{2\pi}$, where Ω is the angle potion in the propagation medium. And $G(r_s, r)$ is the Green's function we derived previously. The $\frac{\partial}{\partial n}(r_0, r)$ term denotes the partial derivative in the normal direction of ∂D.

In the current study, the functions on the discretized elements are approximated via the Galerkin method:

$$\bar{G}_n(\xi) = (1-\xi)G_n + \xi G_{n+1}\,, \tag{3.3}$$

$$\bar{\beta}_n(\xi) = (1-\xi)\beta_n + \xi\beta_{n+1} \tag{3.4}$$

and

$$\bar{p}_n(\xi) = (1-\xi)p_n + \xi p_{n+1} \tag{3.5}$$

are the shape function for the three functions.

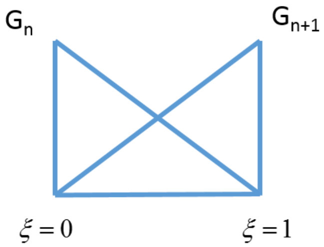

Figure 3-3. The first order shape function for the pressure in one element.

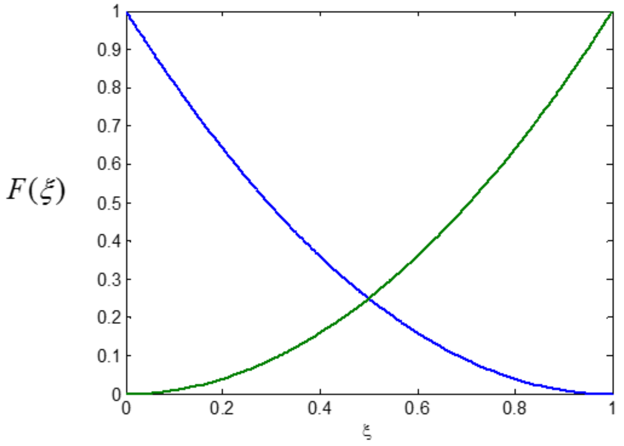

Figure 3-4. The shape of the function in one element.

where $G_n = G(\mathrm{r}_0(\mathrm{n}),\mathrm{r})$, which is the value of the function $G(\mathrm{r}_0(\mathrm{n}),\mathrm{r})$ at the n^{th} node in the mesh. G_{n+1} is the value of $G(\mathrm{r}_0(\mathrm{n}),\mathrm{r})$ at the (n+1) th node of the mesh. $\bar{G}_n(\xi)$ is the shape function of $G(\mathrm{r}_0(\xi),r)$ on the n^{th} element of the mesh. In every element, every function with location variables, G, β, and p are approximated with the same shape function. The variable r is mapped to ξ. Since the transformation is one dimensional, the Jacobian matrix for the mapping is

$$J_n = [\mathrm{h}_n] \tag{3.6}$$

where h_n is the length of the n^{th} element. Curves are approximated by straight lines.

In many previous studies, the value of the functions on the elements are assumed to be constant in each element. The necessary number of the elements to obtain a good approximation is much smaller following our proposed approached. Gaussian quadrature integration method can be more effective when the lengths of elements are different. This may yield increased accuracy for the same number of function evaluations. However, the advantage of Gaussian quadrature methods is not obvious for the problems under consideration.

The numerical equations can be expressed as:

$$\varepsilon p(r(\mathrm{m}+\frac{1}{2}), r_s) = G(r_s, r(\mathrm{m}+\frac{1}{2}))$$
$$+\sum_{n=1}^{N} \Delta h[G(\mathrm{r}_0(\mathrm{n}), \mathrm{r}(\mathrm{m}+\frac{1}{2}))(-ik\beta(r_0(\mathrm{n}))\,p(\mathrm{r}_0(\mathrm{n}), \mathrm{r}_s)) - \mathrm{p}(\mathrm{r}_0(\mathrm{n}), \mathrm{r}_s)\,\frac{\partial G(\mathrm{r}_0(\mathrm{n}), \mathrm{r}(\mathrm{m}+\frac{1}{2}))}{\partial n(\mathrm{r}_0(\mathrm{n}))}]. \tag{3.7}$$

The [B] matrix contains values for the direct wave at the colocation points:

$$B = \begin{bmatrix} G(\mathrm{r}_s, r(1+1/2)) \\ G(\mathrm{r}_s, r(2+1/2)) \\ \ldots \\ G(\mathrm{r}_s, r(N+1/2)) \end{bmatrix}. \tag{3.8}$$

The [A] matrix is a mapping matrix which connects the nodes and the colocation points:

$$A = \begin{bmatrix} \frac{1}{2} & \frac{1}{2} & 0 & \ldots & 0 \\ 0 & \frac{1}{2} & \frac{1}{2} & \ldots & 0 \\ 0 & 0 & \ldots & \ldots & 0 \\ . & . & . & & \\ . & . & . & \frac{1}{2} & \frac{1}{2} \\ . & . & . & & \\ 0 & 0 & 0 & 0 & 1 \end{bmatrix} \tag{3.9}$$

The left hand side of Equation (3.2) can be expressed as:

$$\varepsilon Ax = \epsilon \begin{bmatrix} \frac{1}{2} & \frac{1}{2} & 0 & \dots & 0 \\ 0 & \frac{1}{2} & \frac{1}{2} & \dots & 0 \\ 0 & 0 & \dots & \dots & 0 \\ . & . & . & & \\ . & . & . & \frac{1}{2} & \frac{1}{2} \\ . & . & . & & \\ 0 & 0 & 0 & 0 & 1 \end{bmatrix} \begin{bmatrix} p_1 \\ p_2 \\ p_3 \\ . \\ p_N \end{bmatrix} . \qquad (3.10)$$

The last value in [*A*] is unity because the pressure at the N^{th} node and at the *N*+1 node are assumed to be the same in the current numerical formulation. As a result, we need the N^{th} node and the *N*+1 node to be far enough from the sound source, so that the error from the two points are negligible.

In the [*C*] matrix,

$$C_m \begin{bmatrix} p_1 \\ p_2 \\ \dots \\ p_N \\ p_{N+1} \end{bmatrix} = (\begin{bmatrix} b_{m1} & b_{m2} & \dots & b_{mn} & 0 \end{bmatrix} + \begin{bmatrix} 0 & c_{m1} & \dots & c_{m(n-1)} & c_{mn} \end{bmatrix}) \begin{bmatrix} p_1 \\ p_2 \\ \dots \\ p_N \\ p_{N+1} \end{bmatrix}, \qquad (3.10)$$

where C_m is the m^{th} row of [*C*] and

$$\begin{aligned} b_{mn} = h_n\{ & \frac{1}{3}[\frac{\partial G(\mathrm{r_0(n), r(m+\frac{1}{2})})}{\partial n(\mathrm{r_0(n)})} - \mathrm{ik}\,\beta G(\mathrm{r_0(n), r(m+\frac{1}{2})})] \\ & + \frac{1}{6}[\frac{\partial G(\mathrm{r_0(n+1), r(m+\frac{1}{2})})}{\partial n(\mathrm{r_0(n+1)})} - \mathrm{ik}\,\beta G(\mathrm{r_0(n+1), r(m+\frac{1}{2})})]\} \end{aligned} \qquad (3.11)$$

$$
\begin{aligned}
c_{mn} = h_n\{\frac{1}{6}[\frac{\partial G(\mathrm{r}_0(\mathrm{n}),\mathrm{r}(\mathrm{m}+\frac{1}{2}))}{\partial n(\mathrm{r}_0(\mathrm{n}))} - \mathrm{ik}\,\beta G(\mathrm{r}_0(\mathrm{n}),\mathrm{r}(\mathrm{m}+\frac{1}{2})]\\
+\frac{1}{3}[\frac{\partial G(\mathrm{r}_0(\mathrm{n}+1),\mathrm{r}(\mathrm{m}+\frac{1}{2}))}{\partial n(\mathrm{r}_0(\mathrm{n}+1))} - \mathrm{ik}\,\beta G(\mathrm{r}_0(\mathrm{n}+1),\mathrm{r}(\mathrm{m}+\frac{1}{2})]\}
\end{aligned}
\tag{3.12}
$$

where h_n is the length of the n^{th} element. When the length of elements are the same, the formulas can be simplified.

Singularities appear when the two location variables are contained within the same element. Several methods have been developed to deal with this issue. For example, we can integrate the Green’s function using the short range approximation for the Hankel function and take advantage of the pole subtraction method as done by Berry to remove singularities. The method of modifying the integration described above can be applied for good measure. The infinite terms in the integration essentially annihilates, which may introduce a small error in the overall predictions. Nonetheless, the approach can provide an efficient and accurate solution compared to other alternatives.

3.2 Validation of BEM

3.2.1 Free Field Scattering

First, the BEM formulation is verified by comparing the simulation results to experimental results by Mir, Anthony, and Colin (Mir, Anthony and Colin, 2010).
The experiment is conducted in a 4.79m × 3.90m × 3.94m anechoic chamber. The scattering obstacle is a hard cylindrical PVC tube mounted on a turntable.

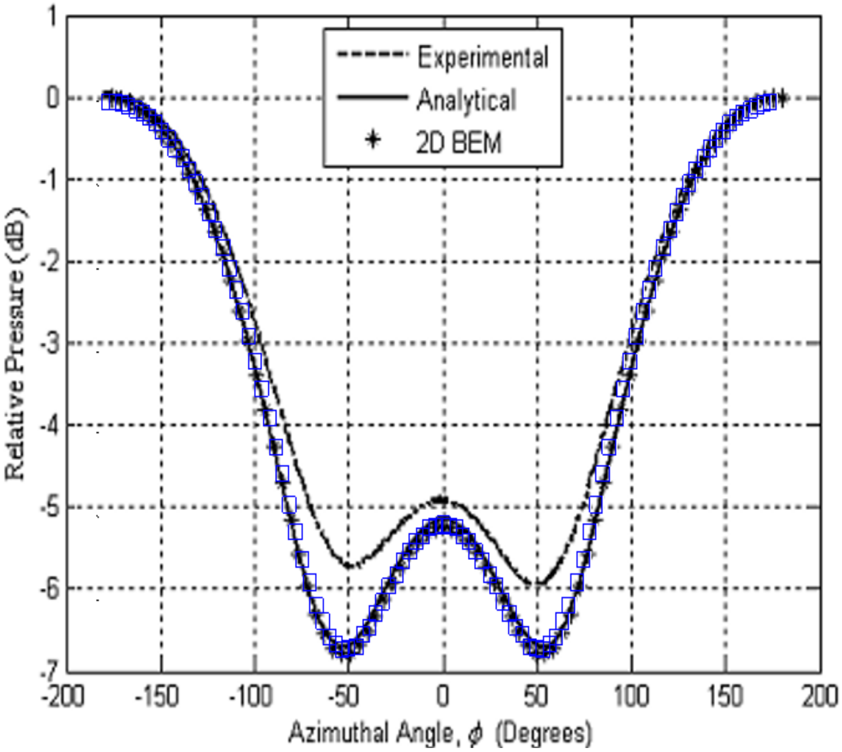

Figure 3-5. The frequency is 700 Hz. The squares are the results calculated with the BEM in the current thesis. Others are labeled in the figure.

The length of the cylinder is 1.446 m and the diameter is 0.114 m. A loudspeaker was placed 4.1m away from the cylinder. In order to eliminate the contribution from the ground reflection, the microphone was placed 1.13 m above the ground. The pressure on the surface of the cylinder is normalized to the maximum pressure to obtain a relative pressure. The results for 700 Hz and 3000 Hz are compared in Figures 2-5 and 3-6. In the BEM, the surface of the cylinder is discretized into elements. For different frequencies, the sizes of the elements are different. The results are calculated with Matlab. The Green’s function in the simulation is free field Green’s function.

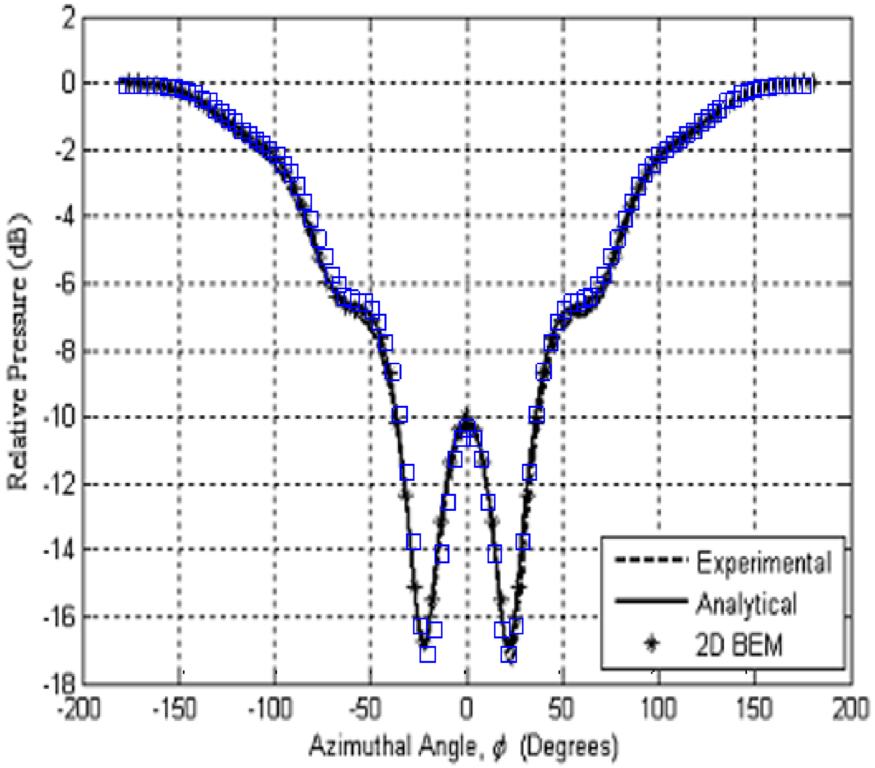

Figure 3-6. The frequency is 3000 Hz. The squares are the results calculated with the BEM in the current thesis. Relative Pressure $= 20\log_{10}(|p|/|\max(p)|)$.

We can see in the figures that the BEM results and the analytical results show excellent agreement with the experimental results at 3000 Hz. At low frequencies, the BEM and analytical predictions are in agreement. However, there is disagreement between the experimental result and the BEM at low frequencies, especially in the shadow zone behind the cylinder. The differences may be attributed to the reflections from the walls and the supporting platform the anechoic chamber. Contributions due to reflections can be significant when the wavelength of the sound is large (i.e., at low frequencies). The BEM formulation for the free field scattering problem by a cylinder has been validated.

3.2.2 Scattering Due to a Barrier Positioned Above a Locally Reacting Ground

Noise barriers are commonly used to reduce the transmission of sound and to deflect some of the acoustic energy away from shielded objects. There are many different methods for predicting the diffraction of sound by a rectangular barrier. In most empirical methods, the barriers need to be thin to obtain a decent approximation. The analytical prediction was first presented by Sommerfeld (Sommerfeld, 1896) and later extended by Carslaw (Carslaw, 1920) and MacDonald (MacDonald, 1915). The solutions are expressed as the summation of two different wave terms. The first term is the contribution from an incident wave and the other term is the contribution due to diffraction.

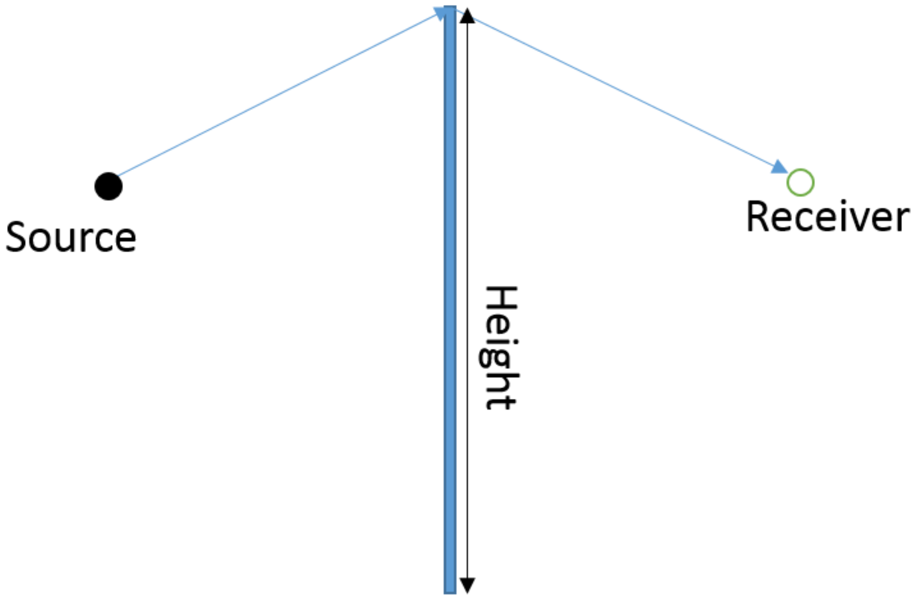

Figure 3-7. Thin barrier scattering geometry.

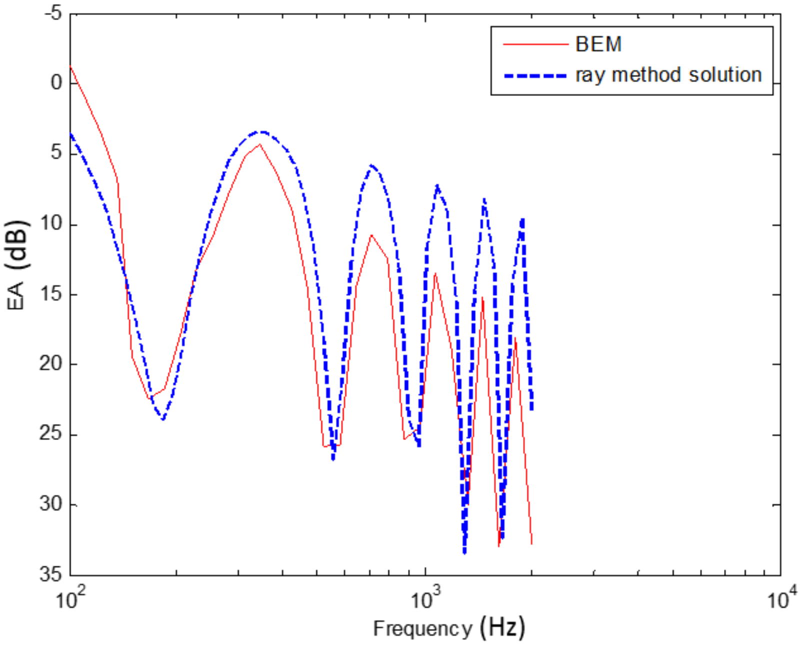

Figure 3-8. Comparison of ray model and BEM predictions for a noise barrier. Source: x=-0.5 m. y=0.5 m; Receiver: x=0.5 m, y=0.5 m. Barrier height=1.2 m.

A comparison is provided in Figure 3-8 for noise propagation through a thin barrier. Good agreement is achieved in predicting the locations of the interference dips. At low frequencies, the differences between the two methods are due to ground reflections. The relative differences in shape and amplitude may be due to ray model assumptions.

Figure 3-9 provides a comparison against the work completed by Hothersall *et al.* (Hothersall, Chandler-Wilde, and Hajmirzae, 1990). Excellent agreement is obtained, which helps establish the validity of our BEM implementation. Additional comparisons against experimental measurement shows good agreement as well.

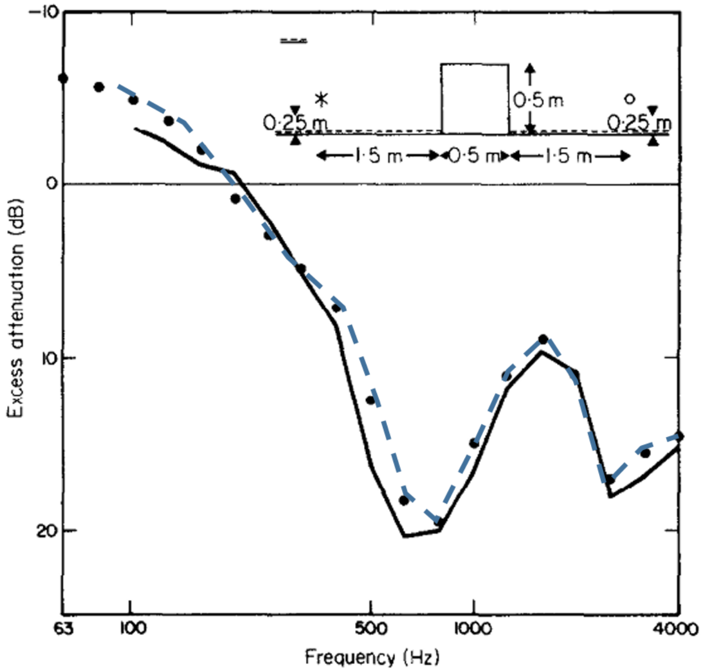

Figure 3-9. Experimental validation of the proposed BEM implementation against measurements made by Hothersall *et al.* (Hothersall, Chandler-Wilde, and Hajmirzae, 1990). Dashed line: our BEM results. Dotted line: Hothersall *et al.*'s BEM. Solid line: experimental data.

To further validate our BEM implementation, several additional measurements were conducted in Herrick Lab's anechoic chamber (with a working dimension of 3.5 m × 3.5 m × 3.5 m). The noise source is a CIE 30W tap loudspeaker, which is attached to a 1.0 m long brass tube with diameter of about 0.03 m. The configuration approximates a monopole source. The microphone in the experiment is a Bruel & Kjaer type 4189 pre-polarized 0.5 inch microphone. The rigid porous medium is represented by spherical glass beads which have diameters in the range of 0.3 mm to 0.4 mm. The barrier is 0.21 m high and 0.015 m thick plywood panel. In the simulations, the barrier is assumed to be rigid. The ground layer is treated as a porous medium.

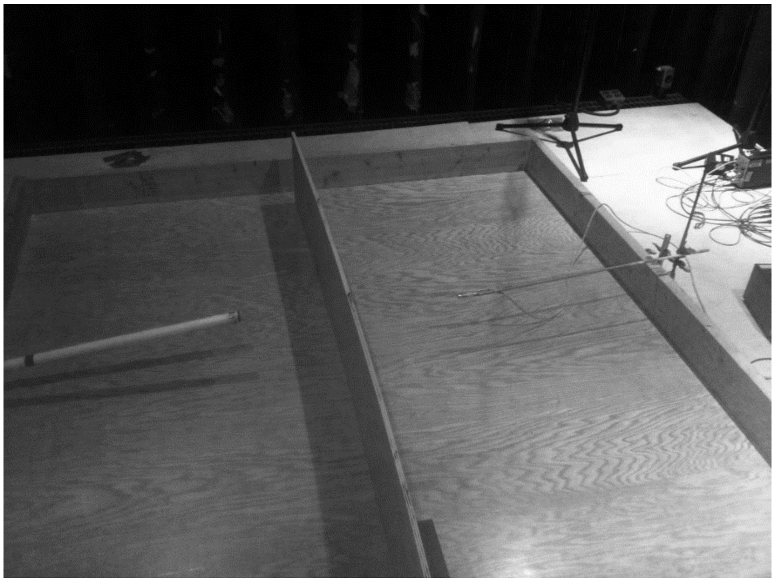

Figure 3-10. Experiment lay out.

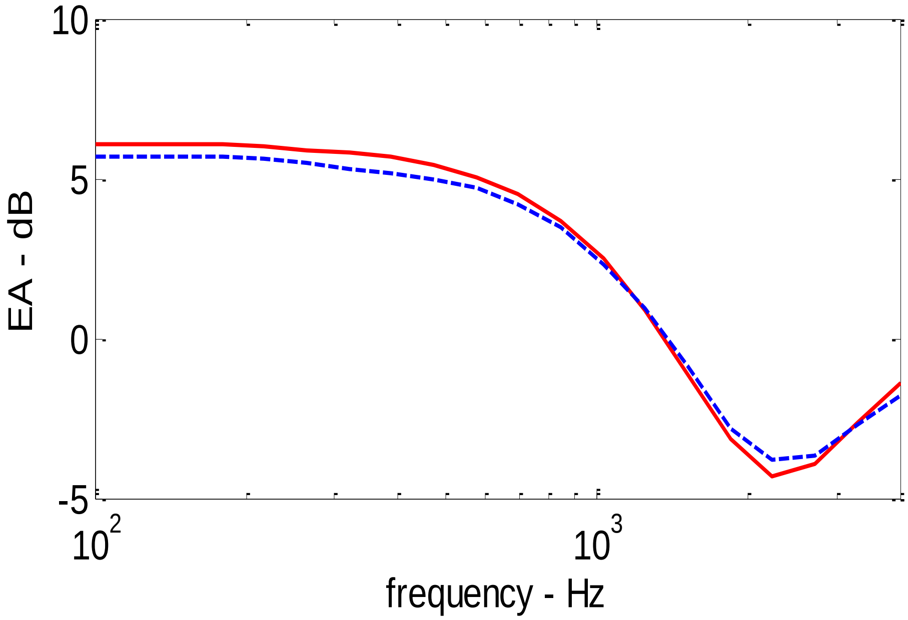

Figure 3-11. Source location: x=-0.54 m, z=13.5 m. Receiver location: x=0.37 m, z=0.178 m. Barrier height=0.21 m and width= 0.015 m. Ground properties: flow resistivity=140,000 Pa m s^{-2}, tortuosity=1.27, porosity=0.4, shape factor=0.8, layer thickness=0.012m. Solid line: BEM; dashed line: experimental result.

The wooden frame is filled with glass beads and modeled using Attenborough's 4 parameter ground impedance model. Excellent agreement is shown in Figure 3-11 between the BEM and experimental data. The measurements for a below ground source/receiver are not provided due to limitations on existing equipment capabilities.

Numerical studies are also considered using the validated BEM model. We can observe the effects of interference as shown in Figures 3-13 to 3-15. As the frequency increases, the wavelength will decrease. As a result, the distance between two adjacent interference maxima decreases. The noise level behind the noise barrier indicates that it is working as intended. It can be seen that the performance of the barrier is better at the higher frequency of 1,000 Hz. Sound diffraction and interference effects are clearly visible behind the barrier where one might expect there to be no sound penetration by intuition. The sound field prediction near the barrier surface is not very accurate since the prediction of the sound field near the scattering surface requires more elements. It is one difficulty of the boundary element method.

In the simulations, most of the acoustic energy is reflected backward by the ground and the barrier due to the rigid boundary assumption. The contribution due to underground obstacles cannot be observed. In more realistic situations, the ground has a finite impedance such that some of the incident sound can penetrate into the ground. This enables the possibility for acoustical detection of below ground objects.

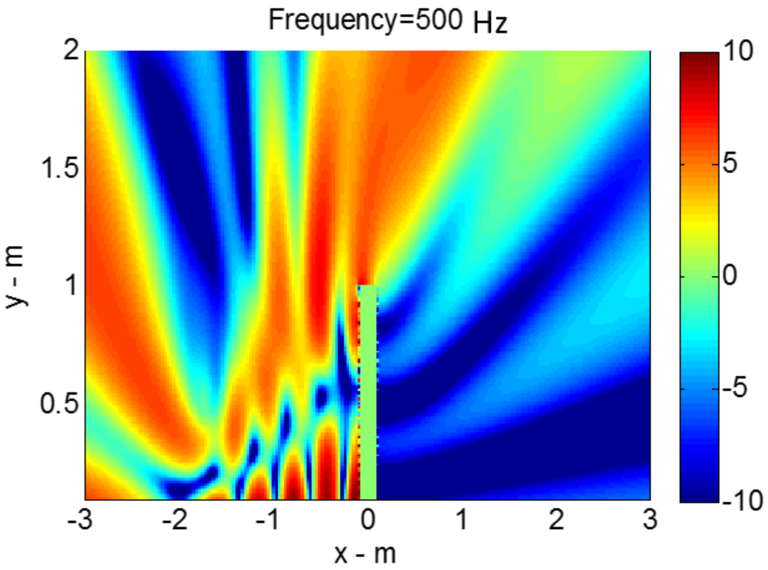

Figure 3-12. Source: location x=-1.75m, y=0.25m, frequency=500 Hz. Barrier height=0.5m. Ground properties: flow resistivity=140,000 Pa m s^{-2}, tortuosity=1.27, porosity=0.4, shape factor=0.8, and thickness=0.012m.

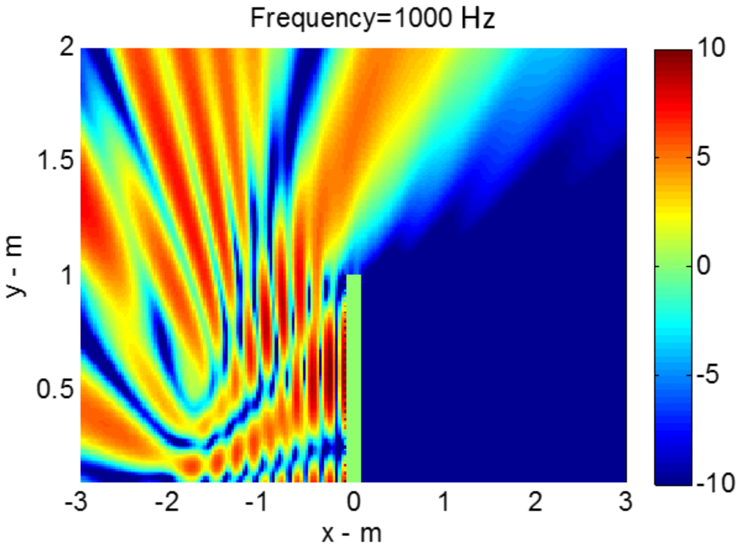

Figure 3-13. Same conditions as Figure 3-12 but for a frequency of 1,000 Hz.

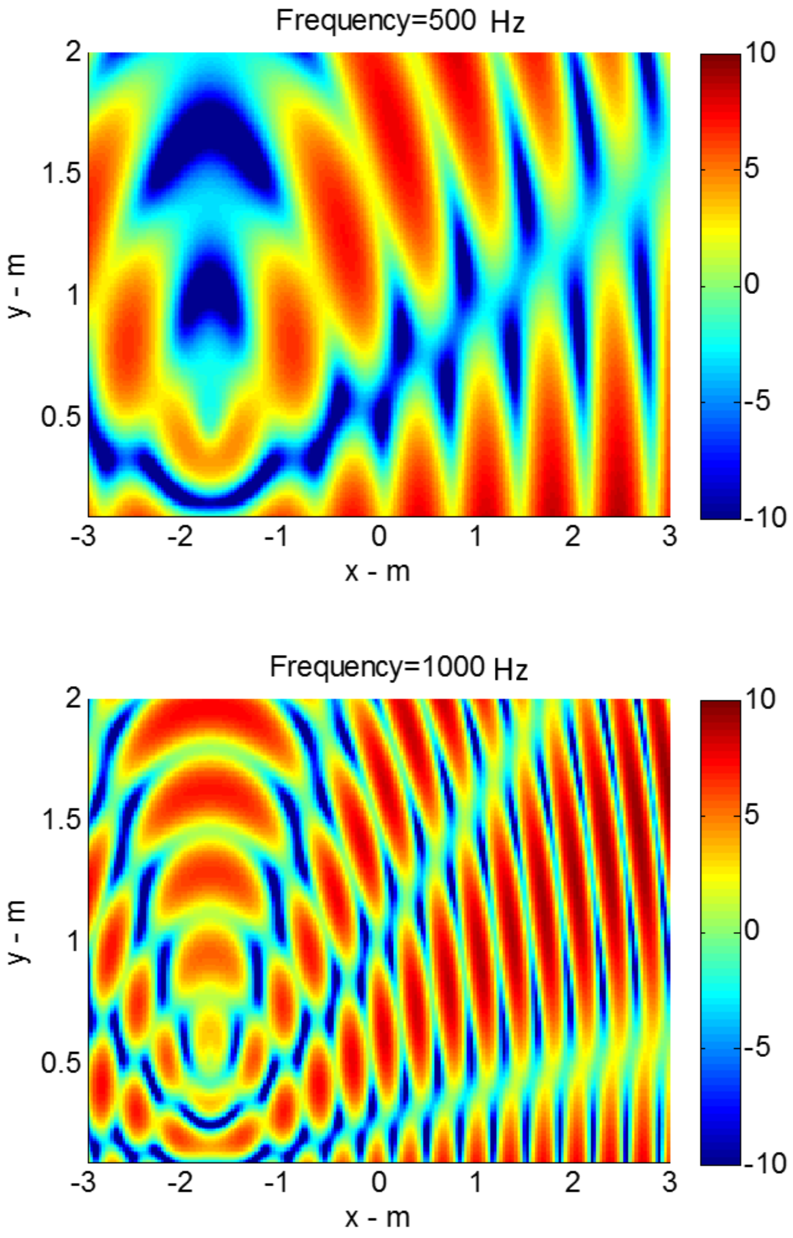

Figure 3-14. Sound field predictions in the absence of a noise barrier. Same conditions as before.

The empirical model can accurately predict the sound field for simple propagation geometries. However, the BEM provides a more general approach. Arbitrarily shaped noise barriers can be considered. In addition, the surface of the barrier can have impedance discontinuities (e.g., use multiple different materials). The primary disadvantage of the BEM is in the longer computational time. This is especially apparent when the barrier has a complicated shape and/or high frequencies are of interest.

3.2.3 Scattering by a Cylindrical Obstacle Located Above a Locally Reacting Ground

The study of sound scattering by spheres and cylinders are of great interest in the transportation noise community. Amplification by the horn-shaped structure formed between the tire/road surface is the primary mechanism for noise generation. Simulation results are compared with experiments data provided by Graf (Graf, 2001). A sphere with a diameter of 0.64 m is placed on the ground surface. A point source is located 0.72 m above the road surface and 2.57 m from the center of the sphere. The receiver is positioned on the center line of the sphere with a distance of d=130 mm. Only the low frequency results are computed due to computational limitations. Excellent agreement is achieved in the range of 100 Hz to 4000 Hz.

Another comparison is performed against the work by Wolfgang, Becot, and Barrelet (Wolfgang, 2000). The BEM predictions are as good as Wolfgang’s model as indicated in Figure 3-17. Note the large deviations at low frequencies while the high frequencies are in good agreement. The low frequency disparity may be attributed to wall reflections in the testing facility.

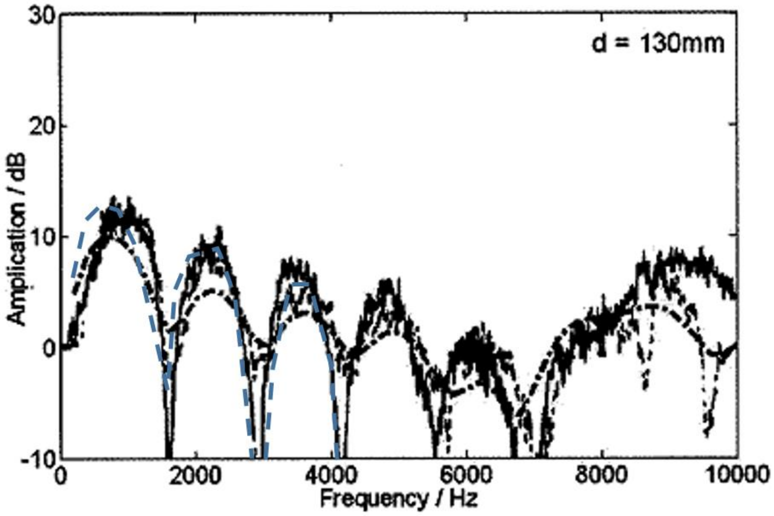

Figure 3-15. Validation of the BEM with the experiments results from Grap *et al.*for d=130mm. Colored line: BEM results.

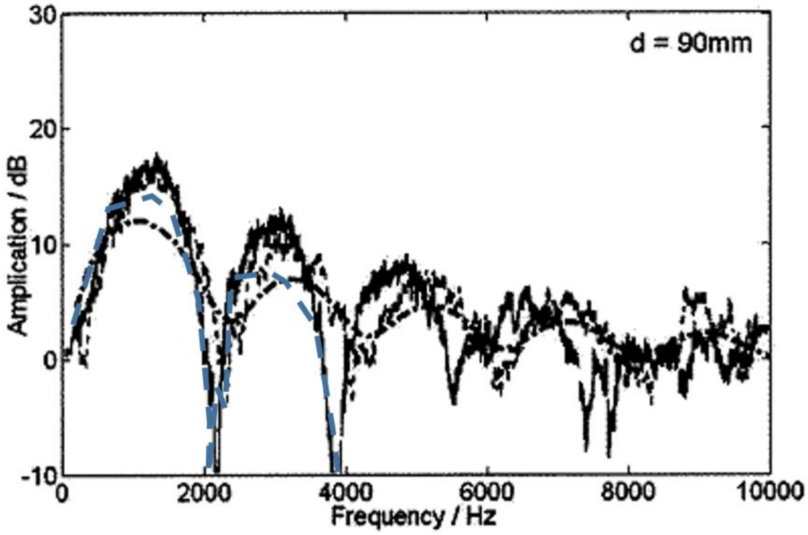

Figure 3-16. Validation of the BEM with the experiments results from Grap *et al.*for d=90mm. Colored line: BEM results.

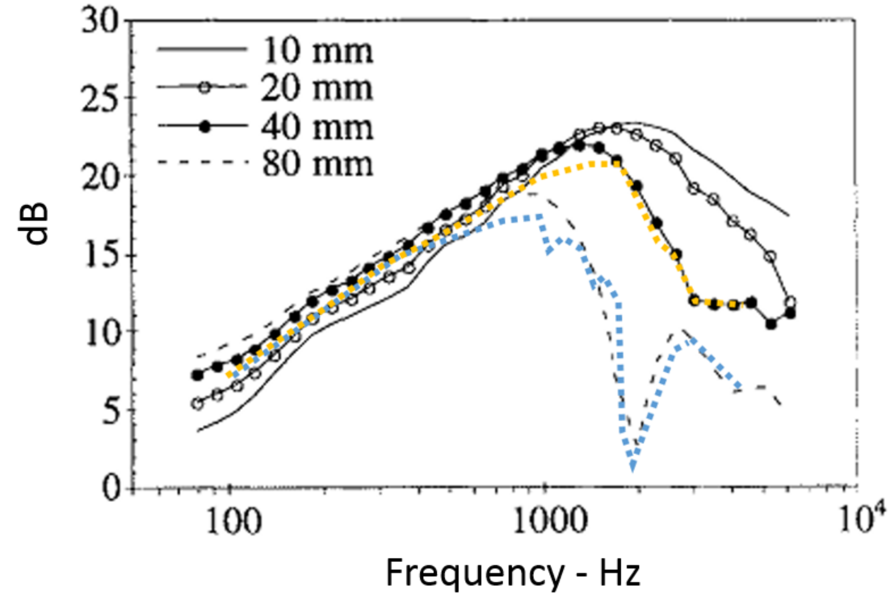

Figure 3-17. Validation against Wolfgang *et al.*'s model. Colored lines: BEM predictions.

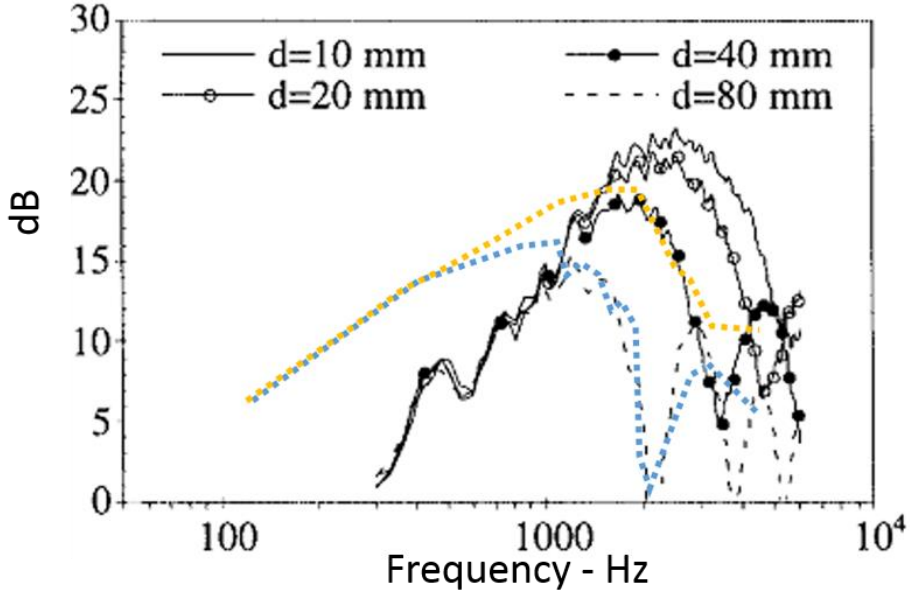

Figure 3-18. Validation against experimental data from Wolfgang *et al*. Colored lines: BEM predictions.

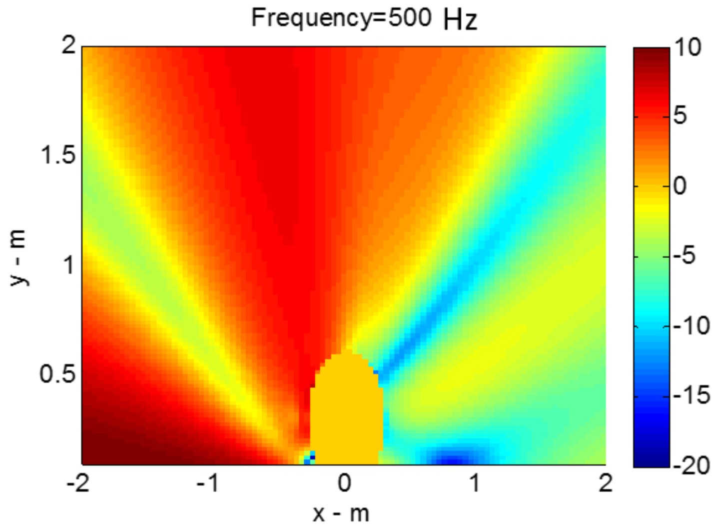

Figure 3-19. Sound field predictions for a cylindrical barrier positioned above a hard-backed ground surface. Ground properties: flow resistivity=140,000 Pa m s^{-2}, tortuosity=1.27, porosity=0.4, pore shape factor=0.8, and thickness=0.012m. Source location: x=-0.4 m, z=0.3 m. Cylinder radius=0.3 m.

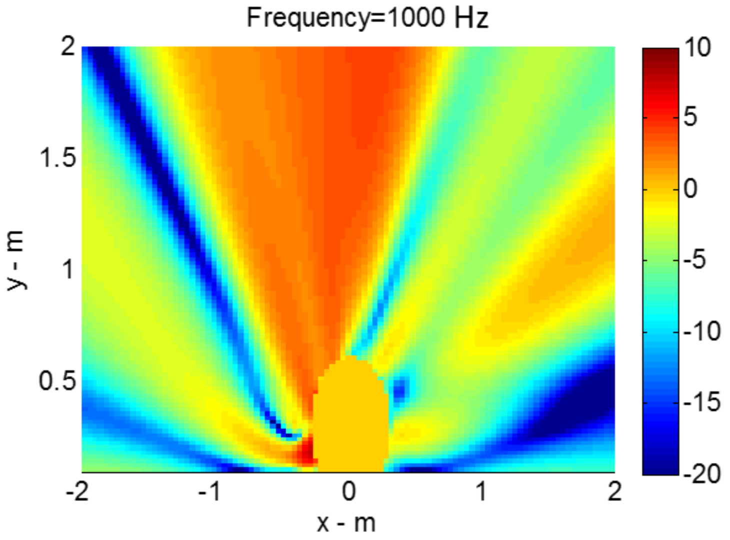

Figure 3-20. Same as Figure 3-19, but at a frequency of 1,000 Hz.

3.2.4 Mixed Ground Surfaces

Typical outdoor sound propagation problems contain multiple types of ground surfaces. For example, the noise generated by a factory may propagate over grassland, pavement, soil, and/or snow. These ground surfaces exhibit a range of acoustical properties. There are several analytical methods which deals with the two-impedance interface boundary condition such as those described by (De Jong, 1987), (Rasmussen, 1982), and (Hothersall and Harriott, 1995). These methods are based on ray theory, which separates the direct and reflected wave contributions. Although a locally reacting ground is different from the porous (non-locally reacting) ground, we can approximate a porous ground as an impedance surface by introducing an effective reflection coefficient. This approximation is valid only for some types of porous mediums and is widely used in semi-empirical models.

Although semi-empirical models are much faster than numerical methods (e.g., FEM and BEM), numerical methods provide greater flexibility and consistency in predicting realistic propagation configurations. A mixed impedance ground with an arbitrary number of impedance discontinuities can be incorporated into a BEM formulation. To validate the BEM, several case studies are performed.

General agreement between the experimental results and the BEM is acceptable as shown in the Figure 3-24. Again, low frequency deviations may be due to wall reflections or the limiting frequency of the anechoic chamber.

The sound field above the ground is shown in the figures 3-25 and 3-26. We can see the asymmetry caused by the impedance discontinuity. The region above the rigid ground has higher SPL than that of the porous ground. This indicates that some of the acoustic waves have been absorbed by the porous medium. The interference pattern depends on

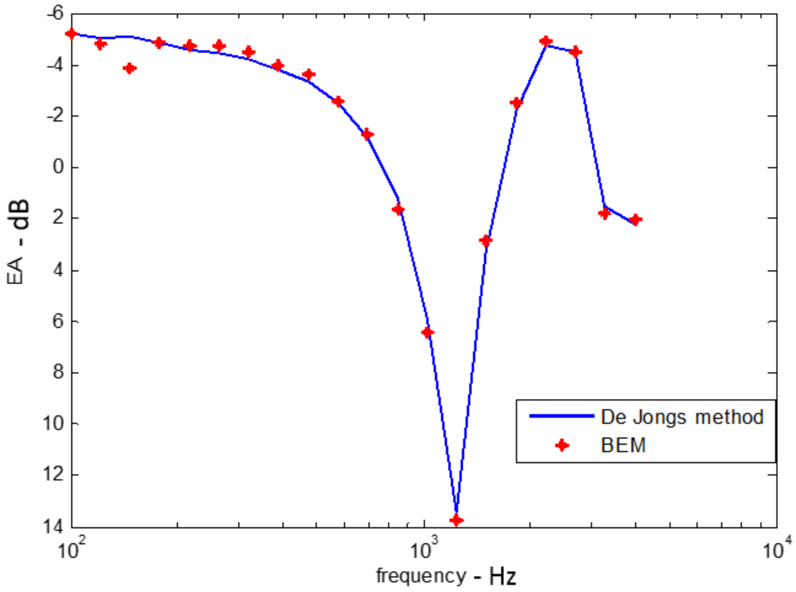

Figure 3-21. BEM result and the ray model result. Source1: x=0.2m y=0.25m; Receiver1: x=-0.15m y=0.25m; Receiver2: x=-0.1m y=0.4m; Right half ground is rigid; Left half is porous ground; Porous ground type same as previous ground type.

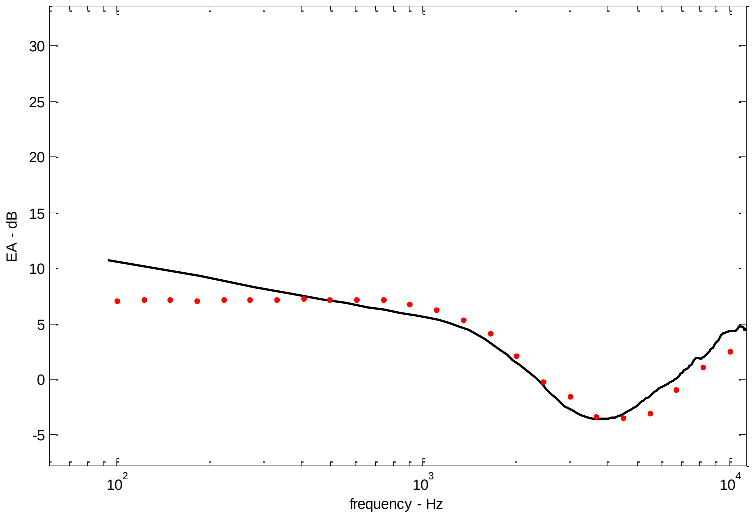

Figure 3-22. Solid line: experimental results; Dotted line: BEM result. Source: x=-0.41m y=0.077m; Receiver: x=38.5m y=0.102m; Left half ground is porous; Right half is a carpet with $\sigma = 110k$ N s m-4 and $\alpha = 850$; Porous ground type same as previous ground type.

the source frequency. The angle formed by the destructive interference region appears to be larger at higher frequencies.The BEM approach is preferable to the semi-analytical methods based on Fresnel diffraction theory since arbitrary impedance discontinuities can be accurately represented. Furthermore, the BEM can predict the sound field above a porous ground without any approximations regarding the boundary conditions. In the BEM formulation, the contribution from the below ground reflection is neglected. This assumption is valid when the flow resistivity is large or when the source is positioned above a locally reacting ground surface. In order to obtain a more general solution, a below ground BEM formulation needs to be developed. This topic is explored in the next chapter.

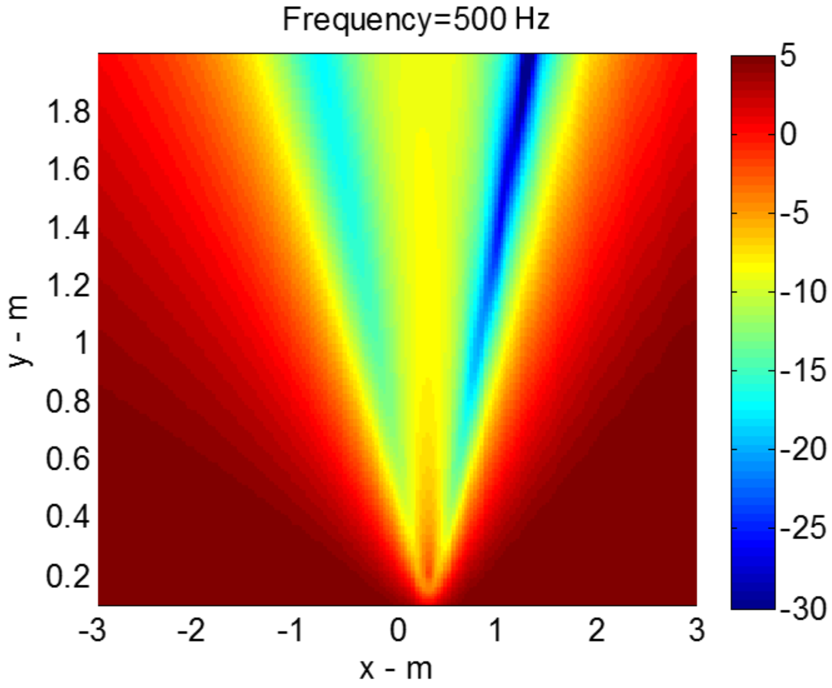

Figure 3-23. Source location: x=0.3m y=0.2m, barrier height=0.5m. Ground properties: flow resistivity=20,000 N s m-4, tortuosity=3.5, porosity=0.15, pore shape factor=1.0.

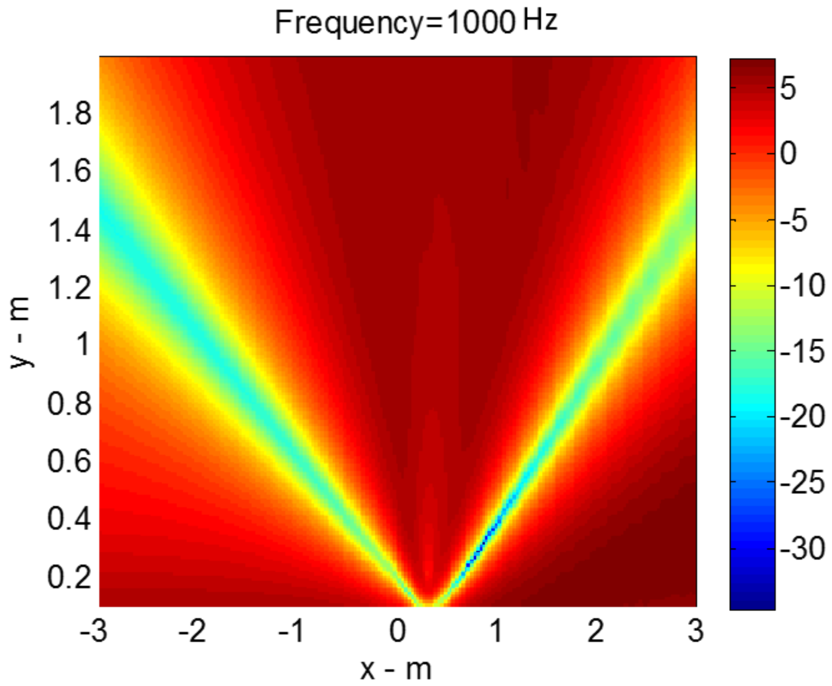

Figure 3-24. Same as Figure 3-23, but for a frequency of 1,000 Hz.

CHAPTER 4. THE BEM FOR THE UNDERGROUND SCATTERING

4.1 BEM Theory for Below Ground Scattering

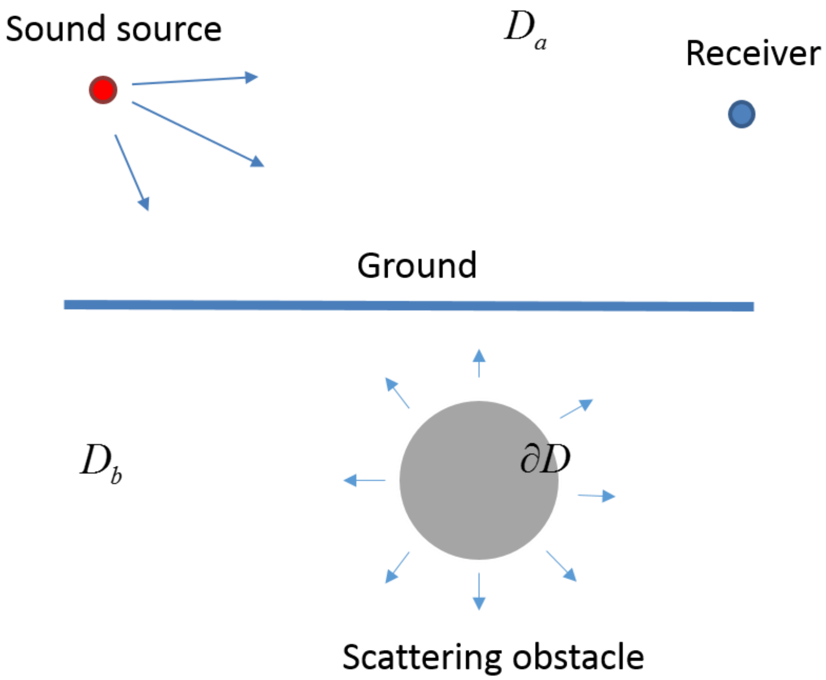

Figure 4-1. The source is located above the ground and the receiver is located either above or below the ground.

The mono-pole source and the scattering surface are not in the same medium. As a result, the integral equations in the previous sections are not valid for this problem. In the formulation of the two–medium BEM, several different types of Green’s functions are required. We define the domain above the ground as D_a and the domain below the interface as D_b.

The medium in D_a is air, and the medium in D_b is a porous material which has complex acoustic wave number. The inhomogeneous Helmholtz equation in D_a can be expressed as

$$\Delta p + k^2 p = -\delta(\mathrm{r} - \mathrm{r}_s), \quad r \in D_a \quad , \tag{4.1}$$

and the Helmholtz equation for the underground domain is

$$\Delta p + k_1^2 p = 0, \quad r \in D_b \quad . \tag{4.2}$$

The boundary condition on the surface of the scattering object is the same as the previous impedance boundary condition. On the interface between the air and the underground medium, the pressure is continuous. The continuity can be expressed as

$$p_+(\mathrm{r}, \mathrm{r}_s) = p_-(\mathrm{r}, \mathrm{r}_s), \quad \mathrm{r} \in \Omega, \ , \tag{4.3}$$

where Ω denotes the interface between the air and the underground medium. Here + means the limit of the pressure as *r* approaches the interface from air, and – means the limiting pressure as *r* approaches the interface from porous medium.

The normal velocity is also continuous on the interface,

$$\frac{1}{\rho}\frac{dp_+}{dz} = \frac{1}{\rho_1}\frac{dp_-}{dz}, \quad r \in \Omega \ . \tag{4.4}$$

Another boundary condition is the Sommerfeld radiation condition, which is the same as the radiation condition in the chapter 2.

To solve the problem with BEM, we need several different types of Green’s functions. The first one is the sound field above ground due to an above the ground sound source. The inhomogeneous Helmholtz equation for it is

$$\Delta G_{11} + k^2 G_{11} = -\delta(\mathrm{r} - \mathrm{r}_s), \quad r, r_s \in D_a \ . \tag{4.5}$$

The second one has the same sound source, but the receiver is below the ground. This Green’s function is named as G_{12}, which denotes the sound field penetrating from the air into the second medium. The inhomogeneous Helmholtz equation for it is

$$\Delta G_{12} + k^2 G_{12} = -\delta(\mathrm{r} - \mathrm{r}_s), \quad r_s \in D_a, \, r \in D_b \ . \tag{4.6}$$

These two Green’s functions share the conditions

$$G_{11}(\mathrm{r}, \mathrm{r}_s) = G_{12}(\mathrm{r}, \mathrm{r}_s), \quad \mathrm{r}_s \in D_a, \mathrm{r} \in \Omega \tag{4.7}$$

and

$$\frac{1}{\rho} \frac{dG_{11}(\mathrm{r}, \mathrm{r}_s)}{dz} = \frac{1}{\rho_1} \frac{dG_{12}(\mathrm{r}, \mathrm{r}_s)}{dz}, \quad \mathrm{r}_s \in D_a, \mathrm{r} \in \Omega. \ . \tag{4.8}$$

The third Green’s function is G_{22}. The inhomogeneous Helmholtz equation for it is

$$\Delta G_{22} + k_1^{\,2} G_{22} = -\delta(\mathrm{r} - \mathrm{r}_s), \quad r_s, r \in D_b, \tag{4.9}$$

where $k_1 = \frac{c}{c_1} k = nk$ is the acoustic wave number in the porous medium and n is the sound speed ratio. The last Green’s function is denoted as $G_{21.}$ The equation is

$$\Delta G_{21} + k_1{}^2 G_{21} = -\delta(\mathrm{r} - \mathrm{r}_s), \quad \mathrm{r} \in D_a, \mathrm{r}_s \in D_b \quad . \tag{4.10}$$

Due to the principle of reciprocity, we can calculate *G21* with *G12*, where

$$G_{21}(\mathrm{r}, \mathrm{r}_s) = \xi G_{12}(\mathrm{r}_s, \mathrm{r}), \;\; \mathrm{r} \in D_a, r_s \in D_b \tag{4.11}$$

The term ξ ensures that the mono-pole source in the lower medium has the same volume strength as the source in the upper medium. The validation of the reciprocity is discussed in the third chapter. We define G as

$$G(\mathrm{r}, \mathrm{r}_s) = \begin{cases} G_{11}(\mathrm{r}, \mathrm{r}_s), \quad \mathrm{r}, \mathrm{r}_s \in D_a \\ G_{12}(\mathrm{r}, \mathrm{r}_s), \quad \mathrm{r} \in D_b, r_s \in D_a \\ \dfrac{1}{\xi} G_{22}(\mathrm{r}, \mathrm{r}_s), \;\; \mathrm{r}, \mathrm{r}_s \in D_b \\ G_{12}(\mathrm{r}_s, \mathrm{r}), \quad \mathrm{r} \in D_a, \mathrm{r}_s \in D_b \end{cases} \tag{4.12}$$

to satisfy reciprocity,

$$G(\mathrm{r}, \mathrm{r}_s) = \mathrm{G}(\mathrm{r}_s, \mathrm{r}), \quad \mathrm{r}, \mathrm{r}_s \in D_a \bigcup D_b \quad . \tag{4.13}$$

In order to get a simple BIE, we need to eliminate the integral term along the interface between the two medium. With Green's theorem we can obtain

$$\epsilon_a p(\mathrm{r}, \mathrm{r}_s) = G(\mathrm{r}_s, \mathrm{r}) + \int_\Omega [G(\mathrm{r}_0, \mathrm{r}) \frac{\partial p(\mathrm{r}_0, \mathrm{r}_s)}{\partial n(\mathrm{r})} - \mathrm{p}(\mathrm{r}_0, \mathrm{r}_s) \frac{\partial G(\mathrm{r}_0, \mathrm{r})}{\partial n(\mathrm{r}_0)}] \mathrm{dr}_0 \tag{4.14}$$

and

$$\begin{aligned}\frac{1}{\xi}\epsilon_b p(\mathrm{r},\mathrm{r}_s) &= -\int_\Omega [G(\mathrm{r}_0,\mathrm{r})\frac{\partial p(\mathrm{r}_0,\mathrm{r}_s)}{\partial n(\mathrm{r}_0)} - \mathrm{p}(\mathrm{r}_0,\mathrm{r}_s)\frac{\partial G(\mathrm{r}_0,\mathrm{r})}{\partial n(\mathrm{r}_0)}]\mathrm{dr}_0 \\ &+\int_\Omega [G(\mathrm{r}_0,\mathrm{r})\frac{\partial p(\mathrm{r}_0,\mathrm{r}_s)}{\partial n(\mathrm{r}_0)} - \mathrm{p}(\mathrm{r}_0,\mathrm{r}_s)\frac{\partial G(\mathrm{r}_0,\mathrm{r})}{\partial n(\mathrm{r}_0)}]dr_0\end{aligned}, \qquad (4.15)$$

where $\epsilon_a = \begin{cases}1, & r\in D_a\\ 0, & r\in D_b\end{cases}$ and $\epsilon_b = \begin{cases}0, & r\in D_a\\ 1, & r\in D_b\\ \epsilon, & r\in\Omega\end{cases}$. ϵ is the term about the solid angle which we have mentioned before. With the two equations above, we can get the BIE we need, which is ready to be solved with the BEM. The BIE is

$$\epsilon p(\mathrm{r},\mathrm{r}_s) = G(\mathrm{r},\mathrm{r}_s) + \xi\int_\Omega [G(\mathrm{r}_0,\mathrm{r})\frac{\partial p(\mathrm{r}_0,\mathrm{r}_s)}{\partial n(\mathrm{r}_0)} - \mathrm{p}(\mathrm{r}_0,\mathrm{r}_s)\frac{\partial G(\mathrm{r}_0,\mathrm{r})}{\partial n(\mathrm{r}_0)}]dr_0. \qquad (4.16)$$

In the (4.16), *r* can be above the ground or below the ground but r_s is above the ground. The detailed proof of the equivalency between the original boundary conditions and the BIE was given by Attenborough, Berry and Chen. (Attenborough, Berry, & Chen, 1990)

In order to predict the sound field in the air and in the porous medium in the problem, collocation method can be applied. In the collocation method, the receiver needs to be put on the surface of the scattering object first.

The BIE can be written as

$$\epsilon p(\mathrm{r}_c,\mathrm{r}_s) = G(\mathrm{r}_c,\mathrm{r}_s) + \xi\int_\Omega \mathrm{p}(\mathrm{r}_0,\mathrm{r}_s)\frac{\partial G(\mathrm{r}_0,\mathrm{r}_c)}{\partial n(\mathrm{r}_0)}dr_0,\ \ r_c, r_s \in \Omega\ . \qquad (4.17)$$

We can conclude from the Equation (4.17) that, we need G_{12} and G_{22} to solve the BIE. And in order to obtain the prediction of the sound field in the air and in the porous medium with the BIE, we also need G_{11} and G_{12}.

The asymptotic solution for G_{11} used in the previous study (Attenborough, Berry, & Chen, 1990) is only valid for certain geometries and ground properties. When the porous ground has low flow resistivity, the asymptotic solution is not accurate enough. When the dissipativity of the porous medium is high, the contribution of the reflected sound wave from underground scattering is negligible. However, when the dissipativity is low, the below ground scattering makes a significant contribution to the sound field above the ground. As a result, a more accurate solution must be utilized to ensure the accuracy of the solution.

The differences between above ground and below ground include sound speed and medium density. For most ground types of interest, the sound speed in the above ground medium is larger than that in the below ground medium, and the density of the below ground medium is relatively larger. Also, we treat air as a non-dissipative medium, and the underground medium is modeled as a dissipative medium, which has complex wave number.

The derivations of different types of Green’s functions are lists below with the steepest descent method. The results are compared with the results calculated with the directly numerical integration.

4.2 Fast Numerical Solutions for Sound Fields Below a Rigid Porous Ground with an Above Sound Source

The study about the sound transmitted into a rigid porous half-plane is of great interest for decades with many practical acoustic engineering applications. The research about the asymptotic solution for the sound fields below a semi-infinite porous ground has been conducted most recently by Kai Ming Li and Sheng Liu. (Li and Liu, 2011) The method of steepest descent is used in the research, and the integral is evaluated asymptotically only at the saddle point.

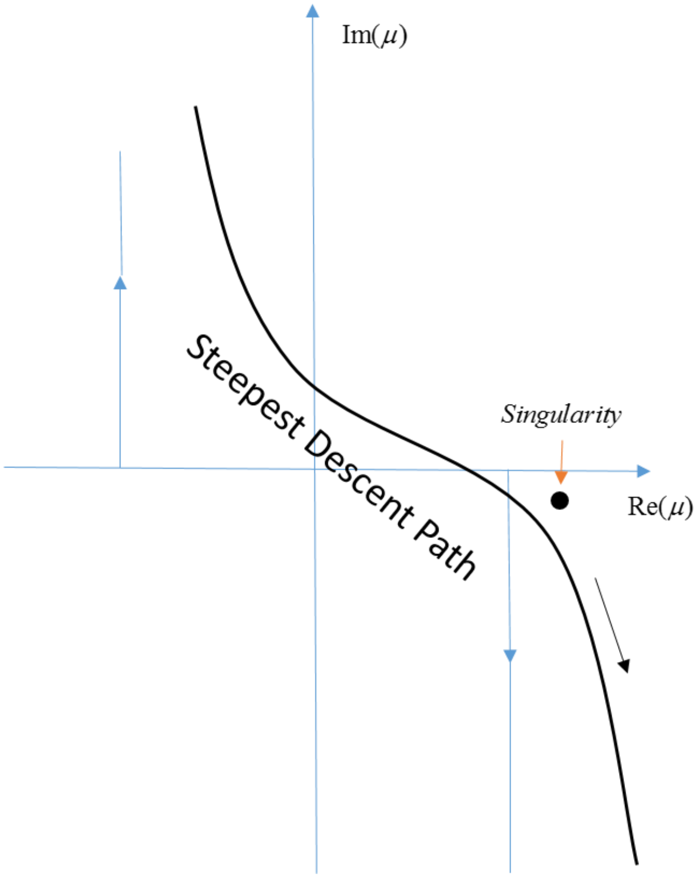

Figure 4-2. The steepest descent path.

In this thesis, a similar method is used to get the fast solution for the Green's function. The function G_{12} is expanded with only one term in Li and Liu's research, however, the path of the steepest descent is found out and the integration is evaluated with 20 terms Gaussian quadrature.

From the boundary conditions, the original integrand can be expressed as:

$$\mathrm{F}(\mathrm{k}_x)=\frac{\mathrm{i}/2\pi}{\mathrm{k}_z+\xi\mathrm{k}_{1z}}\mathrm{e}^{ik_z zs+ik_{1z}D+ik_x r}\ . \tag{4.18}$$

And the total integral can be expressed as

$$p=\int_{-\infty}^{+\infty}\frac{i/2\pi}{k_z+\xi k_{1z}}e^{ik_z zs+ik_{1z}D+ik_x r}dk_x. \tag{4.19}$$

In the equation, D is the vertical distance from the interface to the receive location, and *r* is the horizontal distance between the sound source and the receiver. Before using the steepest descent method, we need to map the integral from k_x plane to μ plane with the mapping

$$k_x=k\sin\mu. \tag{4.20}$$

The integrand becomes

$$\mathrm{F}(\mu)=\frac{i}{2\pi}\frac{\cos\mu}{\cos\mu+\chi}\mathrm{e}^{ikzs\cos\mu+ikD\sqrt{k_1{}^2-(\mathrm{k}\sin\mu)^2}+ikr\sin\mu}\ , \tag{4.21}$$

and the integral becomes

$$p=\int_C \frac{i}{2\pi}\frac{\cos\mu}{\cos\mu+\chi}\mathrm{e}^{ikzs\cos\mu+ikD\sqrt{k_1{}^2-(\mathrm{k}\sin\mu)^2}+ikr\sin\mu}d\mu, \tag{4.22}$$

where the path *C* is the same as the path listed in the previous section.

Li and Liu used a quartic equation to find the saddle point and expanded the integrand at the saddle point. Following the analysis of Li, we can determine the full path of the steepest descent with different quartic equations.

The mapping is

$$\frac{X^2}{2} = ikL - (ikzs\cos\mu + iD\sqrt{k_1{}^2-(\mathrm{k}\sin\mu)^2} + ikr\sin\mu), \tag{4.23}$$

where

$$L = r\sin v + zs\cos v + nD\sqrt{1-\sin v^2/n^2}\ . \tag{4.24}$$

In the Equation (4.24), *v* is the solution of μ when $X=0$. The location of *v* is at the saddle point.

In order to find the steepest descent path. We need to solve the quartic function for every different *X*. Coefficients of $a=\sin\mu$ from order 0 to order 4 can be expressed as

$$\begin{bmatrix} (k^2zs^2-(X^2(i/2)+kL)^2+D^2k1^2)^2-4k^2k1^2zr^2zs^2; \\ 4kr(X^2(i/2)+kL)(k^2zs^2-(X^2(i/2)+kL)^2+D^2k1^2); \\ 4k^2k1^2zr^2zs^2+4k^2r^2(X^2(i/2)+kL)^2- \\ 2(k^2zs^2-(X^2(i/2)+kL)^2+D^2k1^2)(k^2zs^2+k^2r^2+(D^2k1^2)/n^2) \\ +(4k^2k1^2zr^2zs^2)/n^2; \\ -4kr(X^2(i/2)+kL)(k^2zs^2+k^2r^2+(D^2k1^2)/n^2); \\ (k^2zs^2+k^2r^2+(D^2k1^2)/n^2)^2-(4k^2k1^2zr^2zs^2)/n^2 \end{bmatrix} \tag{4.25}$$

The principle for choosing the roots could be found in the work by Li. After obtaining the path of the integration, the solution can be calculated with the Gaussian quadrature of 20 terms. In the evaluation of the integration, the method of pole subtraction is necessary if the path is close to the singularity. The integral is

$$P=\int_C F(\mu)\mathrm{e}^{f(\mu)}\,d\mu\ , \tag{4.26}$$

where

$$F(\mu)=\frac{i}{2\pi}\cos\mu/(\cos\mu+\chi(\mu)) \tag{4.27}$$

and

$$f(\mu)=ik\cos\mu zs+iD\sqrt{k_1^2-(k\sin\mu)^2}+ikr\sin\mu\ . \tag{4.28}$$

Besides, the integration can also be approximated by a 2rd order asymptotic solution

$$I_{asym}=\sqrt{2\pi/(-\mathrm{f''})}e^{f}F, \tag{4.29}$$

which is the same as the asymptotic solution given by Li and Liu. (Li and Liu, 2011)

In order to complete the BEM simulation, the derivatives in the horizontal direction and vertical direction are also necessary. The derivative in the horizontal direction can be evaluated with the same approach. The only difference is

$$F(\mu) = -\frac{k}{2\pi}\cos\mu\sin\mu/(\cos\mu+\chi(\mu)) \quad . \tag{4.30}$$

The derivative in the vertical direction can be evaluated with the approach as well, and the only difference between them is

$$F(\mu) = -\frac{k}{2\pi}\frac{\chi\cos\mu}{\xi(\cos\mu+\chi(\mu))} \quad . \tag{4.31}$$

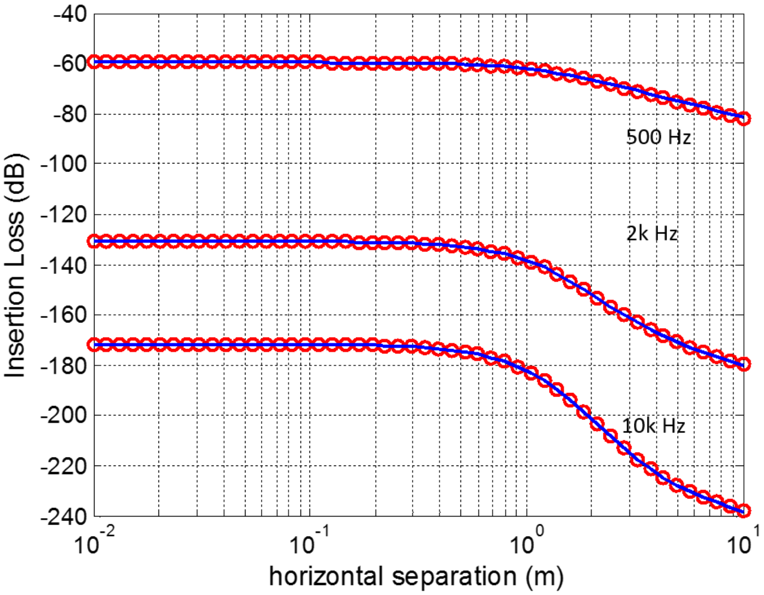

Figure 4-3. Predicted IL versus horizontal separation between the source and receiver. IL=|20log(P/1)|, where the reference is 1 dB; Flow resistivity is 3000 Pa m s^{-2}; Tortuosity is 1.82; Porosity is 0.3; Shape factor is 1; Source location is 1 m above the ground and receiver location is 1 m below the ground. Circle: Fast solutions; Solid: Accurate solutions.

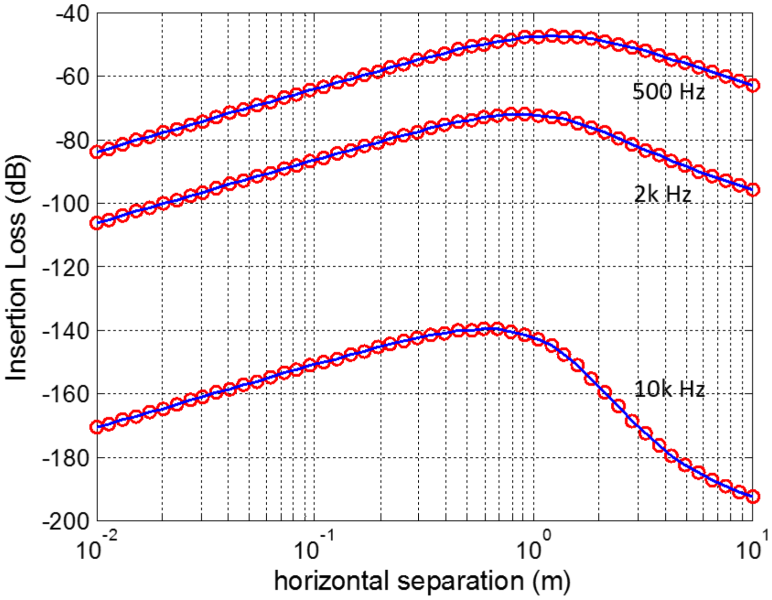

Figure 4-4. Horizontal derivatives. Solid line: fast asymptotic solution; dotted line: exact solution calculated with direct numerical integration.

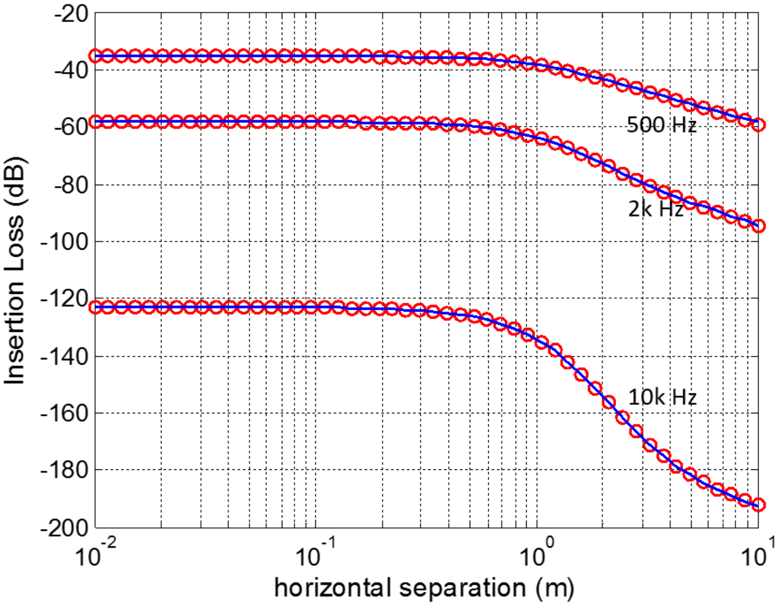

Figure 4-5. Vertical derivatives. Solid line: fast asymptotic solution; dotted line: exact solution calculated with direct numerical integration.

The sound pressure on a straight line are calculated with the steepest descent method and the exactly numerical integration method. The agreements are excellent at different frequencies and for several types of ground. The method of pole subtraction is not implemented into the integration yet because the results are accurate enough for several types of porous ground of interest.

4.3 Fast Numerical Solutions for Sound Fields Below a Rigid Porous Ground with an Underground Sound Source

4.3.1 Theoretical Formulation of G22

When the receiver and the monopole source are both below the ground, we name the Green's function as G22. The differences between G22 and G11 include the wave number a, the density ratio and also the sound speed ratio. In particular, the wave number is complex below the ground because of the property of dissipativity of the porous medium, which brings a positive imaginary part into the wave number. The solution could be approximated with an easy approximation

$$G(r,r_s) = \frac{iH_0^{(1)}(kR_1)}{4} + R_p \frac{iH_0^{(1)}(kR_2)}{4} \;, \tag{4.32}$$

where *Rp* denotes the plane wave reflection coefficient. *Rp* could be calculated with

$$R_p = (\cos\theta - \xi\sqrt{n^2 - sin^2\theta}) / (\cos\theta + \xi\sqrt{n^2 - sin^2\theta}). \tag{4.33}$$

This approximation for the Green's function is used in the BEM formulation by Berry, Chandler-Wilde and Attenborough. (Berry, 1994) The approximation is accurate when

$n >> \sin\theta$, however, if the sound speed ratio $n = c_1 / c_2$ is not far larger than the value of $sin\theta$, this solution is going to be inaccurate. In this section, a more accurate and fast solution for G22 is obtained with the method of the steepest descent. With the boundary conditions and the Helmholtz differential equation, the integral can be expressed as

$$p(\mathrm{r},\mathrm{r}_s) = \frac{-i}{2\pi}\int_C \frac{\zeta\sqrt{n^2-\sin^2\mu}\exp\left[ikf(\mu)\right]}{\cos\mu+\zeta\sqrt{n^2-\sin^2\mu}}d\mu \quad , \tag{4.34}$$

where

$$f(\mu) = r\sin\mu + (z_s + z)\cos\mu = R_2\cos(\mu-\theta). \tag{4.35}$$

Due to the complex wave number and the branch cut in the μ plane, the deformation process of the integral path becomes complicated. The integrand of the G22 integration contains a double-valued function, which is the square root function $\sqrt{n^2-\sin^2\mu}$. The steepest descent path may cross the branch cut and goes into another branch under some conditions. As a result, the function needs to be evaluated carefully along the steepest descent path. Also, the integration along the two sides of the branch cut must be added into the integration under some conditions. The branch integration term is sometimes known as the lateral wave in acoustics. (Brekhovskikh, 2012)

With different geometries, there can be three different types of integral path.

1) When the horizontal distance between source and receiver is short, the steepest descent path will cross the branch cut twice. It means that the path of integration starts from the original branch and goes into another branch and then the path will go back into the original

branch after crossing the branch cut at the second time. (Figure 4-6)

A mapping needs to be introduced to find the steepest descent path, which can be expressed as

$$X^2/2 = ikR_2\cos(\mu-\theta)\ . \tag{4.36}$$

The location of μ_0 in the transformed complex μ plane can be calculated with

$$\mu_0 = \sin^{-1} n, \tag{4.37}$$

where n is the speed ratio c_1/c_2. The branch cuts can be found with

$$\mu = \sin^{-1}(\pm\sqrt{n^2-\frac{x}{k^2}})\ , \tag{4.38}$$

where $x \in [0,\infty)$. In the current problem, the branch cut starts from μ_0 and goes upward to infinity. The relationship between the real part and the imaginary part of the branch cut can be expressed as

$$\mathrm{Re}(\mu) = (A(\mu_i)-\cos^{-1}(\frac{c}{\sqrt{a^2(\mu_i)+b^2(\mu_i)}})/2 - sign(\mu_i)\pi\ , \tag{4.39}$$

where

$$a(\mu_i) = -2\,\mathrm{Re}(k)\,\mathrm{Im}(k)\cosh(2\mu_i), \tag{4.40}$$

$$b(\mu_i) = (\mathrm{Re}(k)^2 - \mathrm{Im}(k)^2)\sinh(2\mu_i)\,, \tag{4.41}$$

and

$$c = -2\,\mathrm{Re}(k)\,\mathrm{Im}(k) \quad . \tag{4.42}$$

With above functions, we could decide the relative location of the steepest descent path to the branch cut.

Through investigation of the shapes of the steepest descent paths, we are able to determine which method should be used. All the curves in the complex plane can be written out analytically. The only inconvenient part is that nearly all of the functions are multi-valued functions. Hence, numerical integration must be conducted carefully. The value of the integrand should be adjusted carefully when the path goes into another branch. In the second branch

$$F(\mu) = \frac{-\zeta\sqrt{n^2-\sin^2\mu}\,\exp\left[ikf\ (\mu)\right]}{\cos\mu-\zeta\sqrt{n^2-\sin^2\mu}}. \tag{4.43}$$

In order to evaluate the integration with Gaussian quadrature, one also need

$$\frac{\partial\mu}{\partial X} = \frac{X}{ikR2\sin(\mu-\theta)}, \tag{4.44}$$

which has a removable singularity when $X = 0$. The singularity could be removed by adding a small value $\delta = 10^{-15}$ at the singular location. The problem could be solved analytically, however, this method is fast and convenient for calculation. To obtain the integral along the steepest path with Gaussian quadrature method, we need to use different functions in different branches. The solution implemented with the Gaussian quadrature method can be calculated with

$$p(\sqrt{2}X_g) = -\frac{i}{\sqrt{2}\pi}\frac{\chi}{\cos\mu+\chi}e^{ikR_2}\frac{\partial\mu}{\partial X}w(\sqrt{2}X_g) \;, \tag{4.45}$$

where *w* is the weighting function for function of the type

$$F = \int_{-\infty}^{+\infty} f(\mathrm{x})e^{-x^2}dx \;, \tag{4.46}$$

and X_g is the abscissae for the Gasussian quadrature of the type in Equation (4.46).

2) As the range increases, we have to incorporate the branch cut integral, which is also known as the lateral wave term. (Brekhovskikh, 2012) In order to complete the integration in the complex plane, one must follow the arrows in the Figure 4-7 to integrate. As a result, an additional term appears in the path of integration. The solution of the original integral becomes

$$p = p_{stp} + p_{lateral} \;, \tag{4.47}$$

where

$$p_{lateral} = p_{branch} + p'_{stp} \;. \tag{4.48}$$

In the Equation (4.48), p'_{stp} denotes another integral on the steepest descent path, which is

$$p'_{stp} = \int_{C_{stp}} \left(-\frac{i}{2\pi}\frac{\chi}{\cos\mu+\chi} + \frac{i}{2\pi}\frac{-\chi}{\cos\mu-\chi}\right)e^{ikR_2\cos(\mu-\theta)}d\mu \;, \tag{4.49}$$

and the path of integration is the pink line in the Figure 4-8.

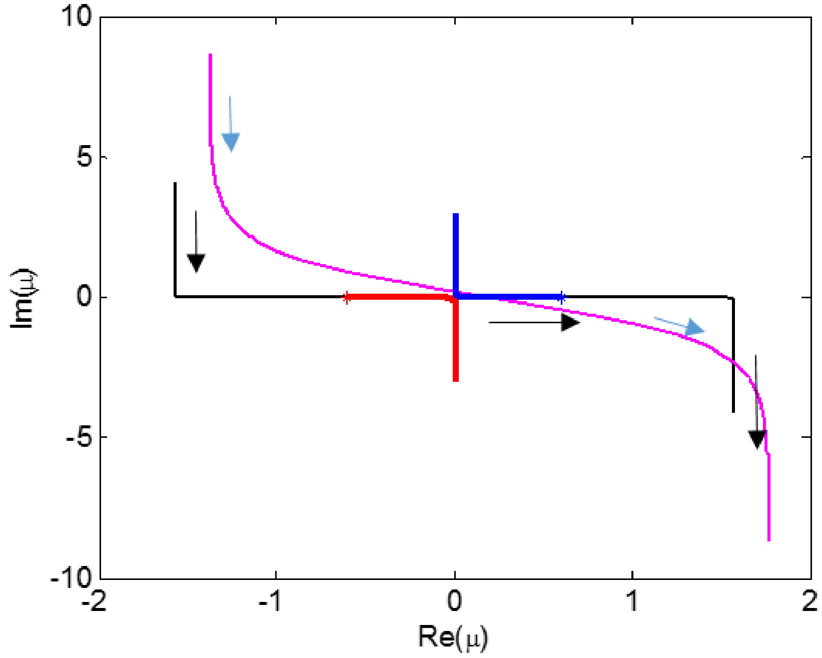

Figure 4-6. The steepest descent paths in the first case.

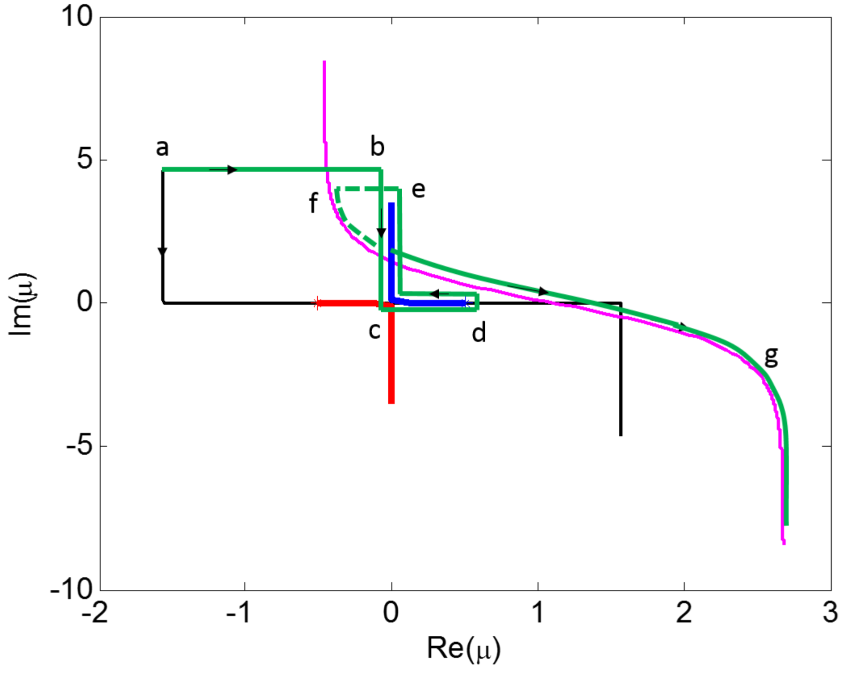

Figure 4-7. The path of the integration and the lateral wave term.

With a similar approach, we could calculate the integration along the branch cut path with the mapping

$$\mathrm{W}{=}ikR_2(\cos(\mu_0\text{-}\theta)\text{-}\cos(\mu\text{-}\theta)) \qquad (4.50)$$

and

$$\mu(\mathrm{W}) = \theta - \cos^{-1}(-\frac{W}{ikR_2} + \cos(\mu_0 - \theta)) \ . \qquad (4.51)$$

The partial derivative is

$$\frac{\partial\mu}{\partial W} = \frac{1}{ikR_2 \sin(\mu - \theta)} \ . \qquad (4.52)$$

And the integral along the branch cut is

$$p_{branch} = \int_{C_{branch}} (-\frac{i}{2\pi}\frac{\chi}{\cos\mu + \chi} + \frac{i}{2\pi}\frac{-\chi}{\cos\mu - \chi})e^{ikR_2\cos(\mu-\theta)}d\mu \ . \qquad (4.53)$$

C_{branch} denotes the branch cut path, which starts from μ_0 and goes to infinity. The integration is evaluated with Gaussian quadrature and the branch cut integral can be written as

$$\begin{aligned} p_{branch} &= (-\frac{i}{2\pi}\frac{\chi(\mathrm{W}_{g1})}{\cos\mu(\mathrm{W}_{g1}) + \chi(\mathrm{W}_{g1})} \\ &+ \frac{i}{2\pi}\frac{-\chi(\mathrm{W}_g)}{\cos\mu(\mathrm{W}_g) - \chi(\mathrm{W}_g)})e^{ikR_2\cos(\mu_0-\theta)}\frac{d\mu}{dW}(\mathrm{W}_g)\,\mathrm{w}_1(\mathrm{W}_g) \end{aligned} , \qquad (4.54)$$

where w_1 is the weighting function for function of the type

$$F = \int_{-\infty}^{+\infty} f(\mathrm{x}) e^{-x} dx, \tag{4.55}$$

and W_g are the abscissae points for the Gaussian quadrature for the type of functions in the Equation (4.55).

In the procedure of integration, any branch cut crossed by the integration path must be took into consideration. The path of integration along the branch cut starts from the branch point then goes along the path where the absolute value of the exponential term decreases most rapidly. In this case, the path goes downward to the infinity. (Figure 4-8)

3) The direction of the branch cut steepest path will change when the range is even larger due to the branch cut of cos^{-1}.

If $\mathrm{Re}(\frac{-\mathrm{Im}(\cos(\mu_0)-\theta)/\mathrm{Im}(\frac{1}{ikR_2})}{ikR_2+\cos(\mu_0-\theta)})$ is less than 1, the third condition is met. Under this condition, the deformed integration path of the branch cut starts from the branch point and goes upward to the infinity, and we only need to add the branch cut term into the solution as

$$p = p_{stp} + p_{branch} \ . \tag{4.56}$$

Also, the integrand should choose different functions in the different branches. In order to the use the BEM in the later chapters, one also need to get the solutions for $\frac{\partial p}{\partial r}$ and $\frac{\partial p}{\partial z}$.

The derivatives could be calculated conveniently with the expression

$$p=\int_{-\infty}^{+\infty}\frac{i}{2\pi}\frac{\xi\sqrt{k_1^2-k_x{}^2}}{k_z(\mathrm{k}_x)+\xi\sqrt{k_1^2-k_x{}^2}}\frac{1}{k_z}e^{ik_xr+ik_z(z_r+z_s)}dk_x\ , \tag{4.57}$$

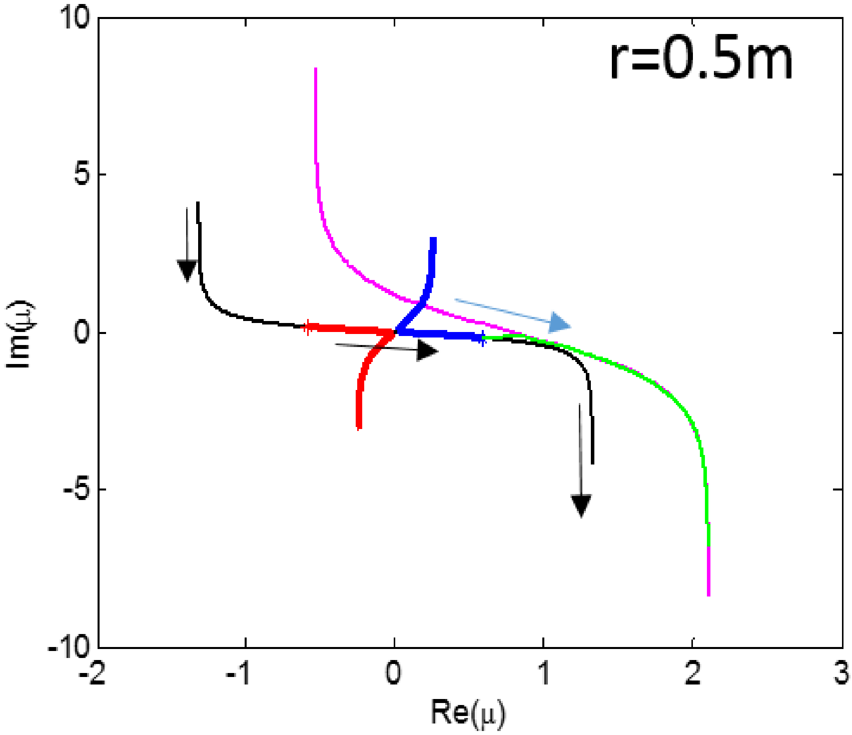

Figure 4-8. The steepest descent paths under the second condition.

The horizontal directional partial derivative is

$$\frac{\partial p}{\partial r}=\frac{-k_x}{2\pi}\frac{\xi\sqrt{k_1^2-k_x{}^2}}{k_z(\mathrm{k}_x)+\xi\sqrt{k_1^2-k_x{}^2}}\frac{1}{k_z}e^{ik_xr+ik_z(z_r+z_s)}\ . \tag{4.58}$$

The Equation (4.58) can be calculated with the equation

$$\frac{\partial p}{\partial r}=\frac{k\sin\mu}{2\pi}\int_{C}\frac{\zeta\sqrt{n^2-\sin^2\mu}\exp\left[ikf(\mu)\right]}{\cos\mu+\zeta\sqrt{n^2-\sin^2\mu}}d\mu\ . \tag{4.59}$$

The integral along the branch cut is

$$\frac{\partial p_{branch}}{\partial r}=ik\sin\mu\int_{C_{branch}}\left(-\frac{i}{2\pi}\frac{\chi}{\cos\mu+\chi}+\frac{i}{2\pi}\frac{-\chi}{\cos\mu-\chi}\right)e^{ikR_2\cos(\mu-\theta)}d\mu\ , \tag{4.60}$$

and the integration could be evaluated with

$$\begin{aligned}\frac{\partial p_{branch}}{\partial r}&=\left(-\frac{i}{2\pi}\frac{\chi(\mathrm{W}_{g1})}{\cos\mu(\mathrm{W}_{g1})+\chi(\mathrm{W}_{g1})}+\frac{i}{2\pi}\frac{-\chi(\mathrm{W}_g)}{\cos\mu(\mathrm{W}_g)-\chi(\mathrm{W}_g)}\right)\\&\times\mathrm{iksin}\,\mu e^{ikR_2\cos(\mu_0-\theta)}\frac{d\mu}{dW}(\mathrm{W}_g)\,\mathrm{w}_1(\mathrm{W}_g)\end{aligned}\ . \tag{4.61}$$

The two-side integral along the steepest descent path becomes

$$\frac{\partial p'_{stp}}{\partial r}=\int_{C_{stp}}\left(-\frac{i}{2\pi}\frac{\chi}{\cos\mu+\chi}+\frac{i}{2\pi}\frac{-\chi}{\cos\mu-\chi}\right)e^{ikR_2\cos(\mu-\theta)}d\mu\ . \tag{4.62}$$

The vertical directional partial derivative is

$$\frac{\partial p}{\partial z}=\frac{k\cos\mu}{2\pi}\int_{C}\frac{\zeta\sqrt{n^2-\sin^2\mu}\exp\left[ikf(\mu)\right]}{\cos\mu+\zeta\sqrt{n^2-\sin^2\mu}}d\mu\ . \tag{4.63}$$

The integral along the branch cut is

$$\frac{\partial p_{branch}}{\partial z}=ik\cos\mu\int_{C_{branch}}\left(-\frac{i}{2\pi}\frac{\chi}{\cos\mu+\chi}+\frac{i}{2\pi}\frac{-\chi}{\cos\mu-\chi}\right)e^{ikR_2\cos(\mu-\theta)}d\mu\ . \tag{4.64}$$

The integration could be evaluated with

$$\frac{\partial p_{branch}}{\partial z} = \Big(-\frac{i}{2\pi}\frac{\chi(\mathrm{W}_{g1})}{\cos\mu(\mathrm{W}_{g1})+\chi(\mathrm{W}_{g1})} + \frac{i}{2\pi}\frac{-\chi(\mathrm{W}_g)}{\cos\mu(\mathrm{W}_g)-\chi(\mathrm{W}_g)}\Big)\mathrm{ik}\cos\mu e^{ikR_2\cos(\mu_0-\theta)}\frac{d\mu}{dW}(\mathrm{W}_g)\,\mathrm{w}_1(\mathrm{W}_g) \, . \tag{4.65}$$

The two-side integral along the steepest descent path becomes

$$\frac{\partial p'_{stp}}{\partial z} = \int_{C_{stp}} \Big(-\frac{i}{2\pi}\frac{\chi}{\cos\mu+\chi} + \frac{i}{2\pi}\frac{-\chi}{\cos\mu-\chi}\Big)e^{ikR_2\cos(\mu-\theta)}d\mu \, . \tag{4.66}$$

The steepest descent paths for p ,$\frac{\partial p}{\partial r}$ and $\frac{\partial p}{\partial z}$ are the same because of the same exponential term $f(\mu)$, which decides the path of the steepest descent.

4.3.2 Validation of the Asymptotic Solutions

In the section 4.3.1, the steepest descent method was used to derive the sound field under the ground due to an underground sound source. For different horizontal separations between the sound source and the receiver, there are three different paths of steepest descent. When the horizontal separation is small, the path is similar to the path used in the above ground case. When the horizontal separation is large, the result must include the lateral wave term, which is also known as branch cut integral.

The lateral wave term can be expressed with Figure 4-10. When the incident angle is larger than the critical angle of the refraction

$$\theta_c = \theta_i = \arcsin(\frac{n_2}{n_1}) \;, \tag{4.67}$$

the effect of total internal reflection occurs. The lateral wave travels along the interface of air/porous and then goes back into the lower medium. The value of the lateral wave is smaller compared to the direct wave term $iH_0^{(1)}(kR_1)/4$, but it brings significant contribution to the total pressure when the horizontal separation is large.

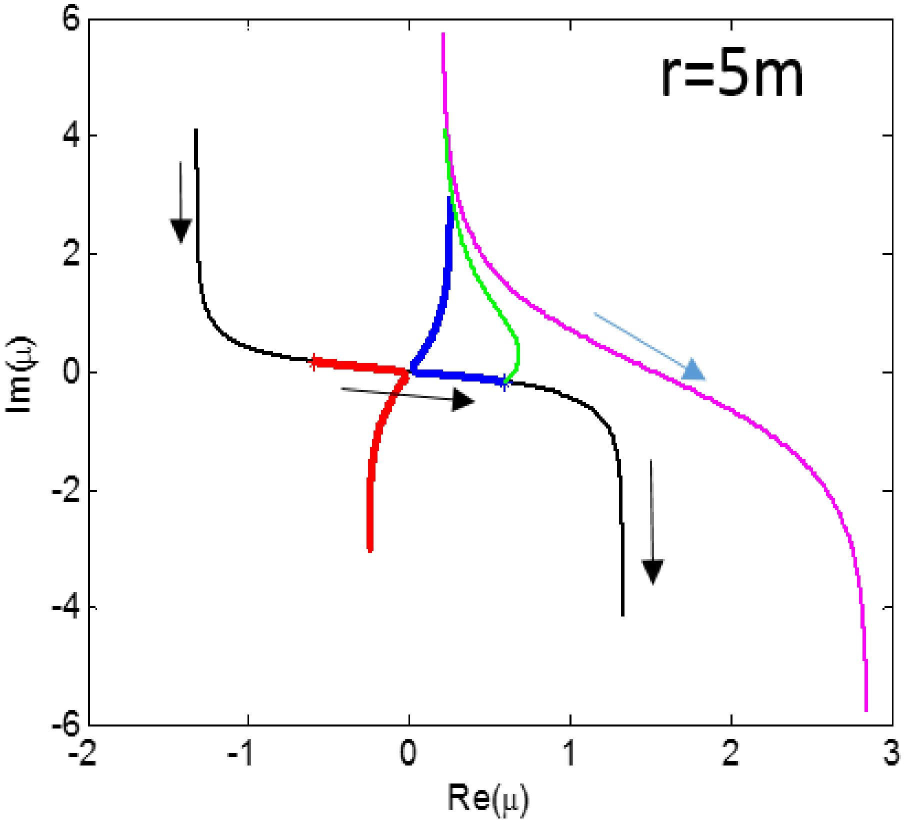

Figure 4-9. The steepest descent paths under the third condition.

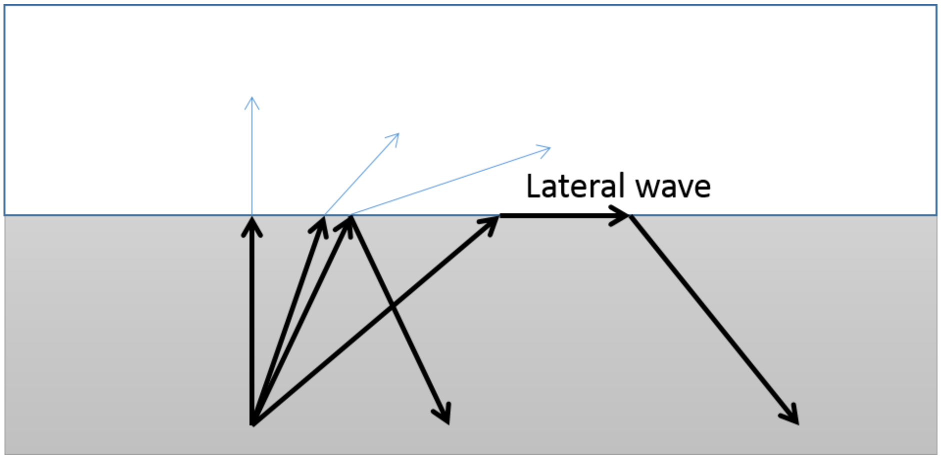

Figure 4-10. Lateral Wave.

The results between the simple asymptotic method, the steepest descent method and the accurate result with integrated exact solution

$$p_{total} = \frac{iH_0^{(1)}(kR_1)}{4} + \frac{iH_0^{(1)}(kR_2)}{4} + \int_{-\infty}^{+\infty} \frac{i}{2\pi} \frac{\xi\sqrt{k_1^2 - k_x^{\ 2}}}{k_z(\mathrm{k}_x) + \xi\sqrt{k_1^2 - k_x^{\ 2}}} \frac{1}{k_z} e^{ik_x r + ik_z(z_r + z_s)} dk_x \tag{4.68}$$

are compared in the Figure 4-11.

In order to obtain the prediction of the sound field below the interface, the Attenborough 4-parameter model is used to obtain the density and the sound speed in the lower medium. (Attenborough, 1985) The effective flow resistivity σ_e of the porous medium is 3000 Pa s m^{-2}. The tortuosity is 1.82 and the porosity is 0.3. The pore shape factor is 1. The results of the simple asymptotic method and the steepest descent method are compared with the accurate solution calculated with the directly numerical integration. The reference pressure for IL is 1 dB

$$IL = 20\log_{10}(|\,\mathrm{p}\,| / |\,\mathrm{p}_{ref}\,|). \qquad (4.69)$$

Figure 4-11 shows that the simple asymptotic solution is accurate for short horizontal distance. The error appears when the separation is larger than 1 m, which could be explained by the appearance of the lateral wave term.

The agreement between the directly integrated exact solution and the steepest descent method solution is excellent for the horizontal distance and the vertical distance as we can see in the Figure 4-11 and Figure 4-12.

In addition, the same porous medium and geometry are used in Figure 4-13 and Figure 4-14 to validate the accuracy of the steepest descent results for horizontal directional derivatives and the vertical directional derivatives. The agreements are excellent in both figures and we can find the contribution of the lateral waves from the results.

All the above comparisons have confirmed the validity of the steepest descent method used in the research, and the solution calculated with the steepest descent method is more accurate than the simple solution derived with the Weyl Van der Pol formula in the long range cases, where the lateral waves appear. In the fifth chapter, the Green's functions derived in this section are implemented into the BEM formulation to solve scattering problems.

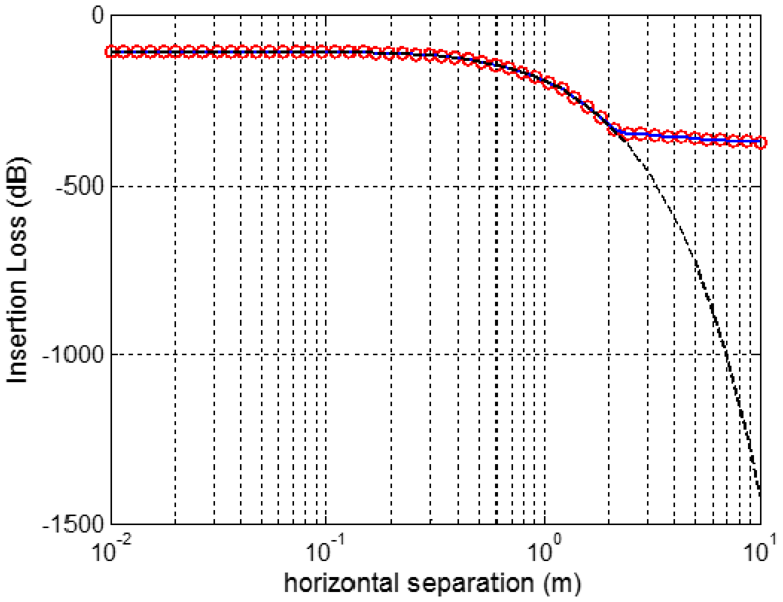

Figure 4-11. The Insertion Loss versus horizontal separation. Source location is 1 m and receiver location is 0.5 m below the interface. Flow resistivity is 3000 Pa m s^{-2}; Tortuosity is 1.82; Porosity is 0.3; Shape factor is 1; Circle: Fast solutions; Solid: Accurate solutions; Dashed: Simple Asymptotic.

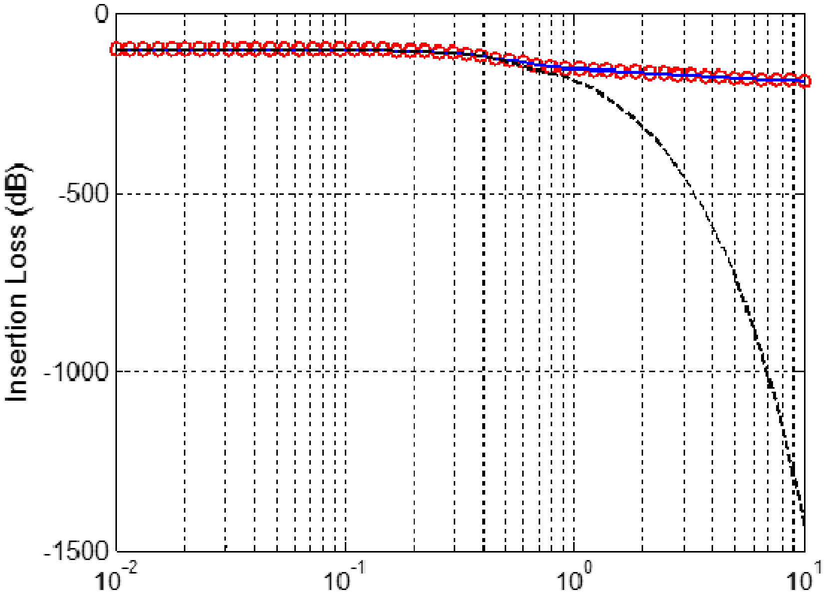

Figure 4-12. Same as previous figure except source location is 0.02m and receiver is at 0.5m below the interface.

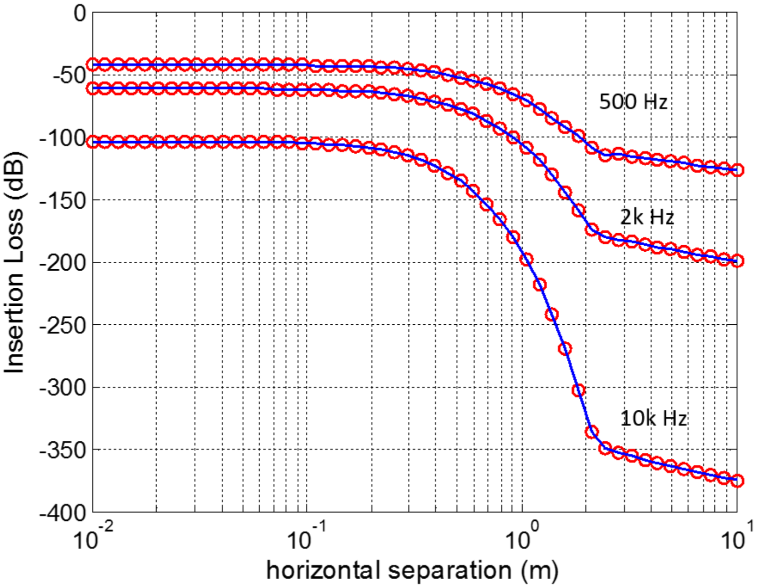

Figure 4-13. Insertion loss versus horizontal separation for 10k Hz, 2k Hz and 500 Hz sound. Flow resistivity is 3000 Pa m s^{-2}; Tortuosity is 1.82; Porosity is 0.3; Shape factor is 1; Source location is 1 m and receiver location is 0.5 m below the interface. Circle: Fast solutions; Solid: Accurate solutions.

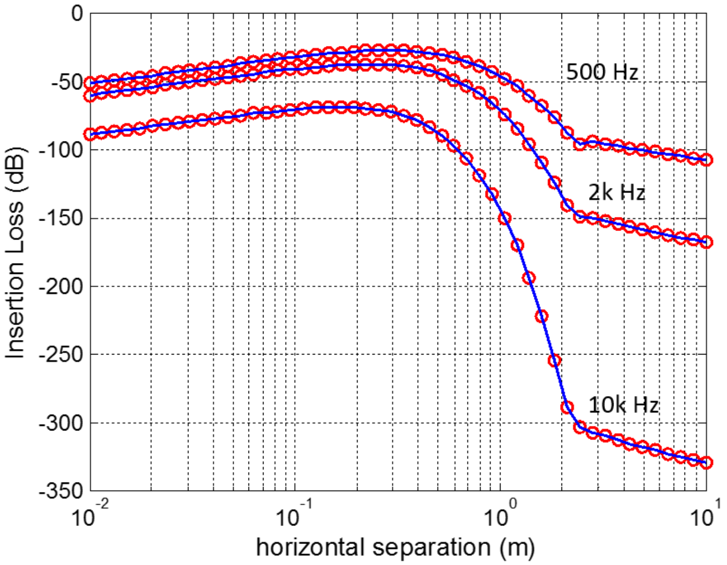

Figure 4-14. Insertion loss for the horizontal directional derivative. Others are the same as the Figure 4-13.

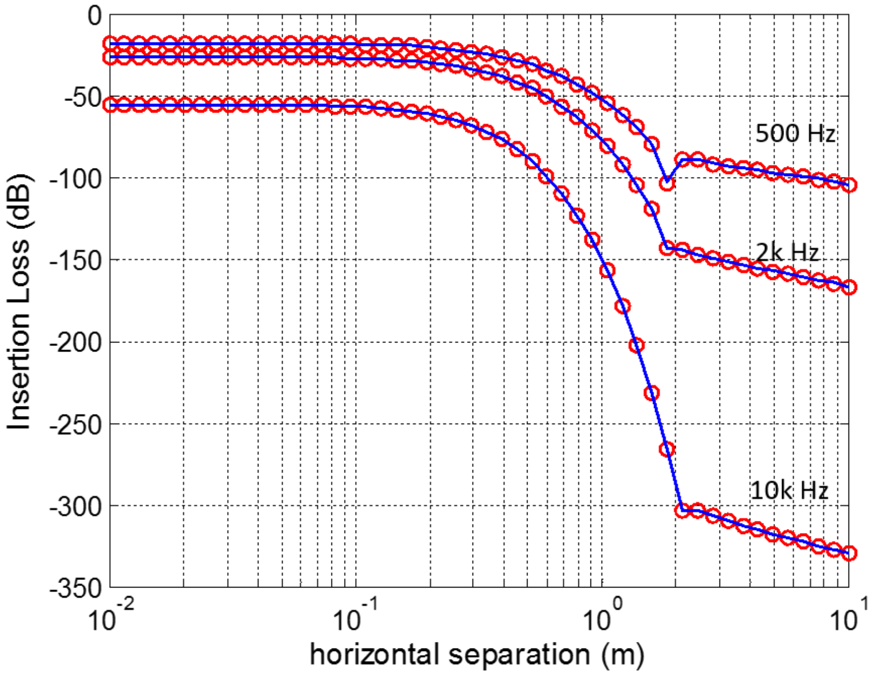

Figure 4-15. Insertion loss for vertical directional derivative; Others are the same as the Figure 4-13.

4.4 Fast Numerical Solutions for Sound Fields Above a Rigid Porous Ground with an Underground Sound Source

G21 is the Green's function whose sound source is below the ground and the receiver of it is above the ground. By interchanging the location of the sound source and the receiver, we can see the reciprocity between the G12 and G21. However, one can also evaluate the G21 integration with the steepest descent method.

The integrand of G21 is similar to that of G12, except for the different density ratio, speed ratio and the wave number. The integrand can be expressed as

$$\mathrm{F}(\mathrm{k}_x)=\frac{\mathrm{i}/2\pi}{\mathrm{k}_z+\xi\mathrm{k}_{1z}}\mathrm{e}^{ik_z zs+ik_{1z}D+ik_x r} \quad . \tag{4.70}$$

First, the function is mapped to another plane with

$$k_x = k\sin\mu. \tag{4.71}$$

The integrand becomes

$$\mathrm{F}(\mu)=\frac{i}{2\pi}\frac{\cos\mu}{\cos\mu+\chi}\mathrm{e}^{ikzs\cos\mu+ikD\sqrt{k_1{}^2-(\mathrm{k}\sin\mu)^2}+ikr\sin\mu} \quad . \tag{4.72}$$

In order to find the steepest descent path, we need to use the transformation

$$\frac{X^2}{2} = ikL - (ikzs\cos\mu + iD\sqrt{k_1{}^2-(\mathrm{k}\sin\mu)^2} + ikr\sin\mu) \quad , \tag{4.73}$$

where

$$L = r\sin v + zs\cos v + nD\sqrt{1-\sin v^2/n^2}. \tag{4.74}$$

In the equation, v is the solution of μ when X=0, and the location of v is the same as the location of the stationary point.

The steepest descent path is influenced by the branch cut in the G21 case because of the influence caused by the square root function in the L term. As a result, the steepest descent path for evaluating G21 is different from that of G12.

In order to find the accurate steepest descent path, we need to solve a quartic function for every different X, where X is a real number on the real axis. Coefficients of a= $\sin\mu$ from order 0 to order 4 can be expressed as

$$\begin{bmatrix} (k^2zs^2-(X^2(i/2)+kL)^2+D^2k1^2)^2-4k^2k1^2zr^2zs^2; \\ 4kr(X^2(i/2)+kL)(k^2zs^2-(X^2(i/2)+kL)^2+D^2k1^2); \\ 4k^2k1^2zr^2zs^2+4k^2r^2(X^2(i/2)+kL)^2 \\ -2(k^2zs^2-(X^2(i/2)+kL)^2+D^2k1^2)(k^2zs^2+k^2r^2+(D^2k1^2)/n^2) \\ +(4k^2k1^2zr^2zs^2)/n^2; \\ -4kr(X^2(i/2)+kL)(k^2zs^2+k^2r^2+(D^2k1^2)/n^2); \\ (k^2zs^2+k^2r^2+(D^2k1^2)/n^2)^2-(4k^2k1^2zr^2zs^2)/n^2 \end{bmatrix} \tag{4.75}$$

1) When the horizontal distance between source and receiver is short, the steepest descent path will cross the branch cut twice, which means that the path starts from the original branch and goes into another branch and then goes back into the original branch. To integrate the integrand on the steepest path with the Gaussian quadrature method, one needs to make sure that the functions are chosen properly in the different branches.

   In the first branch, the function of the integrand is already listed above. When the path is in the second branch, the integrand will change to

$$\mathrm{F}(\mu)=\frac{i}{2\pi}\frac{\cos\mu}{\cos\mu-\chi}\mathrm{e}^{ikzs\cos\mu-ikD\sqrt{k_1{}^2-(\mathrm{k}\sin\mu)^2}+ikr\sin\mu} \quad . \tag{4.76}$$

   With the Gaussian quadrature method for exponential functions, we can evaluate the integration with 20 terms.

2) When the horizontal distance between the sound source and the receiver is long. We need a steepest descent path to keep the start point and the end point of the path in the same

branch. However, there is no such path for any single saddle point we can find. The previous steepest descent path turn back to the left in the μ plane instead of going downward and completing the contour. As a result, we need two saddle points to complete the integration. In other words, we need two different steepest descent paths to keep the start point and the end point in the same branch. The integration along the first path could be calculated with the same approach mentioned above. The sesond path can be calculated with an asympototic solution

$$I_{asym} = \sqrt{2\pi / (-\mathrm{f}")} e^{f} F \quad , \tag{4.77}$$

where

$$F(\mu) = \frac{i}{2\pi} \cos\mu / (\cos\mu + \chi(\mu)) \tag{4.78}$$

and

$$f(\mu) = ik\cos\mu zs + iD\sqrt{k_1^{\,2} - (k\sin\mu)^2} + ikr\sin\mu. \tag{4.79}$$

The contribution from the second saddle path can be named as the evanescent ray, which is caused by the totally reflected energy at the interface. The evanescent ray will decrease exponentially after traveling along the interface. It only contributes a tiny value when the receiver location is well below the ground. The paths are indicated in the Figure 4-16 and the Figure 4-17. The arrows show the direction of the integration. The solid blue lines are the branch cut lines which have important influence to the integration paths and the value of the integrand along the paths.

The property of reciprocity is shown in the figure 4-18. The G12 here is the solution of

$$\Delta G_{12} + k^2 G_{12} = -\delta(\mathrm{r}-\mathrm{r}_s), \quad \mathrm{r}\in D_b, \mathrm{r}_s \in D_a, \qquad (4.80)$$

and G21 is the solution of

$$\Delta G_{21} + k_1^{\,2} G_{21} = -\frac{1}{n}\delta(\mathrm{r}-\mathrm{r}_s), \quad \mathrm{r}\in D_a, \mathrm{r}_s \in D_b \ . \qquad (4.81)$$

The receiver in G12 is the sound source for G21 and the receiver in G21 is the sound source for G21, which means the locations of the sound source and the receiver are interchanged.

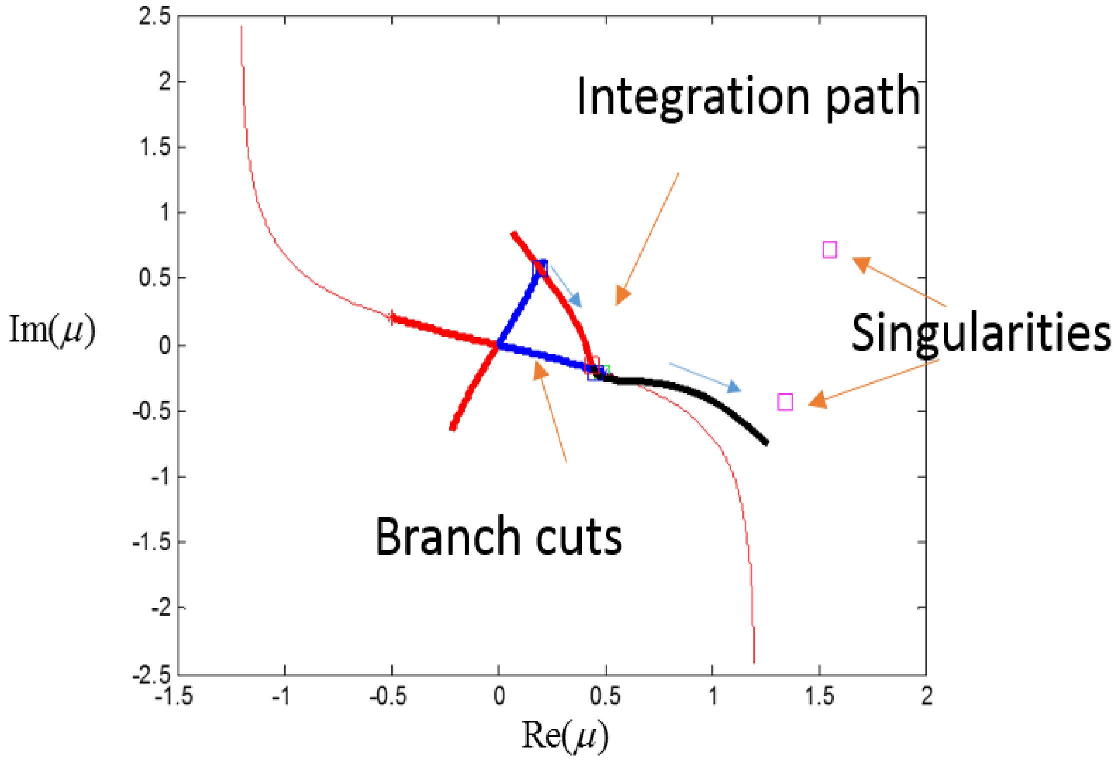

Figure 4-16. The path when the range is short.

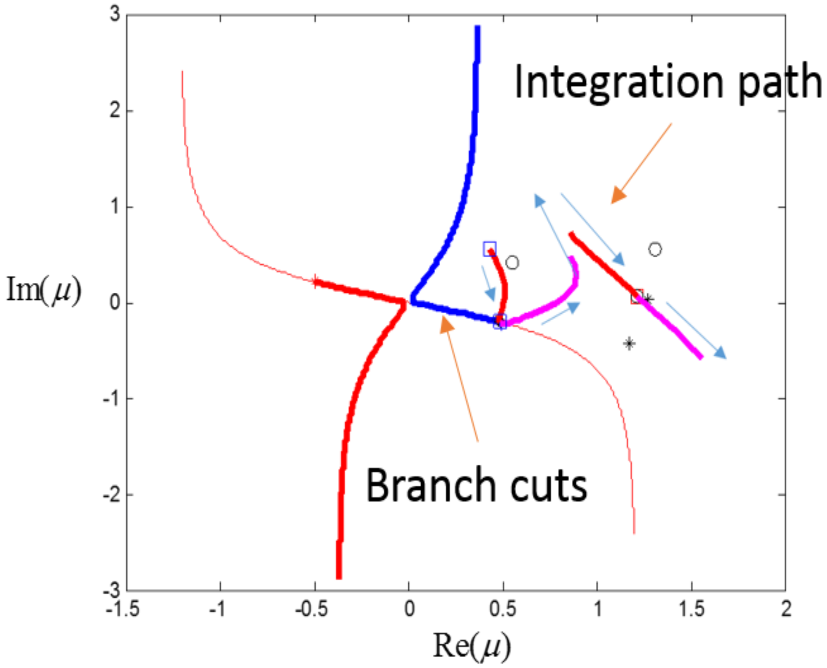

Figure 4-17. The path when the range is long.

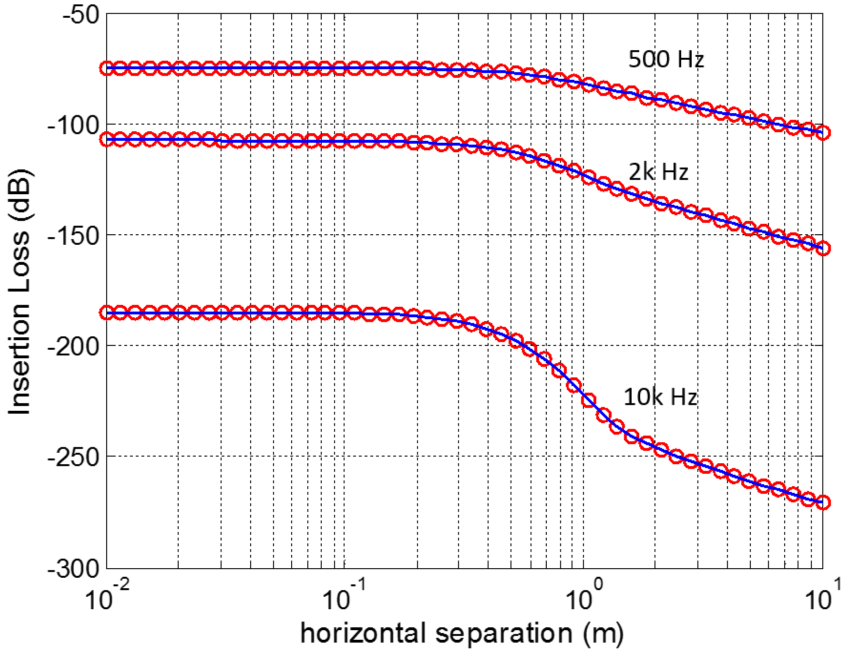

Figure 4-18. Reciprocity of G12 and G21. Solid line: G12; Dotted line: G21. From top to bottom: 10k Hz, 2k Hz and 500 Hz.

We can see that one can use different descent methods to simplify the calculation of the same integration. This inspirational fact provides a possibility to find a better steepest descent method to simplify the evaluations of many integrations, which may be a worthwhile study in the future. Although we calculate G21 with the steepest descent method, the method used in the calculation of G12 is easier. The path of the integration crosses the branch cut several times in the calculation of G21, which makes the evaluation extremely difficult. As a result, the property of reciprocity is used to obtain G21 in the BEM simulation.

All of the necessary Green’s functions are derived in the current chapter. In the next chapter, the Green’s functions are implemented into the BEM formulation to solve the sound field below and above a porous ground due to the scattering effect of an underground obstacle.

CHAPTER 5. THE BEM RESULTS FOR THE UNDERGROUND SCATTERING

Acoustic reflections due to objects below a porous ground can be substantial in a low dissipative medium and/or when the object is located near the air/ground interface. Applications may include detection and identification, or assist in the design of noise barriers. Perhaps the Green's function for a water/sediment interface can be derived which would facilitate underwater acoustics applications.

In the problem of sound scattering by an obstacle below a porous ground, the air is assumed to be non-dissipative. The porous medium is assumed to have a lower

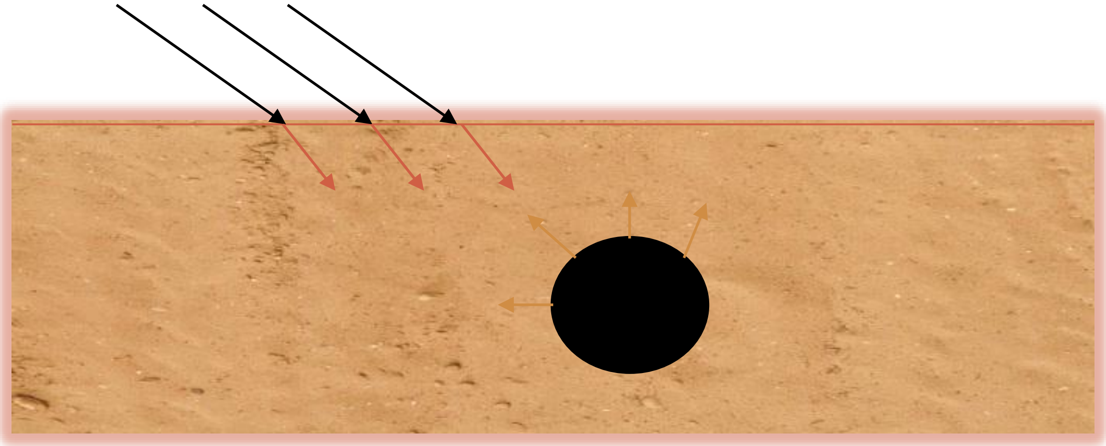

Figure 5-1. Acoustical detection of an underground object.

sound speed and a higher density than air. Also, the porous medium has a complex wave propagation coefficient, which provides the necessary dissipation property.

The problem geometry provided in Figure 5-1. In the BEM, the surface of the obstacle is discretized into boundary elements. The number of the elements depend on the wave-length within the medium and the smoothness of the object's surface. To accurately mesh a complicated shape, more elements are needed. In addition, the rate of change of the pressure along the object's surface needs to be considered. Adaptive meshing can be applied as necessary.

5.1 Below Ground BEM Formulation

The below ground BEM formulation is similar to that of the above ground case. However, there are several notable differences. The pressure field along the surface of the object needs to be determined. The numerical equations can be expressed as:

$$\varepsilon p(r(\mathrm{m}+\frac{1}{2}),r_s)=G(r_s,r(\mathrm{m}+\frac{1}{2}))+$$

$$\xi\sum_{n=1}^{N}\Delta h[G(\mathrm{r}_0(\mathrm{n}),\mathrm{r}(\mathrm{m}+\frac{1}{2}))(-ik\beta(r_0(\mathrm{n}))p(\mathrm{r}_0(\mathrm{n}),\mathrm{r}_s))-\mathrm{p}(\mathrm{r}_0(\mathrm{n}),\mathrm{r}_s)\frac{\partial G(\mathrm{r}_0(\mathrm{n}),\mathrm{r}(\mathrm{m}+\frac{1}{2}))}{\partial n(\mathrm{r}_0(\mathrm{n}))}].$$

(4.82)

The complex density ratio $\xi=\rho_a/\rho_b$ is included within the integral and the equation can be simplified into:

$$\varepsilon Ax = B + \xi \sum_{n=1}^{N} Cx \ . \tag{4.83}$$

The [*B*] matrix contains the direct wave information at colocation points:

$$[B] = \begin{bmatrix} G_{12}(r(1+1/2), \mathrm{r}_s) \\ G_{12}(r(2+1/2), \mathrm{r}_s) \\ \cdots \\ G_{12}(r(N+1/2), \mathrm{r}_s) \end{bmatrix} . \tag{4.84}$$

By reciprocity, the locations of the source/receiver are interchangeable. The mapping matrix, [*A*], remains unchanged. The mapping matrix [*A*] connecting the nodes and the colocation points is still the same. Within the [*C*] matrix,

$$\begin{aligned} b_{mn} = \xi h_n \{ & \frac{1}{3}[\frac{\partial G_{22}(\mathrm{r}_0(\mathrm{n}), \mathrm{r}(\mathrm{m}+\frac{1}{2}))}{\partial n(\mathrm{r}_0(\mathrm{n}))} - \mathrm{ik}\,\beta G_{22}(\mathrm{r}_0(\mathrm{n}), \mathrm{r}(\mathrm{m}+\frac{1}{2})] \\ & + \frac{1}{6}[\frac{\partial G_{22}(\mathrm{r}_0(\mathrm{n}+1), \mathrm{r}(\mathrm{m}+\frac{1}{2}))}{\partial n(\mathrm{r}_0(\mathrm{n}+1))} - \mathrm{ik}\,\beta G_{22}(\mathrm{r}_0(\mathrm{n}+1), \mathrm{r}(\mathrm{m}+\frac{1}{2})]\} \end{aligned} , \tag{4.85}$$

and

$$\begin{aligned} c_{mn} = \xi h_n \{ & \frac{1}{6}[\frac{\partial G_{22}(\mathrm{r}_0(\mathrm{n}), \mathrm{r}(\mathrm{m}+\frac{1}{2}))}{\partial n(\mathrm{r}_0(\mathrm{n}))} - \mathrm{ik}\,\beta G_{22}(\mathrm{r}_0(\mathrm{n}), \mathrm{r}(\mathrm{m}+\frac{1}{2})] \\ & + \frac{1}{3}[\frac{\partial G_{22}(\mathrm{r}_0(\mathrm{n}+1), \mathrm{r}(\mathrm{m}+\frac{1}{2}))}{\partial n(\mathrm{r}_0(\mathrm{n}+1))} - \mathrm{ik}\,\beta G_{22}(\mathrm{r}_0(\mathrm{n}+1), \mathrm{r}(\mathrm{m}+\frac{1}{2})]\} \end{aligned} . \tag{4.86}$$

The pressure distribution vector along the surface of the object is given by $\vec{x}$. Once it has been obtained, we can evaluate the sound field for the entire domain via the BEM.

For the above the ground case:

$$x_{above} = B_a + \xi C_a x \ , \tag{4.87}$$

where

$$C_a \begin{bmatrix} p_1 \\ p_2 \\ \dots \\ p_N \\ p_{N+1} \end{bmatrix} = (\begin{bmatrix} b_1 & b_2 & \dots & b_n & 0 \end{bmatrix} + \begin{bmatrix} 0 & c_1 & \dots & c_{(n-1)} & c_n \end{bmatrix}) \begin{bmatrix} p_1 \\ p_2 \\ \dots \\ p_N \\ p_{N+1} \end{bmatrix} , \tag{4.88}$$

$$\begin{aligned} b_n = \xi h_n \{ & \frac{1}{3}[\frac{\partial G_{12}(\mathrm{r_0(n), r(m+}\frac{1}{2}))}{\partial n(\mathrm{r_0(n)})} - \mathrm{ik}\,\beta G_{12}(\mathrm{r_0(n), r(m+}\frac{1}{2})] \\ & + \frac{1}{6}[\frac{\partial G_{12}(\mathrm{r_0(n+1), r(m+}\frac{1}{2}))}{\partial n(\mathrm{r_0(n+1)})} - \mathrm{ik}\,\beta G_{12}(\mathrm{r_0(n+1), r(m+}\frac{1}{2})]\} \end{aligned} \tag{4.89}$$

and

$$\begin{aligned} c_n = \xi h_n \{ & \frac{1}{6}[\frac{\partial G_{12}(\mathrm{r_0(n), r(m+}\frac{1}{2}))}{\partial n(\mathrm{r_0(n)})} - \mathrm{ik}\,\beta G_{12}(\mathrm{r_0(n), r(m+}\frac{1}{2})] \\ & + \frac{1}{3}[\frac{\partial G_{12}(\mathrm{r_0(n+1), r(m+}\frac{1}{2}))}{\partial n(\mathrm{r_0(n+1)})} - \mathrm{ik}\,\beta G_{12}(\mathrm{r_0(n+1), r(m+}\frac{1}{2})]\}. \end{aligned} \tag{4.90}$$

The Green's function for an above ground source and below ground receiver is G_{12}. To satisfy reciprocity, an additional ξ term is included.

Similarly, the below the ground sound field is given by:

$$x_{below} = B_a + \xi C_a x \ , \tag{4.91}$$

where

$$C_a\begin{bmatrix} p_1 \\ p_2 \\ \dots \\ p_N \\ p_{N+1} \end{bmatrix} = (\begin{bmatrix} b_1 & b_2 & \dots & b_n & 0 \end{bmatrix} + \begin{bmatrix} 0 & c_1 & \dots & c_{(n-1)} & c_n \end{bmatrix})\begin{bmatrix} p_1 \\ p_2 \\ \dots \\ p_N \\ p_{N+1} \end{bmatrix}, \qquad (4.92)$$

$$\begin{aligned} b_n = \xi h_n \{ & \frac{1}{3}[\frac{\partial G_{22}(\mathrm{r}_0(\mathrm{n}), \mathrm{r}(\mathrm{m}+\frac{1}{2}))}{\partial n(\mathrm{r}_0(\mathrm{n}))} - \mathrm{ik}\,\beta G_{22}(\mathrm{r}_0(\mathrm{n}), \mathrm{r}(\mathrm{m}+\frac{1}{2}))] \\ & + \frac{1}{6}[\frac{\partial G_{22}(\mathrm{r}_0(\mathrm{n}+1), \mathrm{r}(\mathrm{m}+\frac{1}{2}))}{\partial n(\mathrm{r}_0(\mathrm{n}+1))} - \mathrm{ik}\,\beta G_{22}(\mathrm{r}_0(\mathrm{n}+1), \mathrm{r}(\mathrm{m}+\frac{1}{2}))]\} \end{aligned} \qquad (4.93)$$

and

$$\begin{aligned} c_n = \xi h_n \{ & \frac{1}{6}[\frac{\partial G_{22}(\mathrm{r}_0(\mathrm{n}), \mathrm{r}(\mathrm{m}+\frac{1}{2}))}{\partial n(\mathrm{r}_0(\mathrm{n}))} - \mathrm{ik}\,\beta G_{22}(\mathrm{r}_0(\mathrm{n}), \mathrm{r}(\mathrm{m}+\frac{1}{2}))] \\ & + \frac{1}{3}[\frac{\partial G_{22}(\mathrm{r}_0(\mathrm{n}+1), \mathrm{r}(\mathrm{m}+\frac{1}{2}))}{\partial n(\mathrm{r}_0(\mathrm{n}+1))} - \mathrm{ik}\,\beta G_{22}(\mathrm{r}_0(\mathrm{n}+1), \mathrm{r}(\mathrm{m}+\frac{1}{2}))]\} \end{aligned} . \qquad (4.94)$$

5.2 BEM Validation

The sound field above and below a hard-backed ground is validated against existing analytical solutions in this section. A monopole source is positioned above the air/ground interface. An analytical solution for the sound field underground is given by:

$$p_1 = B_1(\mathrm{e}^{-ik_{1z}z} + U_1 e^{ik_{1z}z}), \qquad (4.95)$$

which represents contributions from both an upward and downward traveling wave. The sound field in the air can be given as:

$$p = \frac{i}{2k_z}(\mathrm{e}^{ik_z|z-z_s|} + U_0 e^{ik_z(z+z_s)}) \ , \tag{4.96}$$

where

$$U_0 = \frac{(\mathrm{k}_z/\rho)(\mathrm{U}_1+1)+(\mathrm{k}_{1z}/\rho_1)(\mathrm{U}_1-1)}{(\mathrm{k}_z/\rho)(\mathrm{U}_1+1)-(\mathrm{k}_{1z}/\rho_1)(\mathrm{U}_1-1)}, \tag{4.97}$$

and

$$U_1 = e^{2ik_{1z}d_1} \ . \tag{4.98}$$

d_1 is the thickness of the porous medium. (Attenborough, 2006)

The analytical result for the sound field above a hard-backed ground is calculated with the numerical integration, which is the same as the method used in the calculation of the accurate solution for the Green's functions.

In the comparison, Figure 5-2 demonstrates the good agreement between the analytical result and the BEM result. Low agreement could be observed in some regions, but the absolute error is low enough to be neglected. At the end of the interface, poor agreement is the result of the limitation of the BEM elements. A simulation with a larger element number can solve the problem. Besides, a finitely long surface must be used to approximate the infinitely long ground, which would definitely introduce error into the simulation due to the truncation.

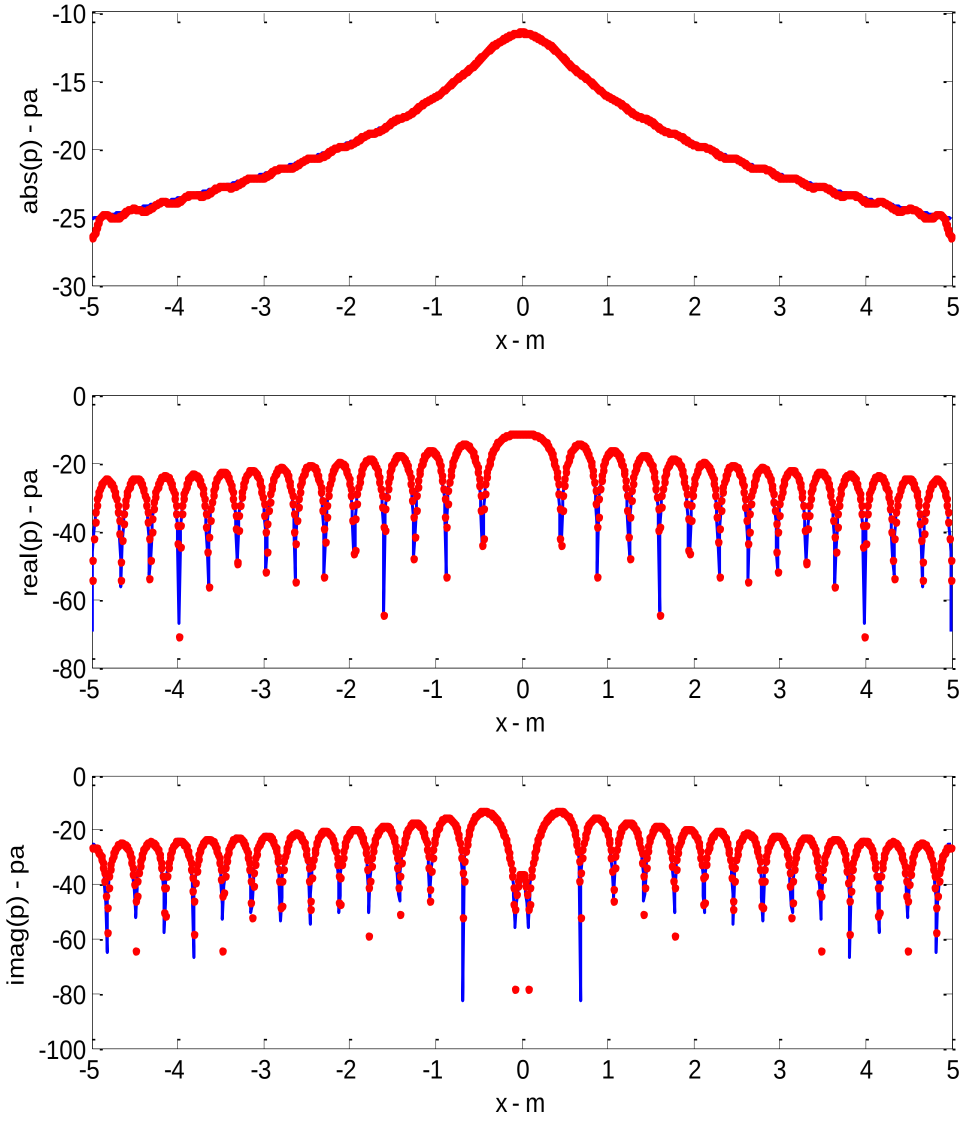

Figure 5-2. Sound pressure field predictions along the hard backing layer at a depth of 0.05 m below the ground. Ground properties: flow resistivity = 3000 Pa m s^{-2}, tortuosity = 1.7, porosity = 0.3, and pore shape factor = 1. The source is located at x_s = 0.5 m, z_s = 0.5 m, with a frequency of 500 Hz. Red dots: BEM predictions. Blue line: analytical model.

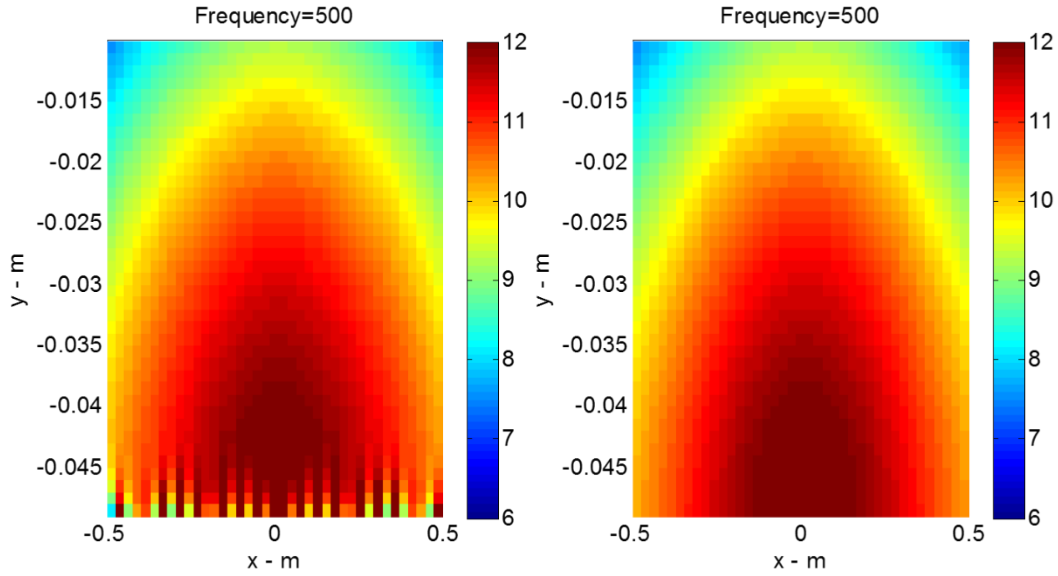

Figure 5-3. Simulation result below the interface. The hard surface is 0.05 m below the ground; The width of the surface is 5 m; Flow resistivity is 3000 Pa m s^{-2}; Tortuosity is 1.7; Porosity is 0.3; Shape factor is 1; The source point is located at x=0 m, z=0.5 m; Frequency is 500 Hz; Left: BEM result; Right: Analytical result.

Figure 5-3 and Figure 5-4 demonstrate the good agreement between the analytical solution and the BEM, except in regions where the SPL is very low. Poor agreement in these regions is inevitable, but an absolute error below -20 dB can usually be satisfactory in practical applications. More elements are required to increase the resolution of the visualization; however, this would require a considerable amount of additional computational resources. In the vicinity of the interface, poor agreement may be attributed to discretization error which fails to capture the rapidly varying pressure fluctuations. The stripes near the bottom interface (z=-0.05 m) indicates that more elements are needed to resolve the sound field.

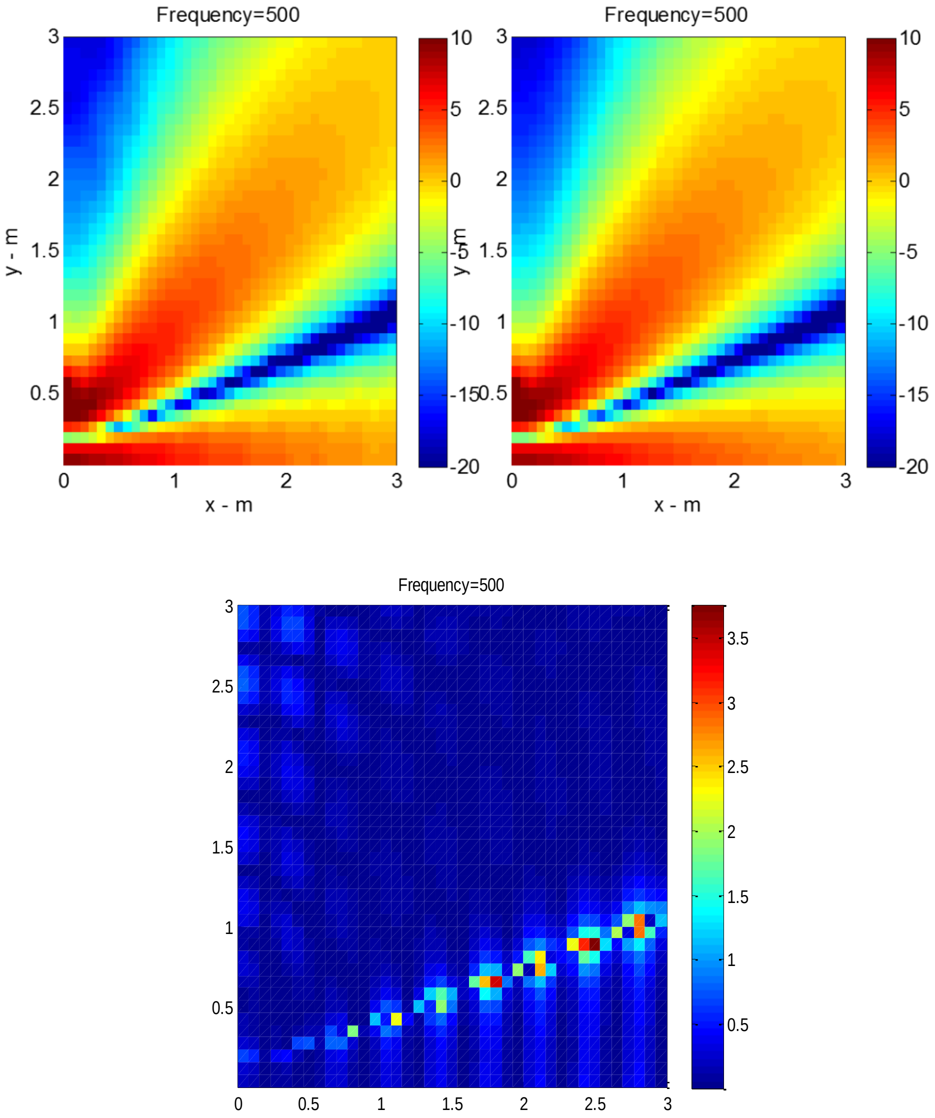

Figure 5-4. Same as Figure 5-3, but for the above ground propagation. The bottom figure shows the relative difference in EA in the absence of the below ground obstruction.

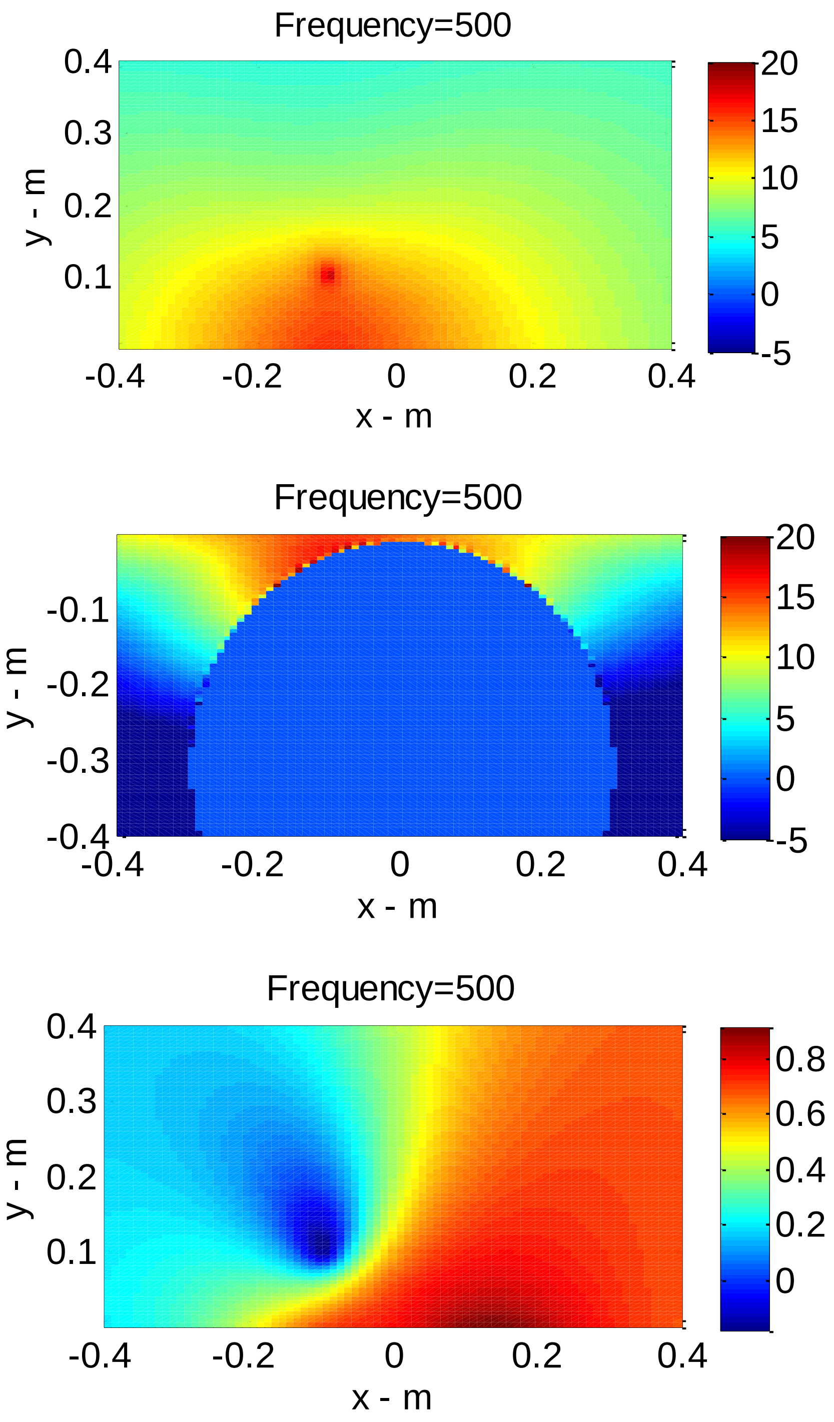

Figure 5-5. EA contour plots for the above ground, below ground, and relative EA in the absence of the below ground obstruction (ordered from top to bottom). A cylinder of 0.3 m radius is buried 0.01 m below the ground.

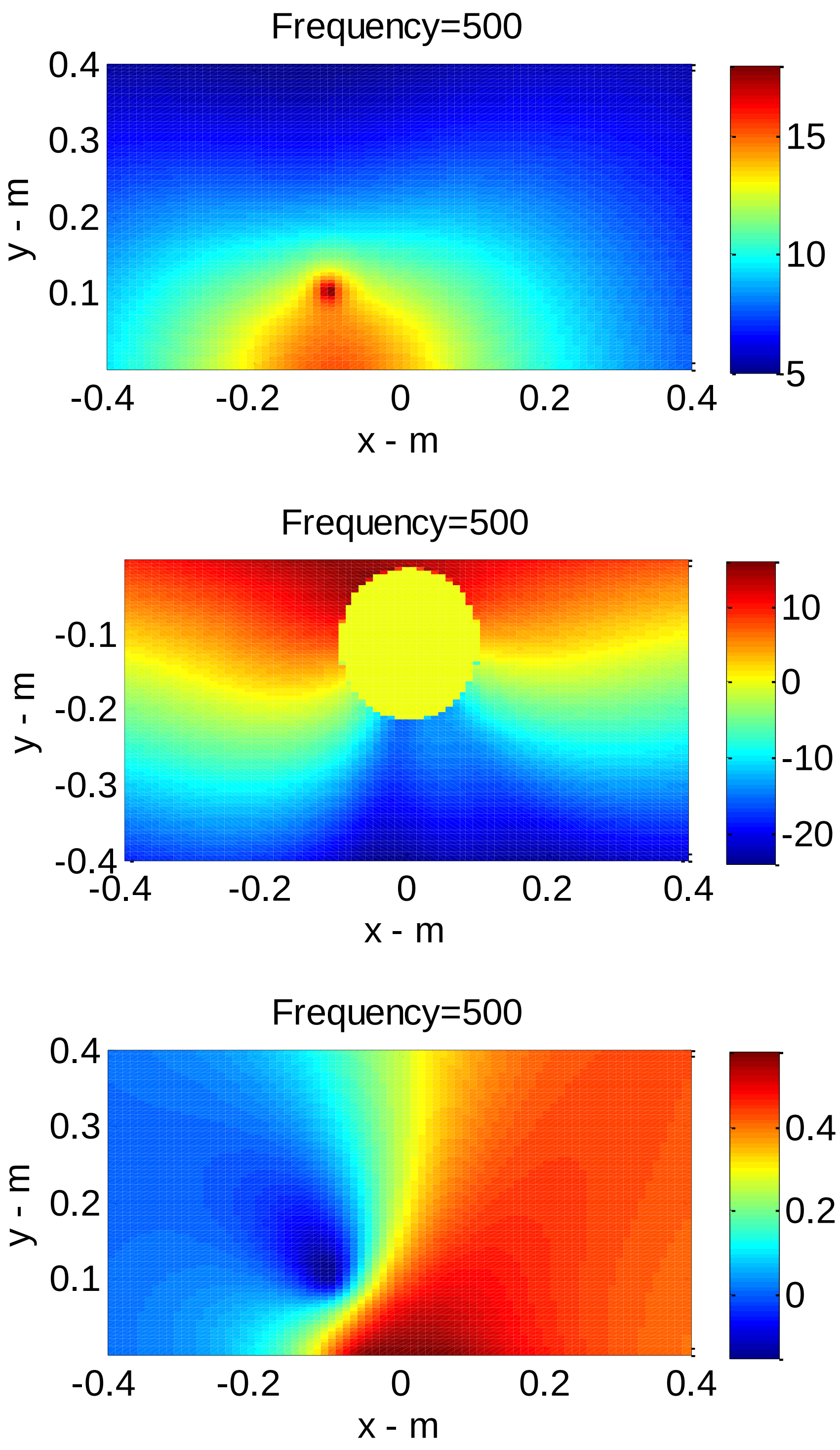

Figure 5-6. Same as Figure 5-5, but for a cylinder of 0.1m radius.

The EA difference is greater in Figure 5-5 than in Figure 5-6, which indicates that the larger cylinder is a more effective noise barrier. From the above ground sound field, one can determine the properties of below ground objects, assuming the porous medium properties are already known. This technique can be applied to underground object detection and acoustical material design. For example, we may consider the acoustical properties of a material which has beams or other obstructions consisting of rigid surfaces (e.g., rocks, roots, etc.) embedded below the ground. The prediction of the sound field above coble ground covered by snow or sand can also be considered.

Figure 5-8 illustrates the influence of the obstacle's proximity to the ground surface. A stronger signal can be obtained by the near-surface object as indicated by the lower plot. The method can also be used to evaluate the acoustic properties of porous materials at oblique angles of incidence.

Additional simulations for a hard-backed ground in the absence of barriers indicates the validity of our BEM formulation in the limiting cases. We can be assured that the proposed BEM provides reasonable sound field predictions based on the physical trends observed for below ground objects. The shape, size, and location of the objects have a significant impact on the sound field both above and below the ground, especially when in the vicinity of the air/ground boundary. When the flow resistivity is sufficient large, the ground behaves rigidly so the usefulness of below ground object detection diminishes.

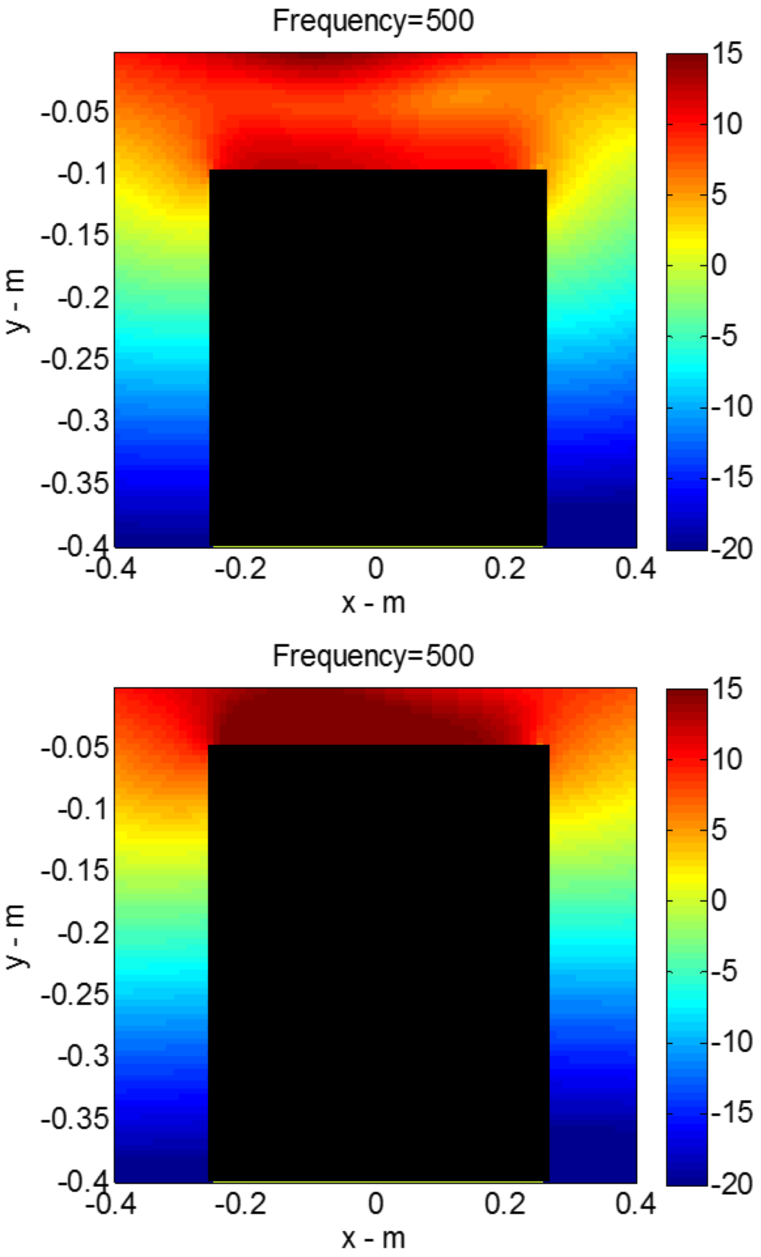

Figure 5-7. Below ground sound field due to a square object of 0.5 m width buried at two different depths. Source location: x_s=0.1 m, z_s=0.1 m. The object is buried 0.1 m and 0.05 m below the ground in the top/bottom figures, respectively.

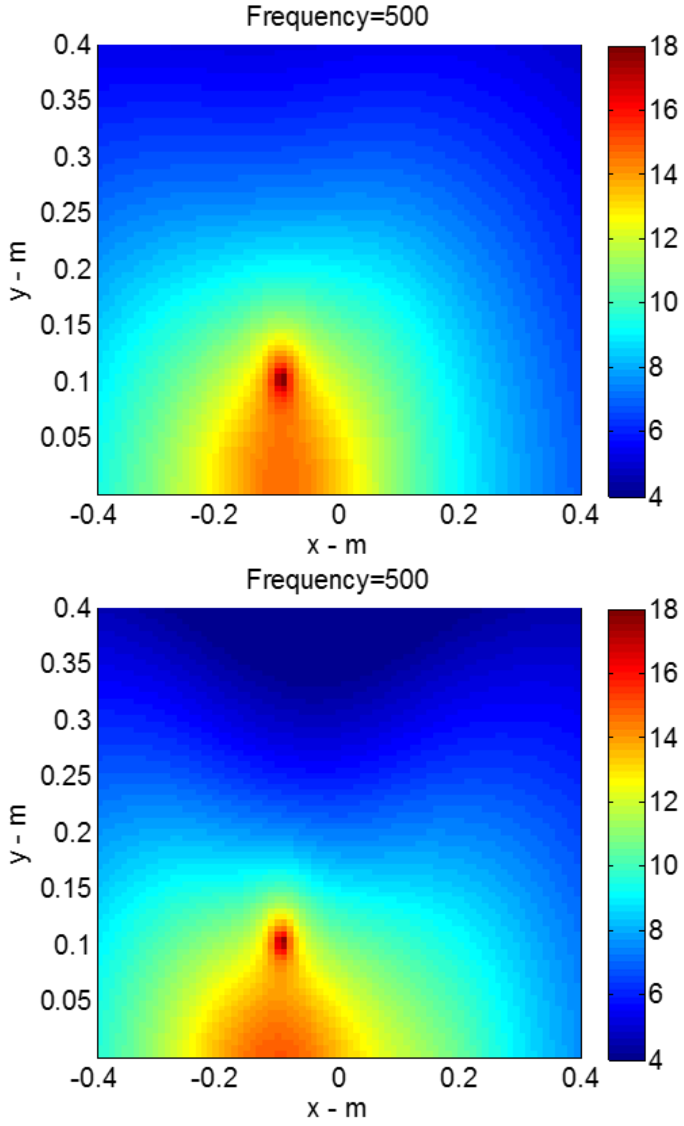

Figure 5-8. Same as Figure 5-7, but for the above ground sound field.

CHAPTER 6. CONCLUSION AND FUTURE WORK

6.1 Conclusions

An efficient asymptotic solution for the sound field below and above the ground due to a coherent line source was presented. The results are compared against analytical solutions or direct numerical solutions where applicable. Excellent agreement has been achieved, except for G_{12} at very low frequencies. This is an inherent problem in the method of steepest descent due to a violation of the rapidly varying phase assumption. However, the Green's function can be used along with direct numerical integration to obtain an accurate solution.

The Green's function is first implemented in the BIE to evaluate the sound field above the ground due to a scattering obstacle positioned above the ground. The sound field predictions in the presence of a noise barrier and mixed impedance ground are validated against experimental measurements. For the sound field below and above the ground due to scattering by an underground obstacle, numerical simulations are conducted using the derived Green's function. Good agreement between the proposed approximation scheme and the analytical solution was achieved in the situation of a hard-backed ground. This indicates that the proposed approximation provides a sufficient and numerically efficient alternative to the standard integration approach. We can be assured that the proposed BEM formulation is capable of predicting the sound field from an obstacle positioned above and/or embedded below a porous ground surface.

6.2 Discussion of Future Work

The prediction of the sound below the ground with a coherent line source below the ground is accurate for the most ground types. However, if the imaginary part of the wave number in the porous medium is large, the path may become distorted. In this case, the validity of the underground Green's function may require further investigation. An improved method could be implemented along with the method of steepest descent to evaluate the integration in the vicinity of the singularity.

The detection object on the seafloor is of great interest to the underwater acoustics community. Predictions based on sonar is influenced by the acoustical properties of the sediment and the topography of the land. The BEM can be applied to efficiently investigate such phenomena. However, the Green's function above the seafloor would be required. A different steepest descent method should be applied to solve the Green's function for the underwater case.

Additionally, the performance of the BEM is unsatisfied at high frequencies due to the large numbers of elements needed to represent the rapidly varying Green's function. There is great interest in developing a more robust high frequency BEM approach. A summary of potential research opportunities is listed below:

- Improve sound field predictions below the ground due to an above ground line source by modifying the steepest descent method to incorporate the phase term outside of the exponential term

- Derive faster solutions for the Green’s function evaluation for the water/sediment interface problem
- Apply state-of-the-art methods to evaluate the integral in the vicinity of singularities
- Design and conduct underground scattering experiments to validate BEM results
- Implement a high frequency BEM in the current work to explore high frequency scattering phenomena
- Investigate the acoustical properties of rough ground surfaces (e.g., rigid beams placed over a porous medium)

LIST OF REFERENCES

LIST OF REFERENCES

Abramowitz, M., & Stegun, I. A. (1972). Handbook of mathematical functions (Vol. 1, No. 5). New York: Dover.

Attenborough, K., Li, K. M., & Horoshenkov, K. (2006). Predicting outdoor sound. CRC Press.

Abarbanel, S., Gottlieb, D., & Hesthaven, J. S. (1999). Well-posed perfectly matched layers for advective acoustics. Journal of Computational Physics, 154(2), 266-283.

Ahmad, S., & Banerjee, P. K. (1988). Multi‐domain BEM for two‐dimensional problems of elastodynamics. International journal for numerical methods in engineering, 26(4), 891-911.

Allard, J. F., Jansens, G., & Lauriks, W. (2002). Reflection of spherical waves by non-locally reacting porous media. Wave motion, 36(2), 143-155.

Attenborough, K., Hayek, S. I., & Lawther, J. M. (1980). Propagation of sound above a porous half‐space. The Journal of the Acoustical Society of America, 68(5), 1493-1501.

Attenborough, K. (1985). Acoustical impedance models for outdoor ground surfaces. Journal of Sound and Vibration, 99(4), 521-544.

Baños, A. (1966). Dipole radiation in the presence of a conducting halfspace (Vol. 9). Pergamon.

Berry, D. L., Chandler-Wilde, S. N., & Attenborough, K. (1994). Acoustic scattering by a near-surface obstacle in a rigid porous medium. Journal of sound and vibration, 170(2), 161-179.

Bleistein, N. (1966). Uniform asymptotic expansions of integrals with stationary point near algebraic singularity. Communications on Pure and Applied Mathematics, 19(4), 353-370.

Brekhovskikh, L. (2012). Waves in Layered Media 2e (Vol. 16). Elsevier.

Chandler-Wilde, S. N., & Hothersall, D. C. (1985). Sound propagation above an inhomogeneous impedance plane. Journal of Sound and Vibration, 98(4), 475-491.

Chandler-Wilde, S. N., & Hothersall, D. C. (1995). Efficient calculation of the Green function for acoustic propagation above a homogeneous impedance plane. Journal of Sound and Vibration, 180(5), 705-724.

Chien, C. F., & Soroka, W. W. (1975). Sound propagation along an impedance plane. Journal of Sound and Vibration, 43(1), 9-20.

Chien, C. F., & Soroka, W. W. (1975). Sound propagation along an impedance plane. Journal of Sound and Vibration, 43(1), 9-20.

Chin, B., Stanley, A, Davis, J. A., & Evans, R. B. (1982). Nature of the lateral wave effect on bottom loss measurements. The Journal of the Acoustical Society of America, 71(6), 1433-1437.

Dinapoli, F. R. (1970). Fast Field Program. The Journal of the Acoustical Society of America, 47(1A), 100-100.

Elleithy, W. M., & Tanaka, M. (2003). Interface relaxation algorithms for BEM–BEM coupling and FEM–BEM coupling. Computer Methods in Applied Mechanics and Engineering, 192(26), 2977-2992.

Fokkema, J. T., & van den Berg, P. M. (2013). Seismic applications of acoustic reciprocity. Elsevier.

Frisk, G. V., & Überall, H. (1976). Creeping waves and lateral waves in acoustic scattering by large elastic cylinders. The Journal of the Acoustical Society of America, 59(1), 46-54.

Graf, R. A. G., Kuo, C. Y., Dowling, A. P., & Graham, W. R. (1999). Horn amplification at a tyre/road interface-part I: experiment and computation. In Proceedings of Internoise 99-the 1999 International Congress on Noise Control Engineering Held in Fort Lauderdale, Florida, USA, 6-8 December 1999, Volume 1.

Ingard, U. (1951). On the reflection of a spherical sound wave from an infinite plane. The Journal of the Acoustical Society of America, 23(3), 329-335.

Junger, M. C., & Feit, D. (1972). Sound, structures, and their interaction (Vol. 225). Cambridge, MA: MIT press.

Kropp, W., Bécot, F. X., & Barrelet, S. (2000). On the sound radiation from tyres. Acta Acustica united with Acustica, 86(5), 769-779.

Kawai, T., Hidaka, T., & Nakajima, T. (1982). Sound propagation above an impedance boundary. Journal of Sound and Vibration, 83(1), 125-138.

Lawhead, R. B., & Rudnick, I. (1951). Acoustic wave propagation along a constant normal impedance boundary. The Journal of the Acoustical Society of America, 23(5), 546-549.

Li, K. M., & Liu, S. (2011). Fast asymptotic solutions for sound fields above and below a rigid porous ground. The Journal of the Acoustical Society of America, 130(3), 1103-1114.

Li, K. M., & Liu, S. (2012). Propagation of sound from a monopole source above an impedance-backed porous layer. The Journal of the Acoustical Society of America, 131(6), 4376-4388.

Li, K. M., & Tao, H. (2013). On the asymptotic solution of sound penetration into a rigid porous half-plane: A modified saddle point method. Journal of Sound and Vibration, 332(19), 4584-4596.

Li, K. M., & Tao, H. (2014). Heuristic approximations for sound fields produced by spherical waves incident on locally and non-locally reacting planar surfaces. The Journal of the Acoustical Society of America, 135(1), 58-66.

Morse, P. M. (1948). Vibration and sound (Vol. 2). New York: McGraw-Hill.

Morse, P. M., & Bolt, R. H. (1944). Sound waves in rooms. Reviews of modern physics, 16(2), 69.

Norton, K. A. (1937). The propagation of radio waves over the surface of the earth and in the upper atmosphere. Radio Engineers, Proceedings of the Institute of, 25(9), 1203-1236.

Paul, D. I. (1957). Acoustical radiation from a point source in the presence of two media. The Journal of the Acoustical Society of America, 29(10), 1102-1109.

Rayleigh, J. W. S. B. (1896). The theory of sound (Vol. 2). Macmillan.

Stephens, G. L. (1984). Scattering of plane waves by soft obstacles: anomalous diffraction theory for circular cylinders. Applied optics, 23(6), 954-959.

Richards, T. L., & Attenborough, K. (1986). Accurate FFT-based Hankel transforms for predictions of outdoor sound propagation. Journal of sound and vibration, 109(1), 157-167.

Stepanishen, P. R., & Benjamin, K. C. (1982). Forward and backward projection of acoustic fields using FFT methods. The Journal of the Acoustical Society of America, 71(4), 803-812.

Seybert, A. F., Soenarko, B., Rizzo, F. J., & Shippy, D. J. (1985). An advanced computational method for radiation and scattering of acoustic waves in three dimensions. The journal of the acoustical society of America, 77(2), 362-368.

Sommerfeld, A. (1909). Propagation of waves in wireless telegraphy. Ann. Phys, 28(3), 665-736.

Sommerfeld, A. (1909). Über die Ausbreitung der Wellen in der drahtlosen Telegraphie. Annalen der Physik, 333(4), 665-736.

Tindle, C. T. (1983). Ray calculations with beam displacement. The Journal of the Acoustical Society of America, 73(5), 1581-1586.

Westwood, E. K. (1989). Complex ray methods for acoustic interaction at a fluid–fluid interface. The Journal of the Acoustical Society of America, 85(5), 1872-1884.